

Electronic Thesis and Dissertation Repository

12-16-2016 12:00 AM

Measuring Brain Serine With Proton Magnetic Resonance Spectroscopy At 3.0 Tesla

Homa Javadzadeh, *The University of Western Ontario*

Supervisor: Dr. Jean Théberge, *The University of Western Ontario*

A thesis submitted in partial fulfillment of the requirements for the Master of Science degree in Medical Biophysics

© Homa Javadzadeh 2016

Follow this and additional works at: <https://ir.lib.uwo.ca/etd>



Part of the [Other Psychiatry and Psychology Commons](#)

Recommended Citation

Javadzadeh, Homa, "Measuring Brain Serine With Proton Magnetic Resonance Spectroscopy At 3.0 Tesla" (2016). *Electronic Thesis and Dissertation Repository*. 4344.
<https://ir.lib.uwo.ca/etd/4344>

This Dissertation/Thesis is brought to you for free and open access by Scholarship@Western. It has been accepted for inclusion in Electronic Thesis and Dissertation Repository by an authorized administrator of Scholarship@Western. For more information, please contact wlsadmin@uwo.ca.

Abstract

Proton magnetic resonance spectroscopy (MRS) non-invasively measures regional human brain chemistry *in vivo*, providing concentration estimates for several metabolites in a pre-selected region of interest. MRS has been applied to investigations of disease-related metabolic and neurochemical alterations in schizophrenia since the early 90's.

The objective of this research is to implement a metabolite-selective MRS method to quantify endogenous concentrations of human brain serine. Serine is a naturally-occurring amino acid and an important co-modulator of the N-Methyl D-aspartic Acid (NMDA) glutamate receptor. Glutamate abnormalities have been implicated in the pathophysiology of schizophrenia, especially its so-called negative and cognitive symptoms, which can be relieved by D-serine supplements.

Measurements of serine have been impossible using standard MRS due to its low concentration and strongly coupled spins. In this thesis, we implement and test an advanced MRS pulse sequence, called DANTE-PRESS, using a narrow band radiofrequency (RF) pulse to isolate the serine signals from the human brain spectra for the first time on a 3.0 Tesla clinical scanner.

Test-retest reliability of *in vitro* serine measurements in brain-mimicking samples was verified using ten repeated acquisitions from two serine samples with concentrations of 0.732 mM (similar to "*in vivo*") and 1.464 mM ("double *in vivo*") at baseline and one week later. Within- and between-session reproducibility was measured with the coefficient of variation (CV) and one-way ANOVA, respectively. Average serine "*in vivo*" concentration at baseline, one week later, "double *in vivo*" at baseline, and one week later were 1.13 ± 0.09 (CV = 8.3%), 1.06 ± 0.10 (CV = 9.9%), 2.18 ± 0.13 (CV = 5.7%) and 2.23 ± 0.14 (CV = 6.5%), respectively.

The thesis also presents the first 3.0 Tesla application of DANTE-PRESS in a human brain region relevant to schizophrenia as proof-of-concept. Future studies can extend the work to implementation of DANTE-PRESS at 7.0 Tesla and *in vivo* test-retest.

Keywords:

Proton magnetic resonance spectroscopy, reproducibility, schizophrenia, brain, serine, DANTE-PRESS, single-voxel spectroscopy.

Co-Authorship Statement

This thesis contains materials for one manuscript in preparation to be submitted to a peer-reviewed journal in the field of MRS. These materials are presented in Chapter 3.

Dr. Peter Williamson and Dr. Nagalingam Rajakumar provided guidance regards to the interpretation of results, and contributed significantly to the review of the report regarding this study.

Dr. Yves Bureau provided invaluable insight regarding issues of statistical analysis for the *in vitro* data contained in this thesis.

Mr. John Butler provided training on the use of the 3.0 Tesla MRI scanner located at St. Joseph's hospital and provided guidance regarding the choice of anatomical regions of interest and the placement of the voxel.

A former Medical Biophysics graduate student, Ms. Karina Quiaoit, along with Mrs. Rebecca McGirr, provided training on preparing the solutions and the construction of brain-mimicking MRI phantoms used for this study.

The study design and the implementation of the advanced ^1H -MRS method, DANTE-PRESS, the modification and the development of the pulse sequence programming on the Siemens platform (under the environments of IDEA and ICE), any other technical developments, the recruitment of the healthy volunteers and the development of the *in vivo* and *in vitro* templates, were all completed by Homa Javadzadeh under the supervision of Dr. Jean Théberge.

Through a collaborative agreement with Siemens Canada, Homa Javadzadeh engaged in developing MRS pulse sequences on the Siemens platform and gained the unique ability to develop MRS pulse sequences and, aside from her own project, helped another faculty member, Dr. Neil Gelman, to develop an MRS sequence to measure lactate in humans. The other advisory committee members, Dr. Rajakumar and Dr. Williamson, provided essential feedback and helpful suggestions by revising the manuscript presented in Chapter 3 prior to submission.

Acknowledgments

Foremost, I wish to thank my supervisor, Dr. Jean Théberge, for his continuous support, infinite patience, encouragement and expert advice he has provided throughout my graduate studies. When faced with the difficulties of carrying out my research project, I always stayed dedicated and committed to overcome any challenges and this is mainly due to the support I received from Dr. Théberge.

Through hard work, perseverance, enormous efforts and the necessary aid provided by Dr. Théberge, I succeeded in implementing a breakthrough novel ^1H -MRS method capable of detecting complex brain metabolites on a clinical scanner. This novel technique will be of substantial benefit to the field of neuropsychiatry, and specifically schizophrenia. I am privileged to have been supervised by an incredible supervisor who cared enormously about my research project, and who responded to my queries so promptly and without his help I would have never achieved my goals as a competent graduate student.

I would also like to thank my committee members, Dr. Peter Williamson and Dr. Nagalingam Rajakumar, for providing their valuable feedback, expert insight and always having a reasonable perspective and outlook towards my achievements. Special thanks to my co-supervisor, Dr. Peter Williamson, for providing me with funding this past year to undertake my research.

Without the contributions of several important faculty members at St. Joseph's Hospital and Lawson Health Research Institute, I would not have been able to accomplish many tasks easily. Special thanks to Mr. John Butler and Ms. Heather Biernaski, for teaching and training me on your knowledge of the 3.0 T system located at St Josephs and allowing me to use the scanner at all times. Thanks to Mr. Lynn Keenlside for his abundant help with building MRI phantoms. Thanks to Mrs. Michele Avon for always accepting my requests and providing help when needed.

I would like to thank Dr. Yves Bureau for helping me with the statistical analysis of the *in vitro* data.

To Dr. Daniel Milej, thank you for passing on your knowledge and guiding me in the right direction every time I needed help without any hesitation while you were occupied with your own work. I wish you nothing but success in your future endeavours.

To, Linden Barton and Dr. Reggie Taylor, my former lab-mates, I thank you for answering my questions regarding MRS and physics.

This journey would not have been possible without the support of my family. To my wonderful father, Hormoz Javadzadeh, a former physics and engineering assistant professor, and my sweet and loving mother, Susan, thank you for your endless love, encouragement and support. I am continually amazed by your willingness to convince me that I am able to accomplish almost anything in life. Being miles away from you did not stop you at any point constantly contacting me and making sure I was doing well. Thank you for everything you have done, and without you I would not have been able to accomplish this task. Many thanks to my incredibly intelligent brother, Houman Javadzadeh, who has earned a Bachelor's Degree in Engineering and a Master of Engineering (M.Eng.) Degree from the University of Toronto, for his continuous support and thank you for encouraging me in all of my pursuits and inspiring me to stay dedicated.

Table of Contents

Abstract	i
Co-Authorship Statement.....	iii
Acknowledgments.....	iv
Table of Contents	vi
List of Tables	ix
List of Figures	x
List of Appendices	xiii
Abbreviations	xiv
Chapter 1	1
1.1 Introduction.....	1
1.1.1 Schizophrenia.....	1
1.1.2 Neural models of schizophrenia:	3
1.1.3 D-Serine as adjuvant to antipsychotic Treatment:	6
1.1.4 Evidence of abnormal levels of D-serine in schizophrenia:	9
1.1.5 Previous ¹ H-MRS studies of serine and glycine:	10
1.1.6 The thesis outline:	11
1.1.7 References:.....	12
Chapter 2.....	28
2 Introduction:.....	28
2.1 Principles of magnetic resonance imaging and spectroscopy:.....	28
2.2 Signal localization:.....	32
2.3 Chemical shift:	33
2.4 J-coupling and spin systems:.....	34

2.5 Proton magnetic resonance spectroscopy:	37
2.6 DANTE-PRESS sequence:	37
2.7 Water suppression:	41
2.8 MRS quantification methods, line shape corrections:	42
2.9 Spectral fitting:	43
2.10 The fitting procedure:	44
2.11 Quantification of metabolites:	45
2.12 Summary:	47
2.13 References:	47
3 Reliability of <i>in vitro</i> measurements of endogenous levels of serine using DANTE-PRESS ¹ H-MRS at 3.0 T.....	54
3.1 Introduction.....	54
3.2 Materials and Methods:.....	59
3.2.1 Phantoms:.....	59
3.2.2 Human participants:	61
3.2.3 Measurements:	61
3.2.4 Experimental:	65
3.3 Results:.....	70
3.4 Discussion:	82
3.5 References:.....	84
Chapter 4.....	90
4 Thesis summary:	90
4.1 General remarks, limitations and implications:	91
4.2 The DANTE-PRESS protocol's advantages and limitations:.....	91
4.2.1 Advantages:.....	91
4.2.2 Limitations and implications:	92

4.3 Biograph mMR PET/MRI 3.0 Tesla scanner:.....	93
4.4 Ultra-high magnetic field of 7.0 Tesla versus 3.0 Tesla:	93
4.5 Caveats and future recommendations:	94
4.6 Future work:.....	95
4.6.1 ¹ H-MRS schizophrenia:	95
4.7 References:.....	98
Curriculum Vitae	125

List of Tables

Table 3-1. A summary of all the brain-mimicking phantoms that were built for this study is presented.....	60
Table 3-2. MRS ratio summary * of all of the <i>in vivo</i> measurements are displayed.	74

List of Figures

Figure 1-1. The limbic basal ganglia thalamocortical circuits.....	5
Figure 2-1. This figure represents the relative population size of the two possible energy states (Eigen states).....	30
Figure 2-2. A three-dimensional single voxel localization process.....	33
Figure 2-3. The chemical structure formula of serine is presented.....	35
Figure 2-4. Resonances of serine and the neighboring metabolites are illustrated.....	36
Figure 2-5. Pulse sequence timing diagram for the ¹ H MRS acquisition protocol (DANTE-PRESS) employed in the experiments reported in this thesis.....	39
Figure 2-6. A frequency selective single-DANTE pulse, generated with bandwidth values of 15 Hz and 100 Hz is illustrated.....	40
Figure 2-7. Top spectrum displays a conventional MRS <i>in vivo</i> data acquired with a symmetrical PRESS sequence and the bottom spectrum displays <i>in vivo</i> data obtained with DANTE-ON.....	41
Figure 2-8. Representative <i>in vivo</i> spectrum obtained from the left anterior cingulate of a healthy participant.....	45
Figure 3-1. Resonances near the 15 Hertz wide region selected by the frequency-selective DANTE RF pulse (simulated FID, 1Hz linewidths).....	56
Figure 3-2. A sequence diagram of the DANTE-PRESS sequence, together with the timing and order of slice selective gradients (G _x ,G _y ,G _z), the frequency selective pulses (RF) and the ADC axis is represented.	58
Figure 3-3. DANTE RF Pulse amplitude waveform in the time domain (top) and the corresponding frequency profile obtained by Fourier Transformation (bottom).....	63

Figure 3-4. Spectra obtained from a phantom containing 30 mM of Ser and 7.5 mM of Cr, using an echo time of 286 ms with D-PRESS (top) and symmetrical PRESS with an echo time of 286 ms (bottom).	67
Figure 3-5. A series of phantoms with the following concentrations of serine were scanned: 20 mM, 10 mM, 5 mM, 2.5 mM, and 1.25 mM.	68
Figure 3-6. This figure illustrates the voxel ($20 \times 20 \times 20 \text{ mm}^3$) positioning in the left anterior cingulate in a healthy participant.	69
Figure 3-7. These spectra illustrate the 10 consecutive <i>in vitro</i> D-PRESS measurements obtained from two phantoms that contain <i>in vivo</i> serine concentrations and double <i>in vivo</i> serine concentrations.....	75
Figure 3-8. The average value of baseline <i>in vivo</i> & one week plus baseline double <i>in vivo</i> & one week are presented in this graph.	76
Figure 3-9. PRESS (A, C) and DANTE-PRESS (B, D) spectra (TE = 286 ms , TR = 2.0 s) were obtained from the anterior cingulate (A, B) and <i>in vitro</i> data acquired from a phantom composed of a solution of Ser and Cr (C, D).....	77
Figure 3-10 . A stack of <i>in vivo</i> DANTE-PRESS spectra obtained at TE=286 ms from the left anterior cingulate of three healthy participants	78
Figure 3-11. Representative of an <i>in vivo</i> spectrum.....	79
Figure 3-12. The “Special Card” illustrates the parameters which interact with the DANTE RF Pulse.	80
Figure 3-13. The inline display illustrates the calibration of the DANTE RF pulse’s chemical shift (CShift) value	81
Figure A-1. The “Special Card” illustrating the parameters which interact with the DANTE RF Pulse.	109

Figure A-2. This figure illustrates the modulation parameters including the drop-down menu for the “Flip Angle Modulation” and the “DANTE Frequency Shift INC” parameters.	111
Figure C-3. The inline display illustrates the calibration of the RF pulse’s flip angle (FA) value of an excitation RF pulse.....	116
Figure C-4. The inline display illustrates the calibration of the RF pulse’s flip angle (FA) value of the two refocusing RF pulses	117
Figure C-5. The inline display illustrates the calibration of the DANTE RF pulse’s chemical shift (CShift) value.	118
Figure C-6. The inline display illustrates the calibration of the DANTE chemical shift for the water peak	119
Figure D-7. This figure illustrates how the gradient crusher areas’ values can be visualized at run-time by the user in response to changes in pulse sequence timing and crusher gradient amplitude.....	121
Figure D-8. Representative of an <i>in vivo</i> spectrum obtained prior to optimizing of the gradient crushers.	122
Figure D-9. Representative of an <i>in vivo</i> spectrum acquired after the optimizing of the gradient crushers was performed.	123

List of Appendices

Appendix A: DANTE-PRESS (the sequence and the special Card)	106
Appendix B: DANTE Radio Frequency (RF) Pulse.....	112
Appendix C: Inline Display	115
Appendix D: Gradient Crusher Optimization	120
Appendix E: Ethics Approval.....	124

List of Abbreviations

β	Damping coefficient
ω_0	Larmor frequency
γ	Gyromagnetic ratio
δ	ppm value (Chemical shift)
τ	Duration
Δt	Period
μs	Microsecond
^1H	Proton
$^1\text{H-MRS}$	Proton magnetic resonance spectroscopy
ABX	A three spin system
ACC	Anterior cingulate cortex
AFA	Actual flip angle value
ANOVA	Analysis of variance
B_0	Static magnetic field, main field
B_1	Rotating magnetic field (radiofrequency range)
CB	Cerebellum
CHES	CHEmical Shift Selective
Cr	Creatine
CNS	Central nervous system
CSF	Cerebral Spinal Fluid
DA	Dopamine
D-Ser	D-Serine
CV	Coefficient of Variation
DANTE	Delays for Alternating with Nutation for Tailored Excitation
D-PRESS	DANTE-PRESS
Dia.	Diameter
DISC1	Disrupted in schizophrenia 1
DSM-5	Diagnostic and Statistical Manual of Mental Disorders, fifth edition
Eth	Ethanolamine

FA	Flip angle
FDP	Frequency domain period
FID	Free Induction Decay
FOV	Field Of View
FWHM	Full Width at Half Maximum
FDFWHM	Frequency Domain Full Width at Half Maximum
G	Linear gradient
GABA	γ -Amino Butyric Acid
Gln	Glutamine
Glu	Glutamate
GLX	Glutamate+Glutamine
GLY	Glycine
Gly-T	Glycine transport
GM	Grey matter
GMS	Glycine modulatory site
$G_{(x,y,z)}$	Gradient in direction x, y, or z
HIP	Hippocampus
HSLVD	Hankel-Lanczos Singular Value Decomposition
ICE	Image Calculation Environment
IDEA	Integrated Development Environment for Applications
Lac	Lactate
LW	Lorentzian Linewidth
M	Magnetization vector (M_x, M_y, M_z)
Mao	Numerically optimized radio frequency inversion pulse by Mao et al.
M_0	Net macroscopic magnetization
MM	Macromolecules
mM	Millimolar
MRI	Magnetic Resonance Imaging
MRS	Magnetic Resonance Spectroscopy
M_x	Projection of magnetisation vector along x axis
M_y	Projection of magnetisation vector along y axis
M_z	Projection of magnetisation vector along z axis
ms	Millisecond

Myo	Myo-inositol
NA	Nucelus accumbens
NA	Number of averages
NAA	N-acetyl Aspartate
NaN ₃	Sodium azide
NMDA	N-methyl D-aspartate
NMDAR	N-methyl D-aspartate receptor
NMR	Nuclear Magnetic Resonance
No.	Number
PBS	phosphate-buffered saline
PEth	Phosphorylethanolamine
PFC	Prefrontal Cortex
PCP	Phencyclidine
PCr	Phosphocreatine
pH	Potential of hydrogen
ppm	Parts per million
PRESS	Point-RESolved Spectroscopy
QUALITY	Quantification Improvement by converting Line Shapes to the Lorentzian
Type	
QUECC	Quality Eddy Current Correction
R	Time-bandwidth product
REP	Repetition number
RF	Radiofrequency
RF ²	The first refocusing 180° RF pulse
RF ³	The DANTE RF pulse
RF ⁴	The second refocusing 180° RF pulse
S	Signal value
SD	Standard deviation
Ser	Serine
SNR	Signal-to-Noise Ratio
SVS	Single voxel spectroscopy
t	Time, Variable delay time
T	Tesla

T ₁	Spin-lattice relaxation time constant.
T ₂	Spin-spin relaxation time constant.
TE	Echo Time
TH	Thalamus
TR	Repetition Time
V	Voltage
VT	Ventral tegmentum
VTA	Ventral tegmental area
WM	White matter
WET	A water suppression scheme
ww	Wet weight

Chapter 1

1.1 Introduction

The goal of this thesis is to describe the implementation of a novel proton magnetic resonance spectroscopy (^1H -MRS) technique in order to measure the *in vivo* concentration of human brain serine. Detection of endogenous levels of serine has been impossible with standard proton MRS and no existing technique can assess *in vivo* brain serine levels on a clinical scanner of 3.0 Tesla (T) or less. The main objective of the thesis is to implement a customized ^1H -MRS technique on a clinical scanner of 3.0 T and evaluate its test-retest reliability in phantoms. The secondary objective is to apply the metabolite-selective MRS technique developed to detect the endogenous concentration of serine in the human brain as an *in vivo* proof-of-concept. Precise and reliable measurements of endogenous serine in the human brain using a customized ^1H -MRS may provide crucial information for research in neuro-psychiatric disorders particularly in patients living with schizophrenia. The following chapter will introduce background information, a brief history and description of schizophrenia, and the main motivation for the development of human brain serine measurements. This chapter will review the literature peripheral to administration of D-serine in patients with schizophrenia as an adjuvant to standard treatment.

1.1.1 Schizophrenia

In 1896, German psychiatrist Emil Kraepelin introduced the concept of dementia praecox, which is now known as schizophrenia.¹ He also differentiated the unitary concept of psychosis into two distinct categories on the basis of their etiology and clinical courses: manic depression and dementia praecox. Subjects who were diagnosed with dementia praecox were described as experiencing positive and negative symptoms (augmented or diminished experiences), including hallucinations and disturbances in behaviour. He significantly contributed to the understanding of psychotic disorders; some of his original

ideas have endured to this day and are comparable to the classification of schizophrenia in the current Diagnostic and Statistical Manual of Mental Disorders, fifth Edition (DSM-5) ² diagnostic classification psychiatric disorders. In the early twentieth century the introduction of the term “schizophrenia” was first discussed by a Swiss psychiatrist named Eugene Bleuler.³

Schizophrenia is a severe mental condition with a high morbidity and mortality rate, which is described as a neuro-developmental brain disorder.⁴ It currently affects approximately 1% of the global population and patients occupy approximately 40% of psychiatric hospital beds.^{5, 6} The onset of symptoms is typically in late adolescence or young adulthood,⁷ and often results in lifetime treatment and therapy with antipsychotic medications. Among the symptoms of this disease, neurocognitive and negative deficits are the most prominent, affecting 40-80% of patients in clinical samples.⁸ Cognitive and negative symptoms account for long term functional impairments. The efficacy of current medications is limited in alleviating these deficits.⁹ Studies have shown that the economic burden caused by schizophrenia remains high in Canada mainly due to the loss of productivity as a result of morbidity.^{10, 11} The global cost of this illness on health care budgets is significant; on average it amounts to about 1.5 to 3 percent of total national health care expenses.¹¹ Currently, there is no cure for schizophrenia, although it is a disorder that is responsive to treatment. Thus, this severe mental disorder is worthy of academic investigation; it is crucial to advance our understanding of the pathophysiology of the disease to maximize our ability to treat schizophrenia.

Numerous reports have investigated the role of genetics or environmental factors in schizophrenia. Studies indicate that environmental stressors including birth complications,¹² infections,¹³ socioeconomic factors, or childhood adversity¹⁴ may make a person more susceptible to developing schizophrenia later in life. Studies of the familial risks and heritability of schizophrenia have indicated that higher levels of risk for schizophrenia exist among relatives.¹⁵ Adoption reports have illustrated that the risk for developing schizophrenia was higher among biologic offspring even when they were adopted by parents who did not have any mental illnesses.¹⁶ In the case of twins, the concordance rates for schizophrenia are far greater among monozygotic twins (almost 50%)¹⁷

compared to fraternal twins who only share approximately 50% of the same genes.^{18, 19} Gene association investigations have identified several risk genes including dysbindin, neuregulin, and Disrupted in schizophrenia 1 (DISC1), each influencing the N-Methyl D-aspartic Acid (NMDA) receptor that contributes significantly to the pathophysiological network of schizophrenia by causing neurotransmitter and synaptic anomalies.²⁰⁻²³ Genetic studies also have provided significant evidence showing dysregulation of certain genes that control the metabolism of D-serine, an important modulator of NMDA receptor (NMDAR).²⁴ While genetic studies do not provide a clear description of specific abnormalities underlying schizophrenia, there does seem to be a heritable genetic component to schizophrenia.¹⁴

1.1.2 Neural models of schizophrenia:

Numerous models of schizophrenia have been developed to rationalize its onset mechanism and the resulting brain abnormalities.²⁵⁻³¹ Separate bodies of evidence have been mounted in support of specific neurotransmitter abnormalities contributing to the manifestation of symptoms. The earliest model recognized as the dopamine (DA) hypothesis proposed that certain dopaminergic pathways are overactive. It was postulated that the dysfunction in dopamine action on the ventral striatum region of the brain surrounding the nucleus accumbens is likely a common feature of all patients with schizophrenia.²⁵ It had been postulated that over-activity of DA neurons situated in the mesolimbic pathway, extending from the ventral tegmental area to limbic regions, may have mediated positive symptoms.³² This hypothesis was initially suggested based on findings showing that dopamine-blocking agents that generated symptoms similar to those of acute paranoid and positive syndromes in schizophrenia.²³ Unfortunately, this model does not fully explain all symptoms, especially negative and cognitive symptoms.²⁶ Over the years, it was postulated that a dopamine neural pathway known as the mesocortical pathway, which also originates from the midbrain's ventral tegmental area and projects to the limbic cortex, may have played a role in mediating some cognitive deficits, mainly the negative symptoms of schizophrenia.²⁵ Several investigations also solidified the hypothesis that the hypoactive condition of the DA neurons in the mesocortical region may be responsible for the negative symptoms.^{23, 27, 32}

Subsequently, a theory called the glutamatergic deficiency model of schizophrenia was proposed that explains the appearance of negative symptoms disturbances of glutamatergic neurotransmission upstream from the dopaminergic pathway.²⁸ This model was proposed a few decades ago after phencyclidine (PCP) was found to act on a specific binding site on the NMDAR resulting in channel blockade and inhibiting receptor-mediated glutamate neurotransmission.³⁴ In humans, it was discovered that PCP is capable of inducing all of the symptoms of schizophrenia in healthy subjects, including not only the positive ones but the prominent negative symptoms and cognitive deficits.^{34,}³⁵ The previous literature indicates the abnormalities of glutamatergic neurotransmission that play a vital role in the pathophysiology of schizophrenia and may account for its manifestations.³⁶

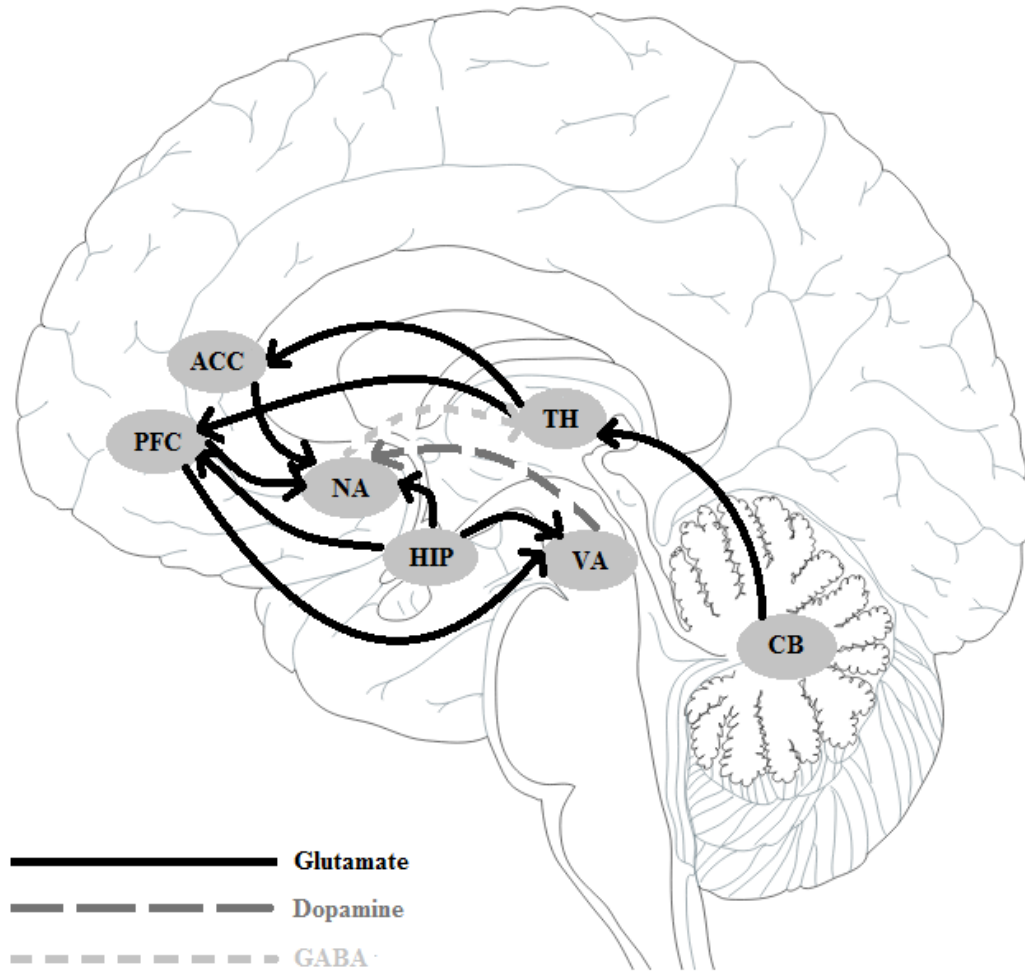


Figure 1-1. The limbic basal ganglia thalamocortical circuits. ACC, anterior cingulate cortex; CB, cerebellum; HIP, hippocampus; NA, nucleus accumbens; PFC, prefrontal cortex; TH, thalamus; VT, ventral tegmentum.

Figure 1-1 illustrates the limbic basal ganglia thalamocortical circuits as two parallel pathways that act contrastingly on the basal output nuclei. It has been suggested that positive, negative, and cognitive deficits in schizophrenia may be associated with dysfunction of the limbic basal ganglia-thalamocortical circuitry.^{31, 37} This pathway is comprised of glutamatergic projections originating in cortical regions that transmit excitatory inputs to the ventral tegmental area, which, in fact, exert an inhibitory output to the thalamus.^{37, 38} Evidence indicates that an imbalance in the glutamatergic pathway, due

to NMDA hypofunction that interacts with the cortex, limbic system and thalamus, contributes to the development of schizophrenia.³⁷ The hypo-functionality of the NMDAR system is believed to prevent the activation of the cortical GABAergic interneurons that, in turn, causes the disinhibition of the glutamatergic inputs in the pyramidal neurons.^{37, 39} The glutamate model of schizophrenia postulates that a disruption of the NMDAR function underlies the induction of the prominent symptoms of schizophrenia, especially the negative and cognitive symptoms. Numerous studies have also revealed possible glutamate-dopamine interactions by altering the activation state of the NMDARs, suggesting the modulation of dopamine release by glutamatergic neurotransmission.^{37, 41-45}

Several lines of evidence support that the hypofunction of the NMDAR is due to its dysregulation rather than a reduction in its numbers. Both clinical trials and pre-clinical investigations indicate that the administration of the agonists of the glycine modulatory site (GMS), that modulates the NMDAR, could restore the NMDAR function.⁴⁶ The activation of the NMDAR relies on the simultaneous binding of glutamate and an agonist D-serine (or glycine). The enhancement of binding to the GMS is more effective than attempts to increase glutamate binding. GMS binding increases NMDAR function effectively, and does not induce neurotoxicity.⁴⁷ Among all GMS ligands, D-serine is known to be the primary co-agonist for synaptic NMDAR.⁴⁸⁻⁵⁵ Thus, it has been proposed to test the validity of D-serine supplementation as a therapeutic agent targeting the GMS in order to augment the NMDAR function.^{56, 57} Some suggest this approach could be a crucial advance for the treatment of the most prominent symptoms of schizophrenia not well controlled by current DA-based medication, i.e. the negative and cognitive symptoms.²⁹

1.1.3 D-Serine as adjuvant to antipsychotic Treatment:

Since it has been postulated that the dysfunction of glutamate neurotransmission mediated by the NMDAR is implicated in the pathophysiology of schizophrenia, the complete and partial agonists of this receptor have been examined in a series of studies as possible modulators of glutamate neurotransmission. Modulation of the NMDAR activity can be

augmented by facilitating glutamatergic signaling via the use of compounds such as NMDA co-agonists (i.e. D-serine, glycine) and glycine transport (Gly-T) inhibitors.⁵⁸ Some promising reports have demonstrated the efficacy of high doses (approximately 60 g/day) of glycine, a direct co-agonist of NMDAR in alleviating the negative and cognitive symptoms of schizophrenia.⁵⁹⁻⁶² Despite confirmation of the efficacy of glycine provided by two meta-analyses,^{63, 64} more investigation should be performed using larger samples to confirm the effectiveness of oral glycine administration in facilitating NMDAR neurotransmission. It has also been noted that the administration of high concentrations of glycine may cause extensive excitotoxicity⁶⁴ and hyperexcitability.⁸³ In contrast, other NMDAR agonists, including D-serine and D-alanine, did not produce any neurotoxicity; previous studies revealed that this condition is a selective effect of glycine.^{82, 83} Gly-T inhibitors may also be used to enhance the glycine synaptic levels by preventing its reuptake without producing any adverse effects.⁶⁵ In preclinical studies Gly-T inhibitors have proven to enhance NMDAR function in schizophrenia,⁶⁷⁻⁷⁸ though the number of studies performed on humans is limited and poorly investigated.^{66,67,79-81}

D-serine enables the activation of the receptor, producing full agonism and induces maximum activation of the NMDAR glycine site, and thus the antagonistic effect produced by other partial agonists is avoided.^{84, 85} Not only does D-serine have a higher affinity for the GMS, it also crosses the blood brain barrier more readily compared to glycine²⁹ and L-serine;⁸⁶ it is enriched within the corticolimbic areas⁸⁷ and its regional distribution and age related changes correlate well with the NMDARs.^{88, 89} Therefore, D-serine is an attractive candidate as an adjuvant to current antipsychotic treatment. A number of clinical trials have examined the co-administration of D-serine along with standard antipsychotic medications in schizophrenia. Unfortunately, some clinical trials have found confounding results in terms of the efficacy of D-serine and glycine administrations to relieve the prominent symptoms, mainly due to their ineffective oral bioavailability.⁴⁷ The confounding results in studies that included the use of D-serine may also be due to variations in pharmacokinetic profiles⁹⁰ and the doses of D-serine being used. A clinical trial investigated the addition of D-serine to treatment of patients with chronic schizophrenia resulting in the significant improvement of positive, negative and cognitive symptoms⁹¹ and another following trial demonstrated a significant reduction in

all of the symptoms in risperidone or olanzapine-treated schizophrenia patients after the administration of D-serine.⁹² Although, a decline in symptoms was observed in previous studies, two clinical trials were performed with a larger sample of acutely ill population,⁹³ and chronic patients⁹⁴ and the results indicated no significant improvements. A double-blind investigation of D-serine at high doses (approximately 60mg/kg and 120mg/kg) verified a significant improvement in neuropsychological scores and the symptoms,⁹⁷ in spite of the concerns raised about its safety issues. More clinical trials are warranted to examine the optimum clinical dose of D-serine that provides a safe and effective therapeutic benefit.^{92, 95, 96} Clinical studies have examined the effects of D-serine addition and its dose-dependency in plasma levels, nonetheless; ideal doses of D-serine need to be determined.^{35, 97} There is currently no method to determine oral dosage of D-serine for a given individual because the amount crossing the blood brain barrier will vary significantly between patients.

Clozapine was revealed to have a greater impact for improving positive and negative symptoms in comparison to other conventional medications.⁹⁸ Unfortunately, it has not been applied as the first-line of treatment due to its serious side effects.⁹⁹ A few studies have indicated that the effectiveness of clozapine in treatment of primary negative symptoms is inadequate.¹⁰⁰ Nevertheless, clozapine is currently part of the standard of care for patients that do not respond to first-line antipsychotic medication. Previous reports have demonstrated the efficacy of the co-administration of D-serine, glycine, and D-cycloserine, a partial agonist, in conjunction to non-clozapine conventional neuroleptics for improving negative deficits in patients with schizophrenia.^{5, 91, 97, 101-105} The co-administration of D-cycloserine which caused deterioration of positive and negative symptoms,¹⁰⁶⁻¹¹⁰ glycine,¹¹¹ and D-serine did not have any potentiated effect nor did it worsen the symptoms⁸⁵ when administered with clozapine. The combination of non-clozapine antipsychotic drugs along with effective adjuvants aimed at glutamate modulation through the GMS may provide potential therapeutic effects for patients with schizophrenia.

A recent meta-analysis has revealed the inefficacy of certain glutamate positive modulators on cognitive functions in patients with schizophrenia.¹⁰³ This systematic

review mostly highlights studies that target and enhance glutamatergic neurotransmission. These reports indicate the ineffectiveness of the use of compounds that mainly act on the AMPA receptors or positively modulate the NMDARs and some few reports investigating the action of amino acids (i.e. D-serine, D-cycloserine and glycine) on the glycine site of the NMDAR. On the contrary, other studies have proven the beneficial effects of NMDA-enhancing agents via the glycine site.⁵⁷ The doses of D-serine and glycine that were administered in these studies were not monitored properly and not adjusted for body weight (an important factor when considering the administration of glycine).⁴³ Clinical trials often include a wide range of participants who may have several types of responses to the treatment. Because schizophrenia is such a heterogeneous disease, it is important to properly stratify patients for fear of obtaining inconclusive results due to inclusion of subgroups with confounding responses to the treatment. There has not been very good means or methods by which to stratify participants in clinical trials so far. Therefore, this review may indicate the poor efficacy of agents that act on the glutamate receptors directly but lacks conclusive information on the inefficacy of compounds that modulate the NMDAR at the GMS in improving cognition function in patients with schizophrenia.¹⁰³

1.1.4 Evidence of abnormal levels of D-serine in schizophrenia:

A few other post-mortem studies were conducted in order to assess abnormalities in metabolites for those diagnosed with schizophrenia. Significant irregularities of brain gross anatomy and histology have been identified in specific post-mortem brain structures of adults with schizophrenia compared to controls. A reduction of glycine was observed in the plasma of medication-naïve patients¹¹² and a lower glycine values was proportional to the severity of the negative deficits.¹¹²⁻¹¹⁴ Considerable reductions of D-serine levels were observed in the cerebral spinal fluid (CSF) content of medication-naïve subjects with schizophrenia,^{115, 116} in the serum of patients,¹¹⁷⁻¹¹⁹ and in the putamen of untreated patients.¹²⁰ Conversely, some post-mortem investigations have reported that the levels of total serine (D and L-serine) and glycine showed a higher level of these amino acids in the medial temporal lobe areas of schizophrenics when compared to controls.¹⁴⁶ No changes were observed in the amount of free D-serine in the prefrontal and parietal

cortices in patients with schizophrenia, suggesting regional dysfunction in serine hydroxymethyltransferase (SHMT), an enzyme that cleaves serine to glycine.^{121,144-147} Significant correlations were found between the levels of K_m SHMT and these amino acids in temporal but not in the frontal lobes in schizophrenic patients.¹⁴⁵ It has been suggested that the exposure to neuroleptics could induce the abnormal SHMT activity in the temporal lobes.¹⁴⁵ Other reports indicated a relatively low concentration of D-serine in the cerebellum and spinal cord, which was similar to examinations of rodents¹²¹ and the decreased serum levels of D-serine/total serine ratio in these patients,¹⁴⁸ corroborating the NMDA hypo-function hypothesis of schizophrenia. These studies supported the assumption that the distribution of D-serine and NMDA receptors are correlated in the human central nervous system (CNS), as suggested in the rodent study.^{121,144} *In vitro* studies have indicated that the reduction of D-serine impairs the NMDAR activity¹²²⁻¹²⁷ and, contrastingly, the enhancement of its levels increased the NMDAR activities¹²⁸⁻¹³⁰ and improved symptoms in patients.¹³¹ Post mortem studies have also revealed abnormalities in the expression of D-serine regulatory enzymes.⁹⁶ Consequently, D-serine and its modulatory enzymes may monitor NMDAR functioning, and any irregularities in this pathway may induce NMDAR dysfunction. These studies indicate the importance of quantifying the amino acids and neurotransmitters that interact with the NMDA glycine receptors, and also of developing a refined technique that can monitor the changes in these metabolites because they underlie the pathophysiology of schizophrenia.

1.1.5 Previous ¹H-MRS studies of serine and glycine:

Proton Magnetic Resonance Spectroscopy (¹H-MRS) studies assess and quantify several metabolites and neurotransmitters present in the human brain.¹³² A method for assessing changes in *in vivo* serine and glycine, could be critical to demonstrating abnormalities of endogenous levels in schizophrenia or to the validation of the brain dose achieved in a study using serine/glycine as an adjuvant to standard treatment. Thus far, no ¹H-MRS studies have examined the endogenous levels of serine in the psychiatric population. Conventional ¹H-MRS cannot detect serine due to its relatively low levels in the human brain, a complex spectral signature, and interference from the neighbouring metabolites.¹³³⁻¹³⁵ Previous reports have employed advanced ¹H-MRS techniques,

conducted at higher field strengths of 4.0 Tesla (T)¹³⁴ and 7.0 T¹³⁵, respectively, to measure *in vivo* endogenous serine concentrations in healthy subjects. Until now, no prior investigations have attempted to measure human brain serine on the more widely available, clinical field strength, 3.0 Tesla scanners. There has been no ¹H-MRS schizophrenia study conducted for detecting serine non-invasively. However, the advanced methods mentioned above hold the promise to be applicable to the study of schizophrenia, especially if the technique can be implemented on a 3.0 Tesla scanner.

Since both D-Serine and glycine can bind to the NMDA GMS, it may be relevant to the glutamatergic models of schizophrenia to study glycine in addition to serine.^{136, 137}

Detection of glycine has also been challenging using conventional ¹H-MRS methods at short echo times due to its low concentration and MRS signature overlap with signals from macromolecules and myo-inositol.^{138, 139} Most studies have focused on investigating the glycine levels in cancerous regions¹⁴⁰⁻¹⁴² since it has been detected as a biomarker in brain tumors.¹³⁹ One study has been able to test changes in levels of glycine after its high-dose administration as adjunctive therapy in healthy men using ¹H-MRS.¹⁴³

Until now, conventional ¹H-MRS techniques have been unable to reliably measure important neurochemicals such as serine and glycine due to their low concentrations and low sensitivity due to spectral overlaps with the signal of other metabolites. Thus, it is crucial to develop advanced ¹H-MRS methods capable of detecting these metabolites to enable their application in studies of schizophrenia and its treatment. Chapter 2 will present our implementation of such a technique.

1.1.6 The thesis outline:

This chapter covered background information, a brief history and description of the mental disorder schizophrenia, toward which the work of this thesis is aimed. This chapter also presents a literature review concentrating mainly on investigating the efficacy of the co-administration D-serine along with standard treatments of schizophrenia.

Chapter 2 is a general introduction to the fundamental principles of proton magnetic resonance spectroscopy and its application in *in vivo*. It is meant to expand on the theoretical foundation necessary to understand the material presented in Chapter 3 that would not typically be included in a peer-reviewed article format due to space limitations and less didactic nature.

Chapter 3 describes a report on test-retest reliability protocol performed on phantoms to demonstrate the within and between session variability of the data obtained with the implemented novel DANTE-PRESS ^1H -MRS sequence. The *in vitro* results were used to estimate serine concentration measurement precision and accuracy. This report also demonstrates an *in vivo* proof of concept data, which was acquired in a group of four healthy participants.

Chapter 4 presents a general concluding statement on the material described in Chapter 3 and it discusses the limitations of the presented study. This chapter also provides suggestions in managing the limitations of this study in future studies using the technique and possible future applications to measurements of other metabolites.

1.1.7 References:

1. Kraepelin E. Dementia praecox and paraphrenia (1919). Barclay RM, translator; Robertson GM, editor. Huntington, New York: Robert E Krieger; 1971.
2. American Psychiatric Association. (2013). Diagnostic and statistical manual of mental disorders (5th ed.). Washington, DC: Author.
3. Bleuler EP. Dementia Praecox or the Group of Schizophrenias (Dementia Praecoxoder Gruppe der Schizophrenien). New York: International Universities Press; 1950 (original 1911).
4. Weinberger DR. From Neuropathology to Neurodevelopment. *Lancet* 1995; 346: 552-557.
5. Saha S, Chant D, Welham J, McGrath J. A Systematic Review of the Prevalence of Schizophrenia. Hyman SE, ed. *PLoS Medicine*. 2005; 2(5):-141.

6. Robins LN, Regier DA: Psychiatric Disorders in North America. New York, Free Press, 1991.
7. Grover S, Avasthi A, Chakrabarti S, Kulhara P. Cost of illness of schizophrenia. *Journal of Pakistan Psychiatric Society*. January-June 2006, 3(1).
8. Carbon M, Correll CU. Thinking and acting beyond the positive: the role of the cognitive and negative symptoms in schizophrenia. *CNS spectrums*. 2014 Dec 1; 19(S1):35-53.
9. Harvey PD, Heaton RK, Carpenter Jr WT, Green MF, Gold JM, Schoenbaum M. Functional Impairment In People with Schizophrenia: Focus on Employability and Eligibility for Disability Compensation. *Schizophr Res*. 2012; 140(1-3); 1-8.
10. Andreasen NC. Symptoms, signs and diagnosis of schizophrenia. *Lancet* 1995; 346: 477-481.
11. Goeree R, Farahati F, Burke N, Blackhouse G, O'Reilly D, Pyne J, Tarride JE. The economic burden of schizophrenia in Canada in 2004. *Current medical research and opinion*. 2005 Dec 1; 21(12):2017-28.
12. Mednick S, Huttunen MO, Machón RA. Prenatal influenza infections and adult schizophrenia. *Schizophrenia Bulletin*. 1994 Jan 1; 20(2):263-7.
13. Owen MJ, Sawa A, Mortensen PB. "Schizophrenia." *Lancet (London, England)*. 14 January 2016.
14. Cannon M, Jones PB, Murray RM. Obstetric complications and schizophrenia: historical and meta-analytic review. *American Journal of Psychiatry*. 2002 Jul 1; 159(7):1080-92.
15. Rees E, O'Donovan MC, Owen MJ. Genetics of Schizophrenia, *Current Opinion in Behavioral Sciences*. 2015; 2 (8-14), 8.
16. Kinney DK, Holzman PS, Jacobsen B, Jansson L, Faber B, Hildebrand W, Kasell E, Zimbalist ME. Thought disorder in schizophrenic and control adoptees and their relatives. *Archives of General Psychiatry*. 1997 May 1; 54(5):475-9.
17. Cardno AG, Gottesman II. Twin studies of schizophrenia: from bow-and-arrow concordances to star wars Mx and functional genomics. *American journal of medical genetics*. 2000 Mar 1; 97(1):12-7.

18. Gottesman II: Schizophrenia Genesis: The Origins of Madness. New York: WH Freeman; 1991.
19. Plomin R, DeFries JC, Knopik VS, Neiderhiser JM. Behavioral Genetics (6th ed.). New York, NY: Worth Publishers; 2014.
20. Gu Z, Jiang Q, Fu AK, Ip NY, Yan Z. Regulation of NMDA receptors by neuregulin signaling in prefrontal cortex. *The Journal of neuroscience*. 2005 May 18; 25(20):4974-84.
21. Li B, Woo RS, Mei L, Malinow R. The neuregulin-1 receptor erbB4 controls glutamatergic synapse maturation and plasticity. *Neuron*. 2007 May 24; 54(4):583-97.
22. Hayashi-Takagi A, Takaki M, Graziane N, Seshadri S, Murdoch H, Dunlop AJ, Makino Y, Seshadri AJ, Ishizuka K, Srivastava DP, Xie Z. Disrupted-in-Schizophrenia 1 (DISC1) regulates spines of the glutamate synapse via Rac1. *Nature neuroscience*. 2010 Mar 1; 13(3):327-32.
23. Panatier A, Theodosis DT, Mothet JP, Touquet B, Pollegioni L, Poulain DA, Oliet SH. Glia-derived D-serine controls NMDA receptor activity and synaptic memory. *Cell*. 2006 May 19; 125(4):775-84.
24. Tang TT, Yang F, Chen BS, Lu Y, Ji Y, Roche KW, Lu B. Dysbindin regulates hippocampal LTP by controlling NMDA receptor surface expression. *Proceedings of the National Academy of Sciences*. 2009 Dec 15; 106(50):21395-400.
25. Seeman P. Dopamine receptors and the dopamine hypothesis of schizophrenia. *Synapse*. 1987 Jan 1; 1(2):133-52.
26. Sayed Y, Garrison JM. The dopamine hypothesis of schizophrenia and the antagonistic action of neuroleptic drugs--a review. *Psychopharmacology bulletin*. 1983; 19(2):283.
27. Knable MB, Weinberger DR. Dopamine, the prefrontal cortex and schizophrenia. *Journal of Psychopharmacology*. 1997 Mar 1; 11(2):123-31.
28. Carlsson A, Hansson LO, Waters N, Carlsson ML. A glutamatergic deficiency model of schizophrenia. *The British Journal of Psychiatry*. 1999 Feb.

29. Nunes EA, MacKenzie EM, Rossolatos D, Perez-Parada J, Baker GB, Dursun SM. D-serine and schizophrenia: an update. *Expert review of neurotherapeutics*. 2012 Jul 1; 12(7):801-12.
30. Nakazawa K, Zsiros V, Jiang Z, Nakao K, Kolata S, Zhang S, Belforte JE. GABAergic interneuron origin of schizophrenia pathophysiology. *Neuropharmacology*. 2012 Mar 31; 62(3):1574-83.
31. Williamson, P. C. *Mind, Brain, and Schizophrenia*. (Oxford University Press, 2006).
32. Lieberman JA, Sheitman BB, Kinon BJ. Neurochemical sensitization in the pathophysiology of schizophrenia: deficits and dysfunction in neuronal regulation and plasticity. *Neuropsychopharmacology*. 1997 Oct 31; 17(4):205-29.
33. Goldman-Rakic PS, Muly III EC, Williams GV. D 1 receptors in prefrontal cells and circuits. *Brain Research Reviews*. 2000 Mar 31; 31(2):295-301.
34. Javitt DC, Zukin SR. Recent advances in the phencyclidine model of schizophrenia. *Am J Psychiatry*. 1991 Oct 1; 148(10):1301-8.
35. Krystal JH, Karper LP, Seibyl JP, Freeman GK, Delaney R, Bremner JD, Heninger GR, Bowers MB, Charney DS. Subanesthetic effects of the noncompetitive NMDA antagonist, ketamine, in humans: psychotomimetic, perceptual, cognitive, and neuroendocrine responses. *Archives of general psychiatry*. 1994 Mar 1; 51(3):199-214.
36. Goff DC, Coyle JT. The emerging role of glutamate in the pathophysiology and treatment of schizophrenia. *American Journal of Psychiatry*. 2001 Sep 1.
37. Poels EM, Kegeles LS, Kantrowitz JT, Slifstein M, Javitt DC, Lieberman JA, Abi-Dargham A, Girgis RR. Imaging glutamate in schizophrenia: review of findings and implications for drug discovery. *Molecular psychiatry*. 2014 Jan 1; 19(1):20-9.
38. Alexander GE, Crutcher MD. Functional architecture of basal ganglia circuits: neural substrates of parallel processing. *Trends in neurosciences*. 1990 Jul 31; 13(7):266-71.

39. Dragunow M, Robertson GS, Faull RL, Robertson HA, Jansen K. D 2 dopamine receptor antagonists induce Fos and related proteins in rat striatal neurons. *Neuroscience*. 1990 Dec 31; 37(2):287-94.
40. Coyle JT. NMDA receptor and schizophrenia: a brief history. *Schizophrenia bulletin*. 2012 Sep 1; 38(5):920-6.
41. Carlsson M, Carlsson A. Schizophrenia: A Subcortical Neurotransmitter Imbalance Syndrome? *Schizophrenia bulletin*. 1990; 16(3):425.
42. Grace AA. Cortical regulation of subcortical dopamine systems and its possible relevance to schizophrenia. *Journal of Neural Transmission/General Section JNT*. 1993 Jun 1; 91(2-3):111-34.
43. Buchanan RW, Javitt DC, Marder SR, Schooler NR, Gold JM, McMahon RP, Uriel Heresco-Levy MD, Carpenter WT. The Cognitive and Negative Symptoms in Schizophrenia Trial (CONSIST): the efficacy of glutamatergic agents for negative symptoms and cognitive impairments. *American Journal of Psychiatry*. 2007 Oct 1.
44. Robertson GS, Vincent SR, Fibiger HC. D1 and D2 dopamine receptors differentially regulate c-fos expression in striatonigral and striatopallidal neurons. *Neuroscience*. 1992 Jul 1; 49(2):285-96.
45. Konradi C. Effects of D-cycloserine on striatal c-fos expression. submitted.
46. Field JR, Walker AG, Conn PJ. Targeting glutamate synapses in schizophrenia. *Trends in molecular medicine*. 2011 Dec 31; 17(12):689-98.
47. D'Souza DC, Radhakrishnan R, Perry E, Bhakta S, Singh NM, Yadav R, Abi-Saab D, Pittman B, Chaturvedi SK, Sharma MP, Bell M. Feasibility, safety, and efficacy of the combination of D-serine and computerized cognitive retraining in schizophrenia: an international collaborative pilot study. *Neuropsychopharmacology*. 2013 Feb 1; 38(3):492-503.
48. Mothet JP, Parent AT, Wolosker H, Brady RO, Linden DJ, Ferris CD, Rogawski MA, and Snyder SH. D-serine is an endogenous ligand for the glycine site of the N-methyl-D-aspartate receptor. *Proceedings of the National Academy of Sciences*. 2000 Apr 25; 97(9):4926-31.

49. Yang Y, Ge W, Chen Y, Zhang Z, Shen W, Wu C, Poo M, Duan S. Contribution of astrocytes to hippocampal long-term potentiation through release of D-serine. *Proceedings of the National Academy of Sciences*. 2003 Dec 9; 100(25):15194-9.
50. Gustafson EC, Stevens ER, Wolosker H, Miller RF. Endogenous d-Serine Contributes to NMDA-Receptor–Mediated Light-Evoked Responses in the Vertebrate Retina. *Journal of neurophysiology*. 2007 Jul 1; 98(1):122-30.
51. Stevens ER, Gustafson EC, Miller RF. Glycine transport accounts for the differential role of glycine vs. d-serine at NMDA receptor coagonist sites in the salamander retina. *European Journal of Neuroscience*. 2010 Mar 1; 31(5):808-16.
52. Stevens ER, Gustafson EC, Sullivan SJ, Esguerra M, Miller RF. Light-evoked NMDA receptor-mediated currents are reduced by blocking D-serine synthesis in the salamander retina. *Neuroreport*. 2010 Mar 10; 21(4):239.
53. Matsui TA, Sekiguchi M, Hashimoto A, Tomita U, Nishikawa T, Wada K. Functional comparison of D-serine and glycine in rodents: The effect on cloned NMDA receptors and the extracellular concentration. *Journal of neurochemistry*. 1995 Jul 1; 65(1):454-8.
54. Schell MJ, Molliver ME, Snyder SH. D-serine, an endogenous synaptic modulator: localization to astrocytes and glutamate-stimulated release. *Proceedings of the National Academy of Sciences*. 1995 Apr 25; 92(9):3948-52.
55. Mothet JP, Rouaud E, Sinet PM, Potier B, Jouvenceau A, Dutar P, Videau C, Epelbaum J, Billard JM. A critical role for the glial-derived neuromodulator d-serine in the age-related deficits of cellular mechanisms of learning and memory. *Aging cell*. 2006 Jun 1; 5(3):267-74.
56. Bendikov I, Nadri C, Amar S, Panizzutti R, De Miranda J, Wolosker H, Agam G. A CSF and postmortem brain study of D-serine metabolic parameters in schizophrenia. *Schizophrenia research*. 2007 Feb 28; 90(1):41-51.
57. Iwata Y, Nakajima S, Suzuki T, Keefe RS, Plitman E, Chung JK, Caravaggio F, Mimura M, Graff-Guerrero A, Uchida H. Effects of glutamate positive modulators on cognitive deficits in schizophrenia: a systematic review and meta-analysis of double-blind randomized controlled trials. *Molecular psychiatry*. 2015 Oct 1;20(10):1151-60.

58. de Bartolomeis A, Sarappa C, Magara S, Iasevoli F. Targeting glutamate system for novel antipsychotic approaches: relevance for residual psychotic symptoms and treatment resistant schizophrenia. *European journal of pharmacology*. 2012 May 5;682(1):1-1.
59. Heresco-Levy, U., Javitt, D.C., 2004. Comparative effects of glycine and D-cycloserine on persistent negative symptoms in schizophrenia: a retrospective analysis. *Schizophr. Res.* 66, 89–96.
60. Heresco-Levy, U., Javitt, D.C., Ermilov, M., Mordel, C., Horowitz, A., Kelly, D., 1996. Double-blind, placebo-controlled, crossover trial of glycine adjuvant therapy for treatment-resistant schizophrenia. *Br. J. Psychiatry* 169, 610–617.
61. Heresco-Levy, U., Javitt, D.C., Ermilov, M., Mordel, C., Silipo, G., Lichtenstein, M., 1999. Efficacy of high-dose glycine in the treatment of enduring negative symptoms of schizophrenia. *Arch. Gen. Psychiatry* 56, 29–36.
62. Javitt, D.C., Silipo, G., Cienfuegos, A., Shelley, A.M., Bark, N., Park, M., Lindenmayer, J.P., Suckow, R., Zukin, S.R., 2001. Adjunctive high-dose glycine in the treatment of schizophrenia. *Int. J. Neuropsychopharmacol.* 4, 385–391.
63. Tuominen HJ, Tiihonen J, Wahlbeck K. Glutamatergic drugs for schizophrenia: a systematic review and meta-analysis. *Schizophrenia research*. 2005 Jan 1; 72(2):225-34.
64. Tsai GE, Lin PY. Strategies to enhance N-methyl-D-aspartate receptor-mediated neurotransmission in schizophrenia, a critical review and meta-analysis. *Current pharmaceutical design*. 2010 Feb 1; 16(5):522-37.
65. Farber NB, Newcomer JW, Olney JW. Glycine agonists: what can they teach us about schizophrenia?. *Archives of general psychiatry*. 1999 Jan 1; 56(1):13-7.
66. Hashimoto K. Glycine transport inhibitors for the treatment of schizophrenia. *The open medicinal chemistry journal*. 2010 May 27; 4(1).143. Vandenberg R J, Aubrey K R. Glycine transport inhibitors as potential antipsychotic drugs. *Expert Opin. Ther. Targets*. 2001; 5:507–518.
67. Javitt DC. Glycine modulators in schizophrenia. *Current opinion in investigational drugs (London, England: 2000)*. 2002 Jul; 3(7):1067-72.

68. Millan MJ. N-methyl-D-aspartate receptor-coupled glycineB receptors in the pathogenesis and treatment of schizophrenia: a critical review. *Current Drug Targets-CNS & Neurological Disorders*. 2002 Apr 1; 1(2):191-213.
69. Sur C, Kinney GG. The therapeutic potential of glycine transporter-1 inhibitors. *Expert opinion on investigational drugs*. 2004 May 1; 13(5):515-21.
70. Kinney GG, Sur C. Glycine site modulators and glycine transporter-1 inhibitors as novel therapeutic targets for the treatment of schizophrenia. *Curr. Neuropsychopharmacol*. 2005; 3:35-43.
71. Hashimoto K. Glycine transporter inhibitors as therapeutic agents for schizophrenia. *Recent Patents on CNS Drug Discovery*. 2006 Jan 1; 1(1):43-53.
72. Lechner SM. Glutamate-based therapeutic approaches: inhibitors of glycine transport. *Current opinion in pharmacology*. 2006 Feb 28; 6(1):75-81.
73. Lindsley CW, Wolkenberg SE, Kinney GG. Progress in the preparation and testing of glycine transporter type-1 (GlyT1) inhibitors. *Current topics in medicinal chemistry*. 2006 Sep 1; 6(17):1883-96.
74. Hashimoto K. Glycine transporter-1 inhibitors as novel therapeutic drugs for schizophrenia. *Central Nervous System Agents in Medicinal Chemistry (Formerly Current Medicinal Chemistry-Central Nervous System Agents)*. 2007 Sep 1; 7(3):177-82.
75. Javitt DC. Glycine transport inhibitors and the treatment of schizophrenia. *Biological psychiatry*. 2008 Jan 1; 63(1):6-8.
76. Yang CR, Svensson KA. Allosteric modulation of NMDA receptor via elevation of brain glycine and D-serine: the therapeutic potentials for schizophrenia. *Pharmacology & therapeutics*. 2008 Dec 31; 120(3):317-32.
77. Javitt DC. Glycine transport inhibitors for the treatment of schizophrenia: symptom and disease modification. *Current opinion in drug discovery & development*. 2009 Jul; 12(4):468-78.
78. Hashimoto K. Glycine transporter inhibitors as therapeutic agents for schizophrenia. *Recent Patents on CNS Drug Discovery*. 2006 Jan 1; 1(1):43-53.

79. Lane H Y, Huang C L, Wu P L, Liu Y C, Chang Y C, Lin P Y, Chen P W, Tsai G. Glycine transporter 1 inhibitor, *N*-methylglycine (sarcosine), added to clozapine for the treatment of schizophrenia. *Biol. Psychiatry*. 2006; 60:645–649.
80. Lane HY, Chang Y C, Liu Y C, Chiu C C, Tsai G E. Sarcosine or D-serine add-on treatment for acute exacerbation of schizophrenia: a randomized, double-blind, placebo-controlled study. *Arch. Gen. Psychiatry*. 2005; 62:1196–1204.
81. Lane HY, Liu Y C, Huang C L, Chang Y C, Liao C H, Perng C H, Tsai G. Sarcosine (*N*-methylglycine) treatment for acute schizophrenia: a randomized, double-blind study. *Biol. Psychiatry*. 2008; 63:9–12.
82. Newell DW, Barth A, Ricciardi TN, Malouf AT. Glycine causes increased excitability and neurotoxicity by activation of NMDA receptors in the hippocampus. *Experimental neurology*. 1997 May 31; 145(1):235-44.
83. Barth A, Nguyen LB, Barth L, Newell DW. Glycine-induced neurotoxicity in organotypic hippocampal slice cultures. *Experimental brain research*. 2005 Mar 1; 161(3):351-7.
84. Laborit H, Huguenard P. Lhibernation artificielle par moyens pharmacodynamiques et physiques. *Presse Medicale*. 1951 Jan 1; 59(64):1329-.
85. Tsai GE, Yang P, Chung LC, Tsai IC, Tsai CW, Coyle JT. D-serine added to clozapine for the treatment of schizophrenia. *American Journal of Psychiatry*. 1999 Nov 1.
86. Bauer D, Hamacher K, Bröer S, Pauleit D, Palm C, Zilles K, Coenen HH, Langen KJ. Preferred stereoselective brain uptake of d-serine—a modulator of glutamatergic neurotransmission. *Nuclear medicine and biology*. 2005 Nov 30; 32(8):793-7.
87. Schell MJ, Molliver ME, Snyder SH. D-serine, an endogenous synaptic modulator: localization to astrocytes and glutamate-stimulated release. *Proceedings of the National Academy of Sciences*. 1995 Apr 25; 92(9):3948-52.
88. Balu DT, Coyle JT. The NMDA receptor ‘glycine modulatory site’ in schizophrenia: d-serine, glycine, and beyond. *Current opinion in pharmacology*. 2015 Feb 28; 20:109-15.

89. Hashimoto A, Nishikawa T, Oka T, Takahashi K. Endogenous D-serine in rat brain: N-methyl-D-aspartate receptor-related distribution and aging. *Journal of neurochemistry*. 1993 Feb 1; 60(2):783-6.
90. Tsai GE, Lane HY, VanDenBerg CM, Liu YC, Tsai P, Jann MW. Disposition of D-Serine in Healthy Adults. *The Journal of Clinical Pharmacology*. 2008 Apr 1; 48(4):524-7.
91. Tsai G, Yang P, Chung LC, Lange N, Coyle JT. D-serine added to antipsychotics for the treatment of schizophrenia. *Biological psychiatry*. 1998 Dec 1; 44(11):1081-9.
92. Heresco-Levy U, Javitt DC, Ebstein R, Vass A, Lichtenberg P, Bar G, Catinari S, Ermilov M. D-serine efficacy as add-on pharmacotherapy to risperidone and olanzapine for treatment-refractory schizophrenia. *Biological psychiatry*. 2005 Mar 15; 57(6):577-85.
93. Lane HY, Chang YC, Liu YC, Chiu CC, Tsai GE. Sarcosine or D-serine add-on treatment for acute exacerbation of schizophrenia: a randomized, double-blind, placebo-controlled study. *Archives of General Psychiatry*. 2005 Nov 1; 62(11):1196-204.
94. Lane HY, Lin CH, Huang YJ, Liao CH, Chang YC, Tsai GE. A randomized, double-blind, placebo-controlled comparison study of sarcosine (N-methylglycine) and D-serine add-on treatment for schizophrenia. *International Journal of Neuropsychopharmacology*. 2010 May 1; 13(4):451-60.
95. Tsai GE, Yang P, Chung LC, Tsai IC, Tsai CW, Coyle JT. D-serine added to clozapine for the treatment of schizophrenia. *American Journal of Psychiatry*. 1999 Nov 1.
96. Labrie V, Wong AH, Roder JC: Contributions of the D-serine pathway to schizophrenia. *Neuropharmacology*. 2012, 62:1484-1503
97. Kantrowitz JT, Malhotra AK, Cornblatt B, Silipo G, Balla A, Suckow RF, D'Souza C, Saksa J, Woods SW, Javitt DC. High dose D-serine in the treatment of schizophrenia. *Schizophrenia research*. 2010 Aug 31; 121(1):125-30.
98. Carpenter WT, Buchanan RW (1994): Schizophrenia. *N Engl J Med* 330:681–690.

99. Kane JM, Correll CU. The Role of Clozapine in Treatment-Resistant Schizophrenia. *JAMA Psychiatry*. 2016;73(3):187-188.
100. Arango C, Garibaldi G, Marder SR. Pharmacological approaches to treating negative symptoms: a review of clinical trials. *Schizophrenia research*. 2013 Nov 30; 150(2):346-52.
101. Heresco-Levy U, Javitt DC, Ermilov M, Mordel C, Silipo G, Lichtenstein M. Efficacy of high-dose glycine in the treatment of enduring negative symptoms of schizophrenia. *Archives of general psychiatry*. 1999 Jan 1; 56(1):29-36.
102. Singh SP, Singh V. Meta-analysis of the efficacy of adjunctive NMDA receptor modulators in chronic schizophrenia. *CNS drugs*. 2011 Oct 1; 25(10):859-85.
103. Tsai GE, Lin PY. Strategies to enhance N-methyl-D-aspartate receptor-mediated neurotransmission in schizophrenia, a critical review and meta-analysis. *Current pharmaceutical design*. 2010 Feb 1; 16(5):522-37.
104. Kantrowitz JT, Woods SW, Petkova E, Cornblatt B, Corcoran CM, Chen H, et al. D-serine for the treatment of negative symptoms in individuals at clinical high risk of schizophrenia: a pilot, double-blind, placebo-controlled, randomised parallel group mechanistic proof-of-concept trial. *Lancet Psychiatry*. 2015; 2(5):403–12.
105. Goff DC, Tsai G, Levitt J, Amico E, Manoach D, Schoenfeld DA, Hayden DL, McCarley R, Coyle JT. A placebo-controlled trial of D-cycloserine added to conventional neuroleptics in patients with schizophrenia. *Archives of general psychiatry*. 1999 Jan 1; 56(1):21-7.
106. Goff DC, Tsai G, Manoach DS, Flood J, Darby DG, Coyle JT: d-Cycloserine added to clozapine for patients with schizophrenia. *Am J Psychiatry* 1996; 153:1628–1630.
107. Potkin SG, Jin Y, Bunney BG, Costa J, Gulasekaram B: Effect of clozapine and adjunctive high-dose glycine in treatment-resistant schizophrenia. *Am J Psychiatry* 1999; 156:145–147.
108. Simeon J, Fink M, Itil TM, Ponce D. d-Cycloserine therapy of psychosis by symptom provocation. *Comprehensive psychiatry*. 1970 Jan 31; 11(1):80-8.
109. Cascella NG, Macciardi F, Cavallini C, Smeraldi E. D-cycloserine adjuvant therapy to conventional neuroleptic treatment in schizophrenia: an open-label

- study. *Journal of Neural Transmission/General Section JNT*. 1994 Jun 1; 95(2):105-11.
110. Van Berckel BN, Evenblij CN, Van Loon BJ, Maas MF, Van der Geld MA, Wynne HJ, Van Ree JM, Kahn RS. D-cycloserine increases positive symptoms in chronic schizophrenic patients when administered in addition to antipsychotics: a double-blind, parallel, placebo-controlled study. *Neuropsychopharmacology*. 1999 Aug 1; 21(2):203-10.
111. 85. Potkin SG, Jin Y, Bunney BG, Costa J, Gulasekaram B. Effect of clozapine and adjunctive high-dose glycine in treatment-resistant schizophrenia. *American Journal of Psychiatry*. 1999 Jan 1; 156(1):145-7.
112. Sumiyoshi T, Anil AE, Jin D, Jayathilake K, Lee M, Meltzer HY. Plasma glycine and serine levels in schizophrenia compared to normal controls and major depression: relation to negative symptoms. *The International Journal of Neuropsychopharmacology*. 2004 Mar 1; 7(01):1-8.
113. Neeman G, Blanaru M, Bloch B, Kremer I, Ermilov M, Javitt DC, Heresco-Levy U. Relation of plasma glycine, serine, and homocysteine levels to schizophrenia symptoms and medication type. *American Journal of Psychiatry*. 2005 Sep 1; 162(9):1738-40.
114. Hons J, Zirko R, Ulrychova M, Cermakova E, Doubek P, Libiger J. Glycine serum level in schizophrenia: relation to negative symptoms. *Psychiatry research*. 2010 Apr 30; 176(2):103-8.
115. Hashimoto K, Engberg G, Shimizu E, Nordin C, Lindström LH, Iyo M. Reduced D-serine to total serine ratio in the cerebrospinal fluid of drug naive schizophrenic patients. *Progress in Neuro-Psychopharmacology and Biological Psychiatry*. 2005 Jun 30; 29(5):767-9.
116. Bendikov I, Nadri C, Amar S, Panizzutti R, De Miranda J, Wolosker H, Agam G. A CSF and postmortem brain study of D-serine metabolic parameters in schizophrenia. *Schizophrenia research*. 2007 Feb 28; 90(1):41-51.
117. Hashimoto K, Fukushima T, Shimizu E, Komatsu N, Watanabe H, Shinoda N, Nakazato M, Kumakiri C, Okada SI, Hasegawa H, Imai K. Decreased serum levels of D-serine in patients with schizophrenia: evidence in support of the N-

- methyl-D-aspartate receptor hypofunction hypothesis of schizophrenia. *Archives of general psychiatry*. 2003 Jun 1; 60(6):572-6.
118. Yamada K, Ohnishi T, Hashimoto K, Ohba H, Iwayama-Shigeno Y, Toyoshima M, Okuno A, Takao H, Toyota T, Minabe Y, Nakamura K. Identification of multiple serine racemase (SRR) mRNA isoforms and genetic analyses of SRR and DAO in schizophrenia and D-serine levels. *Biological psychiatry*. 2005 Jun 15; 57(12):1493-503.
 119. Calcia MA, Madeira C, Alheira FV, Silva TC, Tannos FM, Vargas-Lopes C, Goldenstein N, Brasil MA, Ferreira ST, Panizzutti R. Plasma levels of D-serine in Brazilian individuals with schizophrenia. *Schizophrenia research*. 2012 Dec 31; 142(1):83-7.
 120. Kurumaji A, Watanabe A, Kumashiro S, Seminba J, Toru M. A postmortem study of glycine and its potential precursors in chronic schizophrenics. *Neurochem Int* 1996; 29: 239–245.
 121. Kumashiro S, Hashimoto A, Nishikawa T. Free D-serine in post-mortem brains and spinal cords of individuals with and without neuropsychiatric diseases. *Brain research*. 1995 May 29; 681(1):117-25.
 122. Panatier A, Theodosis DT, Mothet JP, Touquet B, Pollegioni L, Poulain DA, Oliet SH. Glia-derived D-serine controls NMDA receptor activity and synaptic memory. *Cell*. 2006 May 19; 125(4):775-84.
 123. Mothet JP, Parent AT, Wolosker H, Brady RO, Linden DJ, Ferris CD, Rogawski MA, Snyder SH. D-serine is an endogenous ligand for the glycine site of the N-methyl-D-aspartate receptor. *Proceedings of the National Academy of Sciences*. 2000 Apr 25; 97(9):4926-31.
 124. Yang Y, Ge W, Chen Y, Zhang Z, Shen W, Wu C, Poo M, Duan S. Contribution of astrocytes to hippocampal long-term potentiation through release of D-serine. *Proceedings of the National Academy of Sciences*. 2003 Dec 9; 100(25):15194-9.
 125. Gustafson EC, Stevens ER, Wolosker H, Miller RF. Endogenous d-Serine Contributes to NMDA-Receptor-Mediated Light-Evoked Responses in the Vertebrate Retina. *Journal of neurophysiology*. 2007 Jul 1; 98(1):122-30.

126. Stevens ER, Gustafson EC, Sullivan SJ, Esguerra M, Miller RF. Light-evoked NMDA receptor-mediated currents are reduced by blocking D-serine synthesis in the salamander retina. *Neuroreport*. 2010 Mar 10; 21(4):239.
127. Daniels BA, Baldrige WH. d-Serine enhancement of NMDA receptor-mediated calcium increases in rat retinal ganglion cells. *Journal of neurochemistry*. 2010 Mar 1; 112(5):1180-9.
128. Martina M, Krasteniakov NV, Bergeron R. D-Serine differently modulates NMDA receptor function in rat CA1 hippocampal pyramidal cells and interneurons. *The Journal of physiology*. 2003 Apr 1; 548(2):411-23.
129. Yang Y, Ge W, Chen Y, Zhang Z, Shen W, Wu C, Poo M, Duan S. Contribution of astrocytes to hippocampal long-term potentiation through release of D-serine. *Proceedings of the National Academy of Sciences*. 2003 Dec 9; 100(25):15194-9.
130. Chapman DE, Keefe KA, Wilcox KS. Evidence for functionally distinct synaptic NMDA receptors in ventromedial versus dorsolateral striatum. *J. Neurophysiol*. 2003; 89, 69-80.
131. Ohnuma T, Sakai Y, Maeshima H, Hatano T, Hanzawa R, Abe S, Kida S, Shibata N, Suzuki T, Arai H. Changes in plasma glycine, L-serine, and D-serine levels in patients with schizophrenia as their clinical symptoms improve: results from the Juntendo University Schizophrenia Projects (JUSP). *Progress in Neuro-Psychopharmacology and Biological Psychiatry*. 2008 Dec 12; 32(8):1905-12.
132. Gruetter R. Automatic, Localized in-vivo Adjustment of All First and Second-Order Shim Coils. *Magnetic Resonance in Medicine* 1993; 29: 804-811.
133. Javadzadeh H, Theberge J. Assessment of serine quantification reproducibility using advanced ¹H-MRS in the human brain. In: *Proceedings of the 24th Annual Meeting of ISMRM, Singapore, 2016 (Abstract 2381)*.
134. Theberge J, Renshaw PF. In vivo measurements of brain serine with ¹H-MRS. In: *Proceedings of the 15th Annual Meeting of ISMRM, Berlin, Germany, 2007 (Abstract 1373)*. 23.
135. Choi C, Dimitrov I, Douglas D, Zhao C, Hawesa H, Ghose S, Tamminga CA. In Vivo Detection of Serine in the Human Brain by Proton Magnetic Resonance

- Spectroscopy (1H-MRS) at 7 Tesla. *Magn Reson Med*. 2009 Oct; 64(4):1042-1046.
136. Eulenburg V, Armsen W, Betz H, Gomez J. Glycine transporters: essential regulators of neurotransmission. *Trends in biochemical sciences*. 2005 Jun 30; 30(6):325-33.
 137. Javitt DC. Glycine transport inhibitors and the treatment of schizophrenia. *Biological psychiatry*. 2008 Jan 1; 63(1):6-8.
 138. Govindaraju V, Young K, Maudsley AA. Proton NMR chemical shifts and coupling constants for brain metabolites. *NMR Biomed* 2000; 13: 129–153.
 139. Davies NP, Wilson M, Natarajan K, et al. Non-invasive detection of glycine as a biomarker of malignancy in childhood brain tumours using in-vivo ¹H MRS at 1.5 tesla confirmed by ex-vivo high-resolution magic-angle spinning NMR. *NMR Biomed*. 2010; 23:80–87.
 140. Lehnhardt FG, Bock C, Rohn G, Ernestus RI, Hoehn M. Metabolic differences between primary and recurrent human brain tumors: a ¹H NMR spectroscopic investigation. *NMR Biomed* 2005; 18: 371–382.
 141. Bobek-Billewicz B, Hebda A, Stasik-Pres G, Majchrzak K, Żmuda E and Trojanowska A 2010 Measurement of glycine in a brain and brain tumors by means of 1H MRS *Folia Neuropathol*. 48 190–9.
 142. Choi C, Ganji SK, DeBerardinis RJ, Dimitrov IE, Pascual JM, Bachoo R, Mickey BE, Malloy CR, Maher EA. Measurement of glycine in the human brain in vivo by 1H-MRS at 3 T: application in brain tumors. *Magnetic resonance in medicine*. 2011 Sep 1; 66(3):609-18.
 143. Kaufman MJ, Prescott AP, Ongur D, Evins AE, Barros TL, Medeiros CL, Covell J, Wang L, Fava M, Renshaw PF. Oral glycine administration increases brain glycine/creatine ratios in men: a proton magnetic resonance spectroscopy study. *Psychiatry Research: Neuroimaging*. 2009 Aug 30; 173(2):143-9.
 144. Hashimoto A, Oka T. Free D-aspartate and D-serine in the mammalian brain and periphery. *Progress in neurobiology*. 1997 Jul 31; 52(4):325-53.

145. Waziri R, Baruah S, Hegwood T S, Sherman A D. Abnormal serine hydroxymethyl transferase activity in the temporal lobes of schizophrenics. *Neurosci. Lett.* 1990; 120:237–40.
146. Waziri R, Baraiah S, Sherman A D. Abnormal serine-glycine metabolism in the brains of schizophrenics. *Schizophrenia Res.* 1992; 8:233–243.
147. Hashimoto K, Shimizu E, Iyo M. Dysfunction of glia-neuron communication in pathophysiology of schizophrenia. *Curr. Psychiatry Rev.* 2005; 1:151–163.
148. Hashimoto K, Fukushima T, Shimizu E, Komatsu N, Watanabe H, Shinoda N, Nakazato M, Kumakiri C, Okada S, Hasegawa H, Imai K, Iyo M. Decreased serum levels of D-serine in patients with schizophrenia: evidence in support of the NMDA receptor hypofunction hypothesis of schizophrenia. *Arch. Gen. Psychiatry.* 2003; 60:572–576.

Chapter 2

2 Introduction:

The discovery made by Stern and his collaborators in 1933 on the magnetic moment of protons inspired Rabi to develop a technique which more precisely detected the magnitude of the moment.^{1,2,3} In September 1937, Dr. Gorter engaged in simulating experiments that determined the nuclear moments from the changes made in the temperature of solids while located in a constant magnetic field.⁴ Later, a molecular beam apparatus was created by Rabi and his team, which was capable of investigating the magnetic resonance properties of individual elements, including Hydrogen,² Lithium,⁴ and Deuterium.^{5,6} It was not until 1946 that Purcell⁷ and Bloch⁸ independently demonstrated the nuclear magnetic resonance (NMR) properties in solids and liquids. In 1952, both scientists were awarded the Nobel Prize in Physics for their discovery of NMR.

The following paragraphs will describe the fundamental principles of nuclear magnetic resonance (NMR) physics and proton magnetic resonance spectroscopy concepts that are related to the work presented in this thesis.⁸⁻⁶⁸

2.1 Principles of magnetic resonance imaging and spectroscopy:

The three main types of magnetic fields used in MRI, i.e, the external main magnetic field (B_0), the radiofrequency (RF) field (B_1) that excites the spin, and linear gradient (G) fields that provide localization, influence the energy state of a nucleus with a nuclear magnetic moment μ . In the presence of an external magnetic field (B_0), these vectors tend to align. The applied force on the magnetic moment due to B_0 induces the magnetic moment to precess at a fixed angle. The relationship between the precession frequency that the nuclear spins exhibit and the magnetic field strength was defined first by Sir Joseph Larmor. It is proportional to the magnetic field strength and is given by the following equation $\omega_0 = \gamma B_0$. The symbol/variable γ stands for the gyromagnetic ratio, which is a property of each type of nucleus. A hydrogen proton possesses a γ value of $267.52 * 10^6$

rad/(s*T), therefore for a 3.0 Tesla (T) field the resonance frequency equals approximately 128 MHz, which is in the FM radiofrequency (RF) range.

Several nuclei (^1H , ^{13}C , ^{19}F , ^{23}Na , ^{31}P) are known to possess a spin angular momentum but among all, hydrogen (with an angular momentum of spin of $\frac{1}{2}$) is the most used atom in the MRI practice since it is the most abundant molecule in the human body. When ^1H nuclei experience an external magnetic field, a slightly greater number of protons will be in the lower energy state (longitudinal magnetization parallel to the main magnetic field) when compared to the higher energy state (anti-parallel to the main magnetic field). The parallel state possesses a lower energy and this condition causes an energy difference between the two states which corresponds to the energy of a photon at the Larmor frequency. The vector sum of all magnetic moments within a small region of space containing spins precessing at the same frequency (a.k.a isochromat) is denoted as net magnetization (M_0), as illustrated in Figure 2-1. The net magnetization acts as a vector with three components with respect to B_0 , each evolving as a function of time, known as longitudinal $M_z(t)$, and transverse planes $M_y(t)$ and $M_x(t)$.

As illustrated in the following figure, a net magnetization M_0 is produced along the parallel state aligned with B_0 .

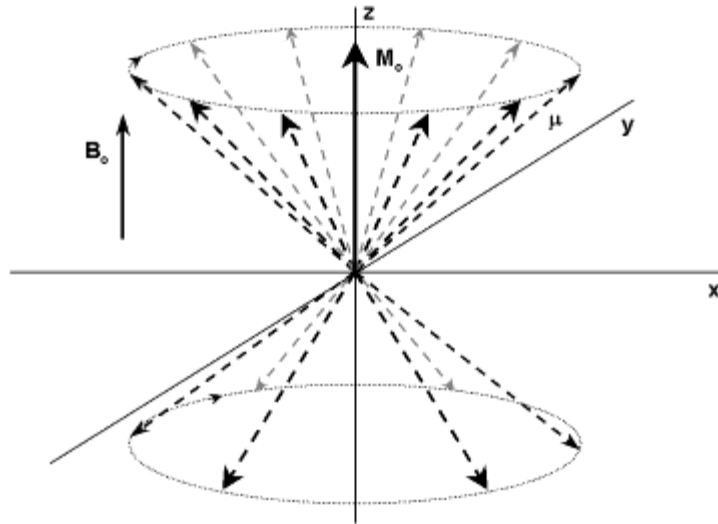


Figure 2-1. This figure represents the relative population size of the two possible energy states (Eigen states). This does not represent the state of individual spins, but any single spin is in a superposition of the two Eigen states. This illustration is adapted from Figure 1-6 in [66].

A condition known as the equilibrium state of magnetization is induced when the net magnetization vector is aligned with the static main field B_0 , where the M_0 will form along the z-direction. In order to generate an MR signal, a non-equilibrium state must be achieved by applying a rotating RF magnetic field (B_1), oscillating at the Larmor frequency in the x-y (transverse) plane. The presence of a rotating RF magnetic field, B_1 , will result in the rotation of the M_0 towards the x-y plane, and will tip it away from its initial direction (z-axis), perpendicular to the direction of the B_0 . The tip angle of the RF pulse applied is dependent on the strength of the RF magnetic field and the duration of the pulse. To achieve maximum signal, a 90° (excitation) pulse must be applied in order to tilt the M_0 completely onto the transverse plane. A 180° flip angle (a refocusing pulse) can be obtained by doubling either the duration or a voltage of an RF pulse (hard pulses). The research presented in this thesis applies a type of spin echo sequence that will be discussed and it consists of an excitation pulse followed by three 180° refocusing pulses, one of which is a frequency-selective RF pulse.

Once the excitation RF pulse is terminated, the net magnetization will continue to precess about the z-direction at the Larmor frequency and the spinning nuclei will return to the equilibrium distribution. The process by which the excited protons return to their original equilibrium orientation is known as relaxation. There are two NMR relaxation states referred to as T_1 and T_2 relaxation time constants; the terms characterize the recovery of M_z , longitudinal or ‘spin-lattice’ relaxation, and the decay of the M_x and M_y components, transverse or ‘spin-spin’ relaxation, respectively. The process of T_1 relaxation time describes an exponential regrowth of longitudinal magnetization, and is the period required for the z component of M to restore 63%, $[1-(1/e)]$, of its initial value. At thermal equilibrium, the phase between the nuclei is incoherent. A collection of spins that are “alike”, meaning they possess the same chemical environment and experience a similar applied magnetic field, are referred to as isochromats. Following an excitation pulse, the spins are tipped onto the transverse plane due to the presence of the B_1 field, and the phase coherence between isochromats is attained. The spin-spin relaxation time (T_2) characterizes the decay of transverse magnetization, and it is caused by random fluctuations of the local field produced from the movement between nearby protons that cause a loss of phase coherence (even within isochromats). Due to static field inhomogeneities (field that varies between isochromats), the transverse magnetization decays more rapidly and accelerates the dephasing of the spins. This observed decay rate of the signal is said to have a characteristic time constant denoted as T_2^* .⁹ Finally, after an excitation pulse is applied, an MR signal is characterized by a Free Induction Decay (FID), which is generated as the net transverse magnetization gradually decreases exponentially in time as the spins lose their phase coherence (FID signal is the sum of signal from a large number of isochromats located within the voxel). A receive coil (for example, a head coil) is capable of detecting the voltage varying at the resonant frequency (ω_0) which is induced in the coil by the precession of M_0 .

2.2 Signal localization:

A pulse sequence consists of the collection of radiofrequency (RF) pulses and gradient pulses with specific durations and timings, capable of generating MR images or spectra. The magnetic field gradients in MR allow for the production of a localized signal which is achieved by applying gradient pulses (known as *slice select* gradient, abbreviated as G_s or G_{ss}) that results in a linear variation of resonance frequencies along any of the three orthogonal planes (the x , y or z axes), and an RF pulse tuned to the Larmor frequency simultaneously. The thickness of the excited slice is determined by the strength of the gradient pulse and the RF pulse's bandwidth. Note that the waveform of an RF pulse (i.e. its time-dependent amplitude modulation) greatly affects the excitation profile of the magnetization. The goal is to only have the signal that is appropriately refocused at the intersection of all three excited planes to generate a signal (the region of interest). This process allows for a selective excitation of a volume at the intersection of the three slabs and generates a voxel with a specific position, size and shape. The simultaneous execution of the 90° RF pulse (the first RF pulse) along with its magnetic field gradient (i.e. along the x -axis) generates a FID which selectively selects spins from a slice. The first spin echo produced by the simultaneous execution of magnetic field gradient perpendicular to the previous gradient (i.e. along the y -axis) and the first slice-selective refocusing pulse (180° RF pulse) contains signal from a bar at the intersection of the two orthogonal slices. The second spin echo is achieved by the simultaneous application of a magnetic field gradient along the last remaining orthogonal axis (i.e. along z -axis) and the second slice-selective 180° RF pulse and will produce signal only from the intersection of the three orthogonal slices, as illustrated in Figure 2-2. Pairs of gradient crushers adjoining the two refocusing 180° RF pulses ensure the selection of the preferred signal and the elimination and the dephasing of any unwanted coherences (echo responses) generated from the outside of the voxel (which may cause artifacts) or from spins having received the wrong flip angle (i.e. at the edge of RF pulse passbands). For more information on the optimization of the gradient crushers for the proper dephasing of the unwanted coherences performed for this study visit Appendix C.

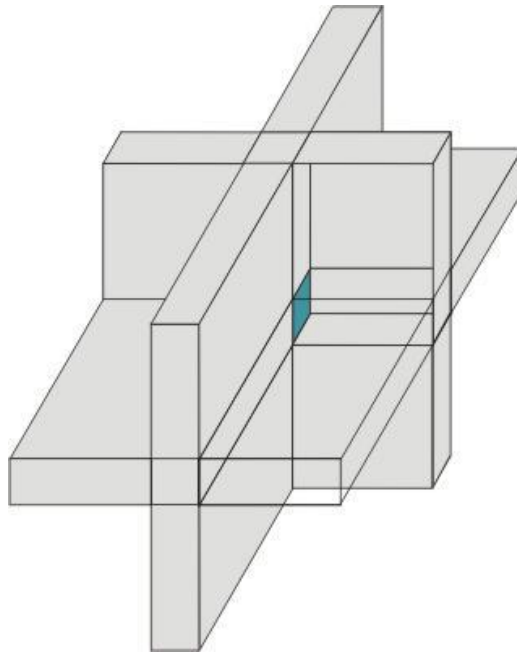


Figure 2-2. A three-dimensional single voxel localization process. The intersection of the three planes selected by the three RF pulses executed simultaneously with their respective slice-selective gradients results in the production of MR signal only from the desired VOI. Signal outside of the VOI is dephased (via the gradient crushing). This image was adapted from Figure 1.8 in [67].

2.3 Chemical shift:

Due to the applied external magnetic field, an induced magnetic field (a secondary magnetic field) is generated by the circulation of electrons surrounding a nucleus. The electrons carry a small charge and therefore exert a smaller effect on the nucleus compared to the external field, sufficient to produce a unique molecular spectrum that distinguishes them. Depending on the extent of nuclei shielding by the surrounding electron cloud, the absorption position shifts either to the right (up field) or to the left (down field) of the NMR spectrum. This phenomenon is known as chemical shift. Chemical shift is expressed as the following ¹⁶:

$$\omega = \gamma B_0 (1 - \sigma)$$

Overall, ω is the local precessional frequency of the resonance that corresponds to a certain molecular compound and σ stands for the electronic shielding constant that is dependent on the chemical environment. As the formula states, the displacement of the resonance frequency is proportional to the main magnetic field B_0 . The change in the strength of the external magnetic field is linearly proportional to the change in the magnitude of a chemical shift represented in Hertz. Therefore, the magnitude of the chemical shift for a given compound is commonly characterized in parts per million (ppm), and is independent of the strength of the external magnetic field. The value for chemical shift is determined by the differences between the absorption peak of a resonance frequency of a particular proton and the absorption peak of a reference proton. In this thesis, for measurements of the naturally occurring metabolite, serine, located at 3.83 ppm, the reference is chosen to be N-Acetylaspartic Acid (NAA), situated at 2.01 ppm. Serine resonates to the left of NAA since its nuclei are less shielded and resonate at a higher frequency. Overall, the magnitude of the chemical shift is dependent on the type of the nucleus and the varying electronic environment of the proton.

2.4 J-coupling and spin systems:

Not all protons have the same resonance frequencies according to their chemical environments and locations. Nuclei subjected to a similar chemical shift or chemical environments are known to be equivalent, while those experiencing different chemical environments are non-equivalent. A J-coupling or spin-spin coupling effect can be observed on the NMR spectrum, when non-equivalent nuclei exert an influence over the effective magnetic field of the adjacent nuclei. The number of peaks represents the number of protons present in a molecule or a compound. In most cases, the NMR spectrum displays a combination of multiple peaks rather than a single peak that has arisen from a solitary proton. Thus, the signal will be split into two or more separate peaks (doublets, triplets, multiplets etc) and the overall area under all these peaks will be the same as the total area under the corresponding singlet peak that would arise in the

absence of the J-coupling effect. The J-coupling constant represents the fixed frequency difference between the centres of the multiplet peaks and, unlike the chemical shift; its value is presented in Hertz. The two factors of J-coupling constant and the chemical shift value aid in describing the spectral signature of each compound in the sample.

This thesis mainly focuses on measuring serine, with a molecular formula of $C_3H_7NO_3$, a strongly coupled metabolite composed of a three spin system known as ABX.⁵⁴

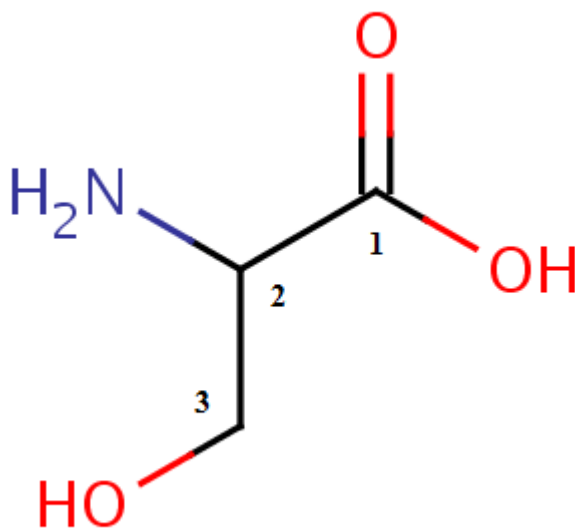


Figure 2-3. The chemical structure formula of serine is presented. This figure was adapted from [68] and was further modified to number the carbon atoms.

The splitting of A resonance occurs in the presence of the two different spins. This spin system is generated by the presence of the 2CH and 3CH_2 groups that form doublet-of-doublets and have closely located resonances of 3.83, 3.94 and 3.98 ppm, respectively.¹⁷ This causes the resonances of serine to overlap, thereby making their identification and quantification difficult. Improved detection of serine with a complex spin system can be achieved through the use of a modified proton magnetic resonance spectroscopy (1H -

MRS) technique, which will be described in more detail in Chapter 2. This method allows the selective excitation of the resonance of serine at 3.83 ppm (the X pattern) as indicated by the arrow in the figure below. This X spin resonance of serine has the least signal contamination from the neighbouring metabolites, including a large singlet methylene resonance of creatine located at 3.92 ppm,⁵⁵ thus making the detection of this spin pattern more ideal when compared to the other two resonances.

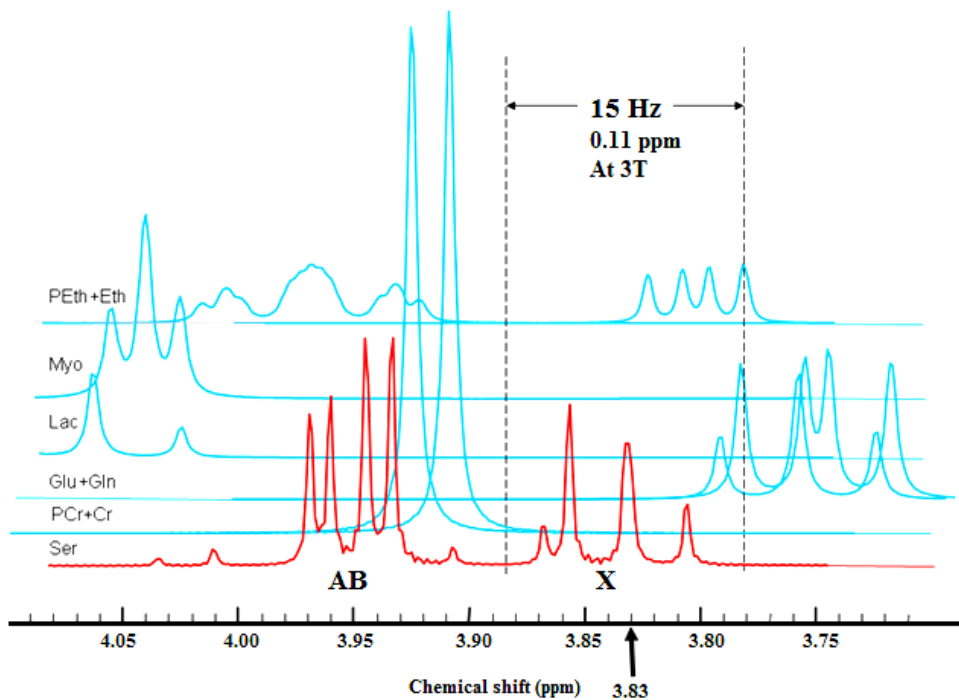


Figure 2-4. Resonances of serine and neighboring metabolites are illustrated above. The ABX pattern is recognized based on its AB and X multiplets. The AB portion consists of an unsymmetrical 8 line pattern, and the X part includes a symmetrical 4 line pattern as shown above. As shown, the X pattern has the least interference from neighboring metabolites (A simulated FID 1Hz LWs).

2.5 Proton magnetic resonance spectroscopy:

Nuclear Magnetic Resonance (NMR) Spectroscopy is a powerful MR-based modality that allows the characterization and determination of the molecular structure of certain metabolites and the examination of biochemical concentrations *in vivo*. The term “nuclear” may lead to misinterpreting its association with nuclear medicine and radiation, thus *in vivo* NMR is otherwise identified as Magnetic Spectroscopy Resonance (MRS). MRS is a valuable modality that can be applied to investigate metabolic changes in neuropsychiatric disorders and to follow the effect of treatment due to its non-invasive and repeatable nature. The investigation of neurochemicals using proton MRS could provide valuable insight into the possible mechanisms underlying neurotransmitter receptor function. Proton MRS allows the measurement of molecules with relatively low concentration levels (0.5-1.0 mM), but this typically requires the use of non-standard MRS pulse sequences. This thesis will focus on the use of an advanced single voxel spectroscopy (SVS) technique known as Delays for Alternating with Nutation for Tailored Excitation (DANTE)-PRESS⁵⁵ that uses very narrow-band RF pulses to selectively refocus the signal from metabolites of interest, thereby simplifying the resulting spectrum. This metabolite-selective DANTE-PRESS technique is of particular interest in the detection of metabolites with strongly J-coupled spin systems.

2.6 DANTE-PRESS sequence:

One of the most commonly used pulse sequences in acquiring *in vivo* single-voxel proton (MRS) data is known as point-resolved spectroscopy (PRESS).²³ Generally a PRESS sequence consists of three broadband radiofrequency pulses (typically a 90° excitation pulse followed by two refocusing 180° RF pulses) that are applied in the presence of gradients along one of three orthogonal axes in order to select a specific three-dimensional volume known as a voxel. A conventional symmetrical PRESS sequence creates a double spin echo that is generated at a time TE/4 after the second 180° refocusing pulse, where TE is the echo time of the sequence. The gradient crusher pairs placed on each side of the two refocusing pulses ensures the dephasing of signal generated outside of the voxel of interest (VOI).

In this thesis, the presented work has been obtained by using a customized, metabolite-selective ^1H -MRS sequence, DANTE-PRESS (D-PRESS),⁵⁵ which required the implementation of a frequency-selective, Gaussian modulated, single-DANTE pulse into a symmetrical PRESS sequence placed at the midpoint between the two 180° refocusing pulses (Figure 2-5).

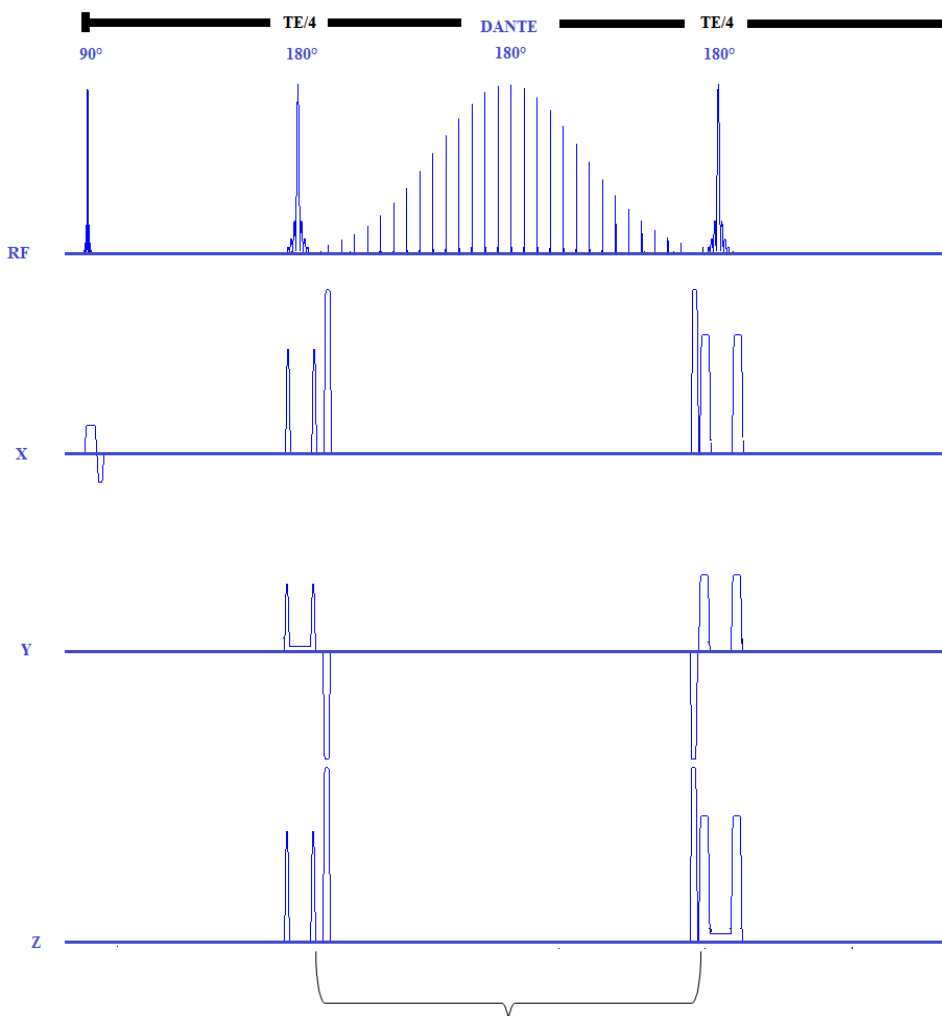


Figure 2-5. Pulse sequence timing diagram for the ^1H MRS acquisition protocol (DANTE-PRESS) employed in the experiments reported in this thesis. This schematic diagram shows the timing and the order of the RF pulses and the gradients pulses. The bracket shows the DANTE module (the DANTE RF pulse and its crusher pairs) added to a standard symmetric PRESS sequence.

The single-DANTE RF Pulse excites a repeating pattern of narrow passbands that can be centered on the 3.83 ppm resonance of serine and a reference metabolite, NAA, by producing a frequency-domain inversion profile with Gaussian passbands (Full width at half maximum, FWHM = 15 Hz) repeating every ~ 223 Hz. The frequency domain period (FDP) is an important parameter that represents the distance (frequency difference) in between two successive passbands of the DANTE pulse in the frequency domain. Depending on the FWHM (a parameter that describes the width of an RF pulse) value of the DANTE RF pulse inputted by the user, the pulse sequence dynamically generates a DANTE pulse with the requested characteristics. Figure 2-6 illustrates the DANTE RF pulse generated by the pulse sequence when the bandwidths requested by the user were 15 Hz and 100 Hz, respectively.

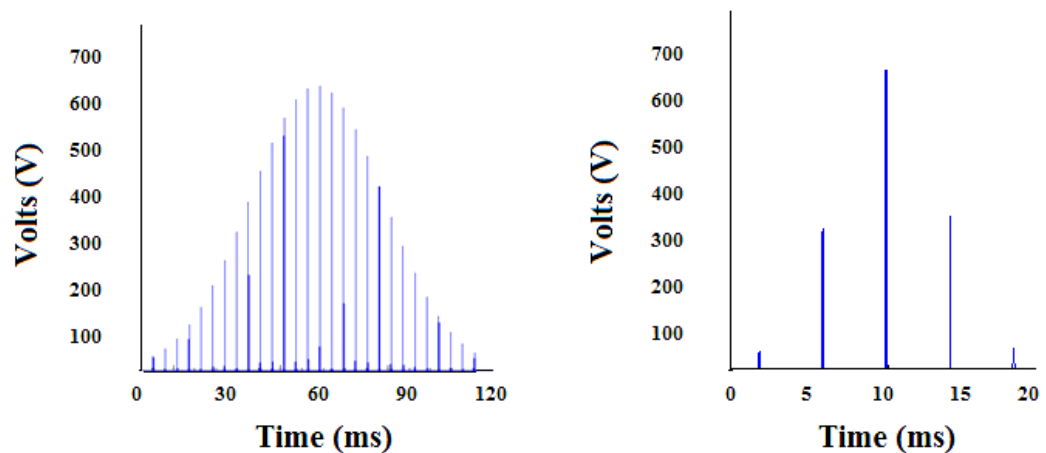


Figure 2-6. A frequency selective single-DANTE pulse, generated with bandwidth values of 15 Hz (on the left; duration of 118.54 ms, with FDP value of 223 Hz) and 100 Hz (on the right; duration of 18.35 ms, with FDP value of 223 Hz), respectively. These simulations were generated in the IDEA pulse programming environment via POET, an offline user interface mimicking the user interface of the MRI scanner (IDEA, Version VB20PSP4, Siemens, Erlangen, Germany).

A bandwidth of $15 \text{ Hz} \cong 0.11 \text{ ppm}$ is sufficient to produce a frequency range needed to excite the X pattern and isolate the resonance of serine at 3.83 ppm at a 3.0 T scanner. This frequency-selective RF pulse enables the selection of serine resonances and elimination of interfering resonances from other metabolites. The signal of unwanted metabolites is destroyed completely due to the optimized crusher gradient pairs placed directly around the DANTE RF pulse along each axis, as demonstrated in figure 2-7. Signals are only produced by the spins that were affected by all four RF pulses of the DANTE-PRESS sequence. Resonances outside the passband of the pulse are eliminated by strong gradient crushing as shown in the image below (Figure 2-7). More details on the DANTE-PRESS sequence are presented in the next chapter.

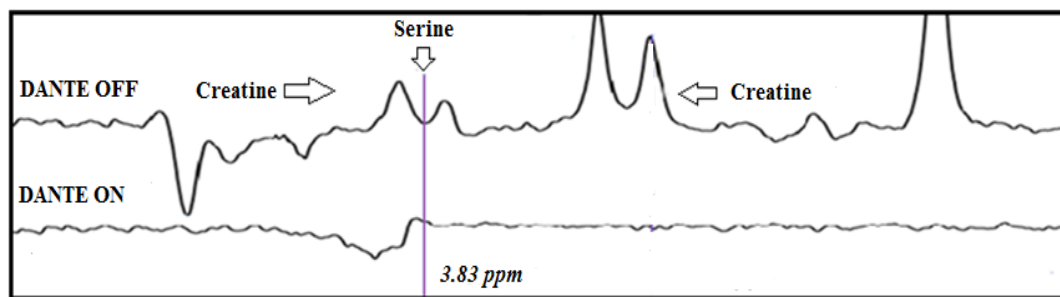


Figure 2-7. Top spectrum displays a conventional MRS *in vivo* data acquired with a symmetrical PRESS sequence (TE=286ms). Bottom spectrum displays *in vivo* data obtained with the serine metabolite-selective protocol (DANTE-PRESS, TE= 286 ms, FDP = 2000 Hz, which only refocuses the serine resonances at 3.83ppm. A slight creatine contamination can be observed).

2.7 Water suppression:

In order to reliably detect metabolites signals of interest within a selected volume of tissue, the water peak must be suppressed. The human brain contains approximately 50,000 mmol/L of water, which is approximately four orders of magnitude larger compared to the concentration of metabolites (approximately 1-10 mmol/L).²³ It is crucial

to saturate the water peak originating at approximately 4.7 ppm to avoid baseline distortions that may affect metabolites with resonances near that range, specifically serine (range of 3.93 ppm to 3.83 ppm).¹⁷ Prior to the measurement of metabolites of interest and the start of the single-voxel localization sequence, a chemical shift selective (CHESS)²⁸ technique is implemented that usually involves a series of three Gaussian shaped narrow-band, frequency-selective RF pulses, centered at the resonance of water. Each of these RF pulses is followed by a spoiler gradient, which ensures the complete dephasing of the selected water signal. These pulses have long durations, which affect signals within a narrow range of frequencies (i.e. 20 to 60 Hz) and avoid the disruption of the spins of the other metabolites. To achieve optimal water saturation, the flip angle values of the CHESS pulses must be optimized after the manual shimming of B_0 is performed. This task ensures best water suppression by iteratively minimizing its residuals via fine adjustment of the RF power of these pulses. Despite careful adjustments, the water peak is usually not eliminated completely. The remaining residuals can be removed during post-processing by using a water subtraction technique such as the Hankel-Lanczos Singular Value Decomposition (HSLVD, using JMRUI software)³⁵ prior to quantifying metabolites. A common problem associated with ^1H -MR Spectroscopy, aside from water contamination, is the presence of broad macromolecule peaks, which are abundant near the resonances of serine.^{52, 53} On a positive note, this thesis focuses on the use of a long echo time that eliminates the interference from the macromolecular signals.

2.8 MRS quantification methods, line shape corrections:

Magnetic field perturbations, eddy currents, arise from switching field gradients.³⁸ Spectral artifacts are generated under the influence of eddy currents and B_0 inhomogeneities resulting in distortions of the lineshape of each peak of the spectrum. A post-processing approach, Quality Eddy Current Correction (QUECC)^{39, 44}, is applied to correct the lineshape distortions caused by the effect of eddy currents and B_0 inhomogeneities in preparation for spectral fitting assuming specific lineshapes. The QUECC technique is a combination of two other methods, QUALITY^{36, 44} and ECC.³⁸ This lineshape correction process is achieved by using a reference peak with a representative lineshape, usually the water peak from a water-unsuppressed acquisition

obtained with the same gradient arrangements. This reference is used to correct for the time-dependent phase and/or the amplitude of the complex signal obtained from the original data. This procedure allows for the restoration of Lorentzian lineshapes that in turn enables the data to be fitted more effectively using spectral models with known lineshapes and better minimize the differences between raw data and the spectral model, known as residuals. The intensity of the water peak is larger than the metabolite of interest and any minimal errors in estimation of fitting the water signal will cause significant error in metabolite concentrations. Thus, it is important to note that both the water reference and the data must be lineshape-corrected.

2.9 Spectral fitting:

After the performance of the lineshape correction and the complete removal of the water peak, the data is ready to be quantified. Each metabolite produces a unique spectral signature and some metabolite signatures can and will overlap in an *in vivo* spectrum. The area under each metabolite signature (sum of its peaks time domain amplitudes) is proportional to the concentration of that particular metabolite. In order to isolate the contribution of the signal of interest among contaminating signals and to quantify a given metabolite's concentration level, it is crucial to develop *a priori* knowledge⁴²⁻⁴⁴ of the metabolite signatures which are specific to the selected pulse sequence and selected timing parameters (i.e. TE). There are two general approaches for generating prior knowledge: scan of metabolite solutions or simulations (density matrix or product operator formalism).^{27, 31, 42-44, 57-65}

In this thesis, we chose to acquire prior knowledge from metabolite solutions. Aqueous phantoms (pH 7.31, similar to *in vivo*) were prepared with metabolites of interest and a reference that have equal concentration levels to the ones expected in the human brain.¹⁷ A prior knowledge template for the metabolites was derived from *in vitro* experiments, obtained from the prepared brain-mimicking phantoms. The *in vivo* template included the modelling of five metabolites (serine, creatine, glutamate, glutamine and N-Acetylaspartic Acid) obtained from *in vitro* experiments. These five metabolites were

selected because they have resonances near the 3.83 ppm serine resonance used in serine-selective acquisitions.

2.10 The fitting procedure:

A locally-developed spectral fitting software (iterative fitting algorithm) called Fitman (Fitman Spectral Analysis Suite)⁴² was used to determine the amplitude of metabolite peaks (area under metabolite signature) in preparation for quantification of the metabolite concentrations. This fitting procedure uses a template created from manual modeling of the resonance pattern of each individual metabolite and incorporating them into a single model (constrained sum of individual metabolite models). These individual metabolite models included the information of all the metabolite peaks (amplitudes, line-widths, chemical shifts, and phases). The spectra were fitted based on the information provided in two separate files known as “.ges” that included the initial estimates of each peak parameter and “.cst”, which contained a set of constraints of the minimization procedure. This process uses a non-linear minimization of the residuals of a fit (i.e. the data subtracted by the fit) and determines an estimate of all of the metabolites’ concentrations.⁴² The following figure illustrates the fitting components of each metabolite, the residual fit, and the data of an *in vivo* spectrum.

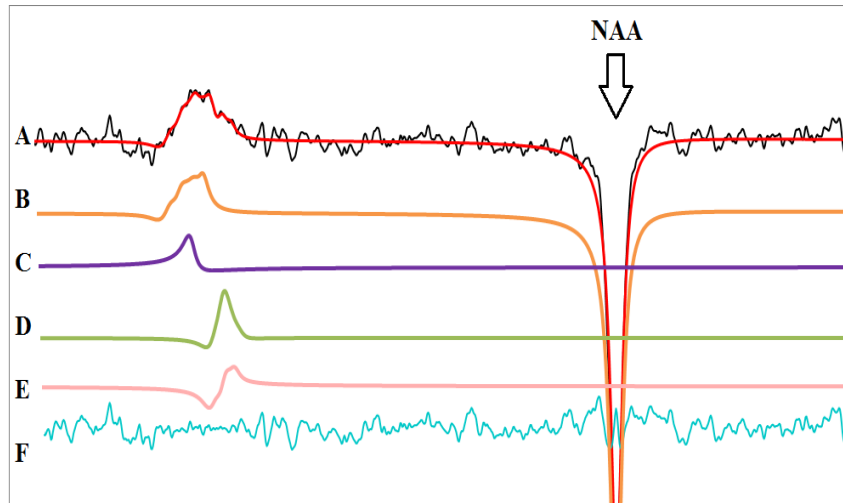


Figure 2-8. Representative *in vivo* spectrum obtained from the left anterior cingulate of a healthy participant. Line (A) represents the data in black and the fitting line in red, lines (B, C) represent the fitting components of serine and creatine in orange and purple, respectively, lines (D, E) illustrate the fitting components of glutamate and glutamine in green and pink, respectively. Line (F) represents the residuals of the fit in blue. (Line broadening factor of 2 Hz was used for display only).

2.11 Quantification of metabolites:

Quantification of magnetic resonance signal amplitude can provide an estimation of a metabolite's concentration based on the metabolite areas determined by fitting of the spectral model. In order to account for scan-to-scan variability in metabolite area estimates, it is essential to obtain an internal concentration reference signal affected by the same sources of variability. The unsuppressed water signal from a voxel is typically used as a concentration reference, which can be seen as the denominator in the following general quantification formula for metabolite concentration in mM:

$$\frac{\frac{\text{Area of Metabolite}}{10^{(\text{Mgain}[\text{dB}]/20)} * \text{Scale}_M} * 55.556 \text{ mol/L} * 1000 \text{ mmol/mol} * \text{water_percent} * \frac{\# \text{ of protons}_W}{\# \text{ of protons}_M}}{\frac{\text{Area of Water}}{10^{(\text{Wgain}[\text{dB}]/20)} * \text{Scale}_W}}$$

Equation (2-1)

Aside from the areas of metabolite(s) and water, as the formula states, the following factors are taken into consideration: **M**gain and **W**gain which represent the receiver gain for the metabolite and water spectra, respectively, Scale_M and Scale_W represent the scaling factors of the raw data and the water data, respectively (occurs during conversion of MRS data file from the manufacturer's format to the fitman ".dat" format), the number of protons of metabolite(s) and water indicated as protons_M and protons_W (i.e. 2 protons per water molecule) and water_percent represents the water content within a voxel.

$$\text{water_percent} = 0.81 \text{ fgrey} * \frac{\frac{\text{water_density}}{\text{water_MW}} * 1000 \text{ cm}^3/\text{L}}{55.5556 \text{ mol/L}}$$

Equation (2-2)

In this thesis, we assumed that the voxel was entirely made up of grey matter (81% water content) and therefore, only the fractional component of grey matter was taken into account. The water_percent formula includes the density of water at 38 Celsius (the body temperature ($0.99299\text{g}/\text{cm}^3$)) and the molecular weight of water at body temperature ($18.0152\text{g}/\text{mol}$) denoted as water_density and water_MW , respectively.

2.12 Summary:

In conclusion, this thesis introduces the implementation of an advanced proton magnetic resonance spectroscopy protocol, DANTE-PRESS, at 3.0 T that enables the detection of metabolites with complex spectral signatures. This chapter has presented a general description of this advanced MRS protocol. This technique is a novel approach that looks promising for *in vivo* applications that will be described more specifically in the following chapter. For more information see Appendices A, B and C.

2.13 References:

1. Frisch, R.; Stern, O. (1933). "Magnetic Deviation of Hydrogen Molecules and the Magnetic Moment of the Proton. I". *Z. Phys.* 85: 4–16.
2. Rabi, I.I.; Kellogg, J.M.; Zacharias, J.R. (1934). "The magnetic moment of the proton". *Physical Review*. 46: 157–163.
3. Esterman, I.; Stern, O. (1933). "Magnetic Deviation of Hydrogen Molecules and the Magnetic Moment of the Proton. I". *Z. Phys.* 85: 17–24.
4. Rabi, I.I.; Zacharias, J.R.; Millman, S. & Kusch, P. (1938). "A New Method of Measuring Nuclear Magnetic Moment". *Physical Review*. 53 (4): 318–327.
5. Esterman, I.; Stern, O. (1934). "Magnetic moment of the deuteron". *Physical Review*. 45: 761(A109).
6. Rabi, I.I.; Kellogg, J.M.; Zacharias, J.R. (1934). "The magnetic moment of the deuteron". *Physical Review*. 46: 163–165.
7. Purcell EM, Torrey HC, Pound RV. Resonance absorption by nuclear moments in a solid. *Phys Rev* 1946; 69:37-38
8. Bloch F. Nuclear Induction. *Phys Rev*. 1946;70(7-8);460–74
9. Chavhan GB, Babyn PS, Thomas B, Shroff MM, Haacke EM. Principles, techniques, and applications of T2*-based MR imaging and its special applications 1. *Radiographics*. 2009 Sep; 29(5):1433-49.

10. Harris, R. K. Nuclear Magnetic Resonance Spectroscopy. (Addison Westley Longman Limited, 1986).
11. Keeler, J. Understanding NMR Spectroscopy. (John Wiley & Sons Ltd., 2005).
12. Haacke, M. E., Brown, R. W., Thompson, Michael, R. & Venkatesan, R. Magnetic Resonance Imaging: Physical Principles and Sequence Design. (John Wiley & Sons Inc., 1999).
13. DW, Moore EA, Graves MJ and Prince MT. MRI from Picture to Proton Cambridge University Press, Feb 15, 2007.
14. Brant WE and de Lange EE. Essentials of Body MRI. Oxford University Press. 2012. Kemp W. Organic Spectroscopy (3rd ed).Palgrave July 26, 1991.
15. Silverstein RM, Webster FX, Kiemle DJ, Bryce DL. Spectrometric Identification of Organic Compounds, (8th Edition) Wiley, September 2014, 2015
16. Nishimura DG, Principles of magnetic resonance imaging. Stranford University, 1996.
17. Govindaraju V, Young K, Maudsley AA. Proton NMR chemical shifts and coupling constants for brain metabolites. NMR in Biomedicine. 2000 May 1;13(3):129-53.
18. Mountford CE, Stanwell P, Lin A, Ramadan S, Ross B. Neurospectroscopy: the past, present and future. Chemical reviews. 2010 Apr 13; 110(5):3060-86.
19. M. van der Graaf, In vivo magnetic resonance spectroscopy: basic methodology and clinical applications, European biophysics journal : EBJ 39 (4), 527-540 (2010).
20. P. Glees, The Human Brain. (Cambridge University Press, 2005).
21. Hahn EL. Spin echoes. Phys Rev 1950; 80:580-594.
22. Keevil, S. F. Spatial localization in nuclear magnetic resonance spectroscopy. Phys. Med. Biol. 51, R579–R636 (2006).
23. Bottomley PA. Spatial localization in NMR spectroscopy in vivo. Annals of the New York Academy of Sciences. 1987 Nov 1;508(1):333-48.
24. de Graaf RA. In Vivo NMR Spectroscopy: Principles and Techniques: John Wiley and Sons Ltd; 1998.

25. Ernst T, Hennig J, Ott D, Friedburg H. The importance of the voxel size in clinical ¹H spectroscopy of the human brain. *NMR in Biomedicine*. 1989 Dec 1; 2(5-6):216-24.
26. van der Graaf M. In vivo magnetic resonance spectroscopy: basic methodology and clinical applications. *European Biophysics Journal*. 2010 Mar 1; 39(4):527-40.
27. Kaiser LG, Young K, Matson GB. Numerical simulations of localized high field ¹H MR spectroscopy. *Journal of Magnetic Resonance*. 2008 Nov 30; 195(1):67-75.
28. Haase A, Frahm J, Hanicke W, Matthaei D. ¹H NMR chemical shift selective (CHESS) imaging. *Physics in medicine and biology* 1985; 30(4):341-344.
29. Frahm J, Bruhn H, Gyngell ML, Merboldt KD, Hanicke W, Sauter R. Localized high resolution proton NMR spectroscopy using stimulated echoes: initial applications to human brain in vivo. *Magn Reson Med* 1989; 9(1):79-93.
30. A. Haase, J. Frahm, W. Hanicke and D. Matthaei, ¹H-NMR chemical shift selective (CHESS) imaging, *Physics in medicine and biology* 30 (4), 341-344 (1985).
31. Smith SA, Levante TO, Meier BH, Ernst RR. Computer simulations in magnetic resonance. An object-oriented programming approach. *Journal of Magnetic Resonance, Series A*. 1994 Jan 31; 106(1):75-105.
32. Christiansen P, Toft PB, Gideon P, Danielsen ER, Ring P, Henriksen O. MR-visible water content in human brain: a proton MRS study. *Magnetic resonance imaging*. 1994 Jan 1; 12(8):1237-44.
33. Ross, B. & Bluml, S. Magnetic resonance spectroscopy of the human brain. *Anat. Rec.* 265, 54–84 (2001).
34. Drost DJ, Riddle WR, Clarke GD. Proton magnetic resonance spectroscopy in the brain: report of AAPM MR Task Group# 9. *Medical physics*. 2002 Sep 1; 29(9):2177-97.
35. Van den Boogaart A, Ala-Korpela M, Jokisaari J, Griffiths JR. Time and frequency domain analysis of NMR data compared: an application to 1D ¹H spectra of lipoproteins. *Magnetic resonance in medicine*. 1994 Apr 1; 31(4):347-58.

36. De Graaf AA, Van Dijk JE, BoéE WM. QUALITY: quantification improvement by converting lineshapes to the Lorentzian type. *Magnetic resonance in medicine*. 1990 Mar 1; 13(3):343-57.
37. Riddle WR, Gibbs SJ, Willcott MR. Removing effects of eddy currents in proton MR spectroscopy. *Medical physics*. 1992 Mar 1; 19(2):501-9.
38. Klose U. In vivo proton spectroscopy in presence of eddy currents. *Magnetic Resonance in Medicine*. 1990 Apr 1; 14(1):26-30.
39. Bartha R, Drost DJ, Menon RS, Williamson PC. Spectroscopic lineshape correction by QUECC: combined QUALITY deconvolution and eddy current correction. *Magn Reson Med* 2000; 44(4):641-645.
40. Stanley JA, Drost DJ, Williamson PC, Terry Thompson R. The use of a priori knowledge to quantify short echo in vivo ^1H MR spectra. *Magnetic Resonance in Medicine*. 1995 Jul 1; 34(1):17-24.
41. de Graaf AA, van Dijk JE, Bovee WM. QUALITY: quantification improvement by converting lineshapes to the Lorentzian type. *Magn Reson Med* 1990; 13(3):343-357.
42. Bartha R, Drost DJ, Williamson PC. Factors affecting the quantification of short echo in vivo ^1H MR spectra: prior knowledge, peak elimination, and filtering. *NMR in biomedicine* 1999; 12(4):205-216.
43. van Dijk JE, Mehlkopf AF, van Ormondt D, Bovee WM. Determination of concentrations by time domain fitting of proton NMR echo signals using prior knowledge. *Magn Reson Med* 1992;27(1):76-96.
44. de Graaf AA, Bovee WM. Improved quantification of in vivo ^1H NMR spectra by optimization of signal acquisition and processing and by incorporation of prior knowledge into the spectral fitting. *Magn Reson Med* 1990; 15(2):305-319
45. Behar KL, Rothman DL, Spencer DD, Petroff OA. Analysis of macromolecule resonances in ^1H NMR spectra of human brain. *Magn Reson Med* 1994; 32(3):294-302.
46. Kraguljac NV, Reid M, White D, Jones R, den Hollander J, Lowman D, Lahti AC. Neurometabolites in schizophrenia and bipolar disorder—a systematic review and meta-analysis. *Psychiatry Research: Neuroimaging*. 2012 Sep 30; 203(2):111-25.

47. Ernst T, Henning J. Coupling Effects in Volume Selective ^1H Spectroscopy of Major Brain Metabolites. *NMR in Biomedicine* 1998;2(6): 216-224.
48. Moonen CT, von Kienlin M, van Zijl PC, Cohen J, Gillen J, Daly P et al. Comparison of single-shot localization methods (STEAM and PRESS) for in vivo proton NMR spectroscopy. *NMR Biomed.* 1989; 2(5-6):201-8.
49. Stanley JA, Drost DJ, Williamson PC, Terry Thompson R. The use of a priori knowledge to quantify short echo in vivo ^1H MR spectra. *Magnetic Resonance in Medicine.* 1995 Jul 1; 34(1):17-24.
50. Frahm J, Bruhn H, Gyngell ML, Merboldt KD, Hanicke W, Sauter R. Localized high-resolution proton NMR spectroscopy using stimulated echoes: initial applications to human brain in vivo. *Magn Reson Med* 1989; 9(1):79-93.
51. Frahm J, Merboldt KD, Hanicke W, Haase A. Simulated Echo Imaging. *Magn Reson Med* 1985; 64:81-93.
52. Behar KL, Rothman DL, Spencer DD, Petroff OA. Analysis of macromolecule resonances in ^1H NMR spectra of human brain. *Magn Reson Med.* 1994; 32:294–302.
53. Soher BJ, Pattany PM, Matson GB, Maudsley AA. Observation of coupled ^1H metabolite resonances at long TE. *Magn Reson Med.* 2005; 53:1283–1287.
54. C, Dimitrov I, Douglas D, Zhao C, Hawesa H, Ghose S, Tamminga CA. In Vivo Detection of Serine in the Human Brain by Proton Magnetic Resonance Spectroscopy (^1H -MRS) at 7 Tesla. *Magn Reson Med.* 2009 Oct; 64(4):1042-1046.
55. Theberge J, Renshaw PF. In vivo measurements of brain serine with ^1H -MRS. In: *Proceedings of the 15th Annual Meeting of ISMRM, Berlin, Germany, 2007* (Abstract 1373).
56. Bartha R, Drost DJ, Menon RS, Williamson PC. Spectroscopic lineshape correction by QUECC: combined QUALITY deconvolution and eddy current correction. *Magn Reson Med* 2000; 44(4):641-645.
57. Vanhamme L, van den Boogaart A, Van Huffel S. Improved Method for Accurate and Efficient Quantification of MRS Data with Use of Prior Knowledge. *J. Magn. Reson.* 1997; 129: 35–43.

58. Mierisová S, van den Boogaart A, Tkáč I, Van Hecke P, Vanhamme L, Liptaj T. New approach for quantitation of short echo time in vivo ¹H MR spectra of brain using AMARES. *NMR Biomed.* 1998; 11: 32–39.
59. Pouillet JB, Sima DM, Simonetti AW, De Neuter B, Vanhamme L, Lemmerling P, Van Huffel S. An automated quantitation of short echo time MRS spectra in an open source software environment: AQSES. *NMR Biomed.* 2006; 20: 493–504.
60. Schulte R, Boesiger P. ProFit: two-dimensional prior-knowledge fitting of J-resolved spectra. *NMR Biomed.* 2006; 19: 255–263.
61. Soher BJ, Young K, Bernstein A, Aygula Z, Maudsley AA. GAVA: spectral simulation for in vivo MRS applications. *Journal of Magnetic Resonance.* 2007 Apr 30; 185(2):291-9.
62. Thompson RB, Allen PS. Sources of variability in the response of coupled spins to the PRESS sequence and their potential impact on metabolite quantification. *Magnetic resonance in medicine.* 1999 Jun 1; 41(6):1162-9.
63. Wilson M, Davies NP, Sun Y, Natarajan K, Arvanitis TN, Kauppinen RA, Peet AC. A comparison between simulated and experimental basis sets for assessing short-TE in vivo ¹H MRS data at 1.5 T. *NMR in Biomedicine.* 2010 Dec 1; 23(10):1117-26.
64. Young K, Matson GB, Govindaraju V, Maudsley AA. Spectral simulations incorporating gradient coherence selection. *Journal of Magnetic Resonance.* 1999 Sep 30; 140(1):146-52.
65. Maudsley AA, Govindaraju V, Young K, Aygula ZK, Pattany PM, Soher BJ, Matson GB. Numerical simulation of PRESS localized MR spectroscopy. *Journal of Magnetic Resonance.* 2005 Mar 31; 173(1):54-63.
66. Jensen, J.E.N. 2002, *High Field In Vivo Phosphorus Magnetic Resonance Spectroscopy: Optimization and Application to the Study of Schizophrenia.* Faculty of Graduate Studies, University of Western Ontario.
67. Théberge, J. 2004, *Short echo time proton magnetic resonance spectroscopy in the study of schizophrenia.* Faculty of Graduate Studies, University of Western Ontario.

68. Retrieved on December 22, 2016 from
http://www.bmrwisc.edu/metabolomics/mol_summary/?molName=DL_serine.

3 Reliability of *in vitro* measurements of endogenous levels of serine using DANTE-PRESS ¹H-MRS at 3.0 T.

3.1 Introduction

Over the last two decades, there has been a growing interest in investigating the *in vivo* assessment of endogenous serine (Ser) levels in the frontal region of the human brain. Researchers have explored its implications for understanding the pathophysiology of neuropsychiatric disorders, especially schizophrenia.¹⁻⁴ Ser is one of the naturally occurring amino acids present in the human brain, regulating glutamate neurotransmission at the glycine site of the N-methyl-D-aspartate (NMDA) receptor, serving as an endogenous co-agonist.⁵⁻⁸ Increasing evidence for dysfunction within the glutamatergic molecular cascade in schizophrenia implies a need for further investigation of glutamate modulatory agents via the NMDAR glycine binding site.⁹ Several lines of evidence suggest that abnormalities of the glutamate neurotransmission system in schizophrenia are possibly caused by the alteration in Ser signaling, suggesting that the administration of D-Ser may provide a new treatment strategy.¹⁰⁻¹¹ It has been suggested that some of the most debilitating features of this mental disorder, including the negative (-) and cognitive (c) symptoms (i.e. avolition (-), memory and attention deficits (c)), have been caused by abnormalities in the glutamatergic system. These symptoms may be relieved by the oral administration of D-serine supplements¹² in addition to standard antipsychotic medication (which mostly mitigate positive symptoms, i.e. auditory hallucinations).

Given that NMDA hypo-functionality has been associated with schizophrenia,⁴⁰ the use of D-Ser, and other agonists that bind to the same receptor site has been investigated as a safer alternative to the administration of glutamate, which could cause neurotoxicity.^{5,13-15} Other amino acid supplements, including glycine and D-cycloserine, enable improvements in negative and cognitive symptoms induced by glutamatergic dysfunction.^{5,16-17} When compared to these amino acids, D-Ser is known to be a full agonist and provides selective action on NMDA-glycine sites, suggesting that it is the

dominant endogenous co-agonist of NMDA receptors.¹⁸⁻²² While the academic literature investigating the role of glycine is extensive, there has been an increasing interest in investigating the contribution of D-Ser as a therapeutic agent in schizophrenia. Furthermore, it is evident that the distribution of D-Ser parallels that of the NMDA receptors more closely than glycine,²³ and it crosses the blood-brain-barrier more readily.²⁴ Taken together, these reports elucidate the important role of D-Ser and its applicability to adjuvant treatment of the negative and cognitive symptoms of schizophrenia. Ultimately, MRS measurements of Ser could provide information on the inter-individual variability of this metabolite in the living human brain and its possible abnormal levels in schizophrenia. In the longer term, detection of human brain Ser could be used as a potential diagnostic marker, as part of tools to properly stratify participants of drug trials likely to respond to glutamate-modulating therapies. This process of stratification could also be a key part of personalized dose titration for D-serine oral supplements, attempting to reach a particular brain dose in the context of a variable ability to cross the blood brain barrier.

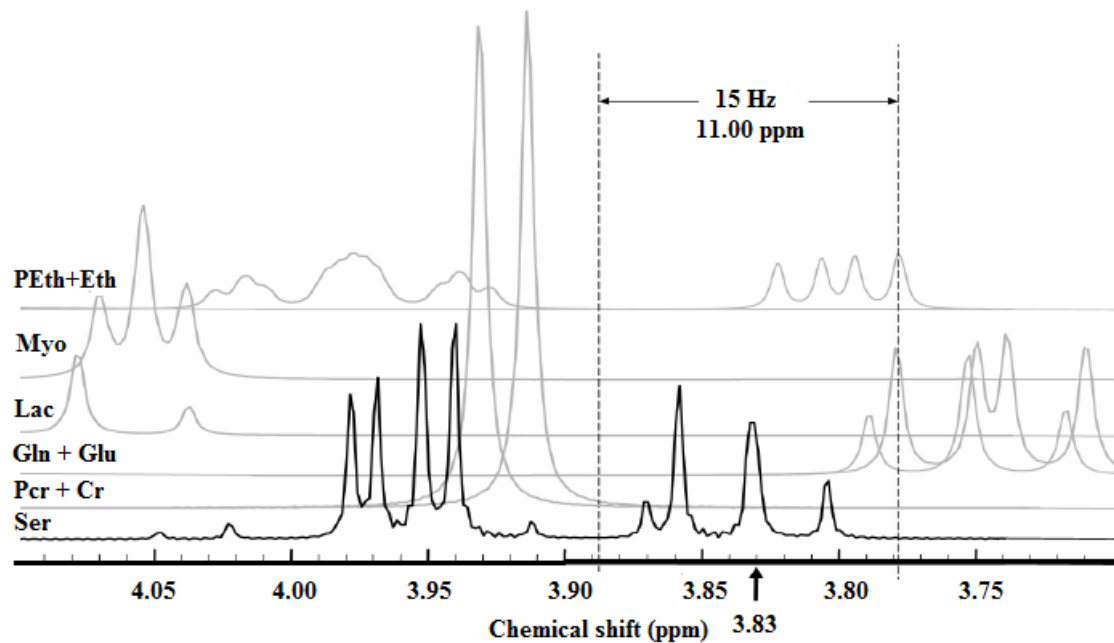


Figure 3-1. Resonances near the 15 Hz wide region selected by the frequency-selective DANTE RF pulse (simulated FID, 1Hz linewidths).

Previously, the assessment of the endogenous Ser concentration in the human brain has been impossible using conventional proton Magnetic Resonance Spectroscopy ($^1\text{H-MRS}$). This is mainly due to Ser's low endogenous concentration at approximately 0.4 -0.8 mmol/kg_{ww} (wet weight).^{25, 45-47} The Ser spectrum consists of multiplets from an ABX spin system formed by interacting protons from the ^2CH and $^3\text{CH}_2$ groups featuring resonances at 3.83, 3.94 and 3.98 ppm, respectively.²⁵ The spectral overlap with the methylene resonance of creatine (Cr) at 3.92 ppm also makes Ser a challenge to quantify in humans. Although, the Cr resonance is the most difficult source of Ser signal contamination to overcome, measurements of Ser are further hindered by overlap with the neighbouring multiplets of glutamate (Glu) (at ~3.74 ppm) and glutamine (Gln) (at ~3.75 ppm) and possibly small contributions from ethanolamine (Eth) (at ~3.82 ppm) and phosphoryl ethanolamine (PEth) (at ~3.98 ppm), as illustrated in Figure 3-1.

Recently developed techniques in metabolite-selective ^1H -MRS of the human brain have offered promising approaches to producing reliable measurements of brain metabolites important in neuropsychiatry research. Most recently, developing a method through the insertion of triple- or quadruple-DANTE frequency selective pulses to an adiabatic PRESS sequence has allowed the group of Choi et al. to measure *in vivo* data consisting of certain metabolites, including Myo-Inositol, Glu and Gln, while eliminating any spectral conflict from the neighbouring metabolites.^{26, 27} A recent study by Choi et al. has been devoted to detecting *in vivo* brain Ser levels from the frontal region of healthy subjects by utilizing an advanced proton magnetic resonance spectroscopy (^1H -MRS) method at a field strength of 7.0 T.²⁸ The Choi et al. study includes the implementation of a constant-TE, triple-refocusing, difference-editing strategy, which involves the collection of two interleaved datasets, retaining only the signals affected by the editing pulses. This technique requires the subtraction of a pair of sub spectra acquired with dissimilar sets of optimized sub echo times (i.e., TE1, TE2 and TE3) which preserves the Ser signal at the CH_2 multiplet by eliminating the interfering Cr singlet at 3.92 ppm. A limitation of this filtering strategy may include minor subtraction errors that may cause the contribution of the contaminants in interfering with Ser measurements by up to 30%²⁸. The subtraction of the two sub spectra may also produce a reduction in the SNR of the Ser measurements. Prior to that project, our research group had developed an analogous technique to that of their previous work and was able to measure low *in vivo* concentrations of Ser using a single-shot technique on a Varian Unity Inova 4.0 Tesla system.²⁹

This project proposes the first attempt to measure endogenous brain Ser levels using a 3.0 T clinical Siemens Biograph mMR scanner. To achieve very selective excitation, a non-invasive spectrally selective novel method known as DANTE-PRESS or D-PRESS^{29, 30} was developed based on similar principles used in the Choi et al studies^{26, 27} with a few key differences, such as use of single-DANTE pulses rather than triple- and quadruple-DANTE pulses, and the use of a double spin echo rather than a triple spin echo sequence. The D-PRESS technique was implemented by incorporating a very frequency-selective single-DANTE pulse to a symmetrical PRESS sequence, placed between the two slice-selective refocusing 180° RF pulses (Figure 3-2).

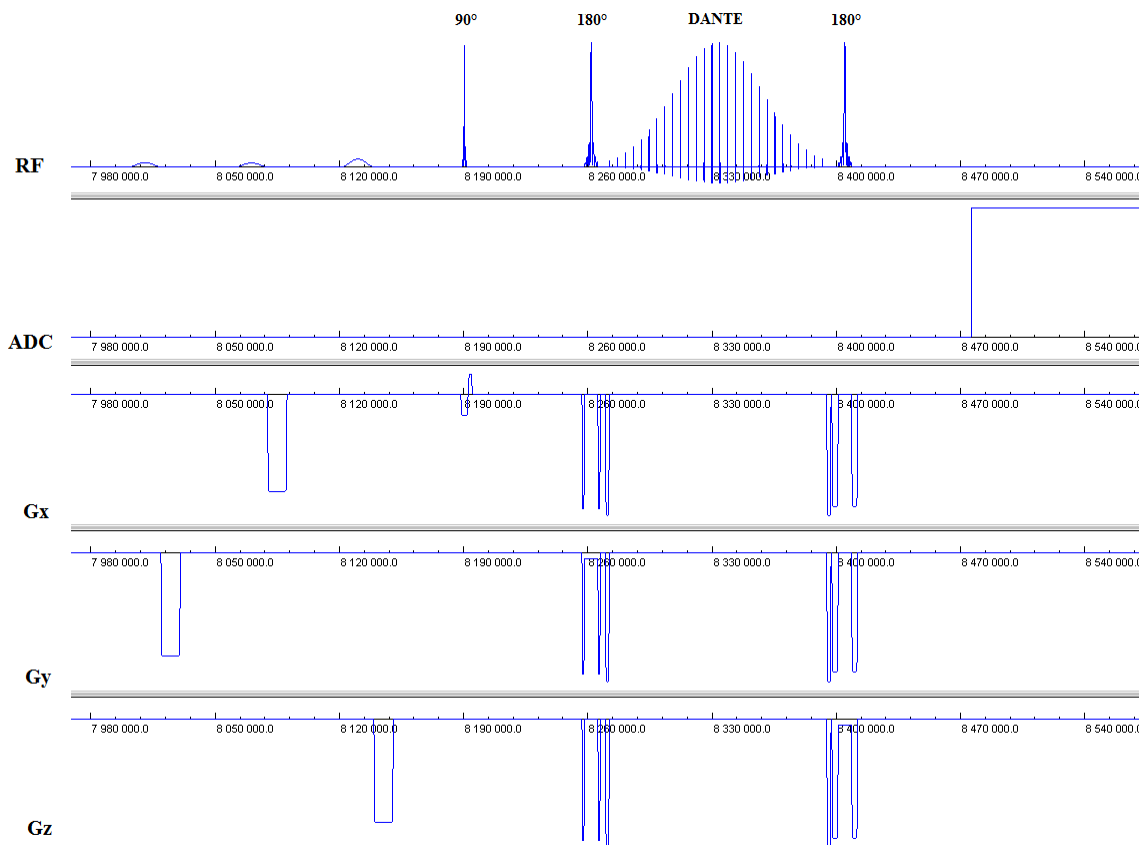


Figure 3-2. A sequence diagram of the DANTE-PRESS sequence, together with the timing and order of the slice selective gradients (G_x , G_y , G_z), the frequency selective pulses (RF) and the ADC axis.

The Ser resonance at 3.83 ppm has the least amount of contamination from other interfering metabolites, making it the ideal target for selective excitation. This manuscript aimed to determine the test-retest reliability of assessments of Ser concentration with D-PRESS in *in vitro* using a series of phantom experiments. The optimized technique was then utilized to obtain *in vivo* proof-of-concept data focusing on measurements of Ser concentration in the frontal brain (left anterior cingulate) of healthy participants, a region of relevance to future applications in psychiatric disorders.^{31, 32}

3.2 Materials and Methods:

3.2.1 Phantoms:

Brain-mimicking phantoms were constructed to examine the ability of the metabolite selective MRS technique in 1) isolating the signal of interest, 2) testing for linearity and 3) determining accuracy and precision of Ser detection. Overall, twelve phantoms were built and their information is summarized in table 3-1. The phantoms consisted of hollow polyethylene spheres (diameter (Dia.) [i.d.] ~5, ~7.5 or ~10 cm) filled with buffered saline (Milli-Q water; 10% phosphate-buffered saline (PBS); pH 7.31; 0.05% sodium azide (NaN_3), to prevent bacterial growth overtime).⁴¹ A phantom (Phantom 3) with a high concentration of Ser (30 mM; S5386-25G; Pcode: 014K06342; Sigma-Aldrich) and *in vivo* level Cr (7.5 mM; C0780-50G; Pcode: 101101933; Sigma-Aldrich) was constructed in order to investigate the J-modulation of the Ser signal acquired at various echo times and with or without the application of the metabolite-selective RF pulse. Four brain-mimicking spherical phantoms (Phantoms 4,5,6 and 7, respectively, inner diameters (Dia.) [i.d.] ~10 cm and ~5 cm) were constructed containing a high concentration of Ser (30 mM), Cr (25 mM), Glu (30mM; 49449-100G; Pcode: 101097293; Sigma-Aldrich), and Gln (30mM; 49419-25G; Pcode: 101095200; Sigma-Aldrich) with *in vivo* concentration N-Acetylaspartic acid (NAA) (8mM, EO03308AO, Sigma-Aldrich) were used in order to develop the templates for *in vivo* data quantification. These separate phantoms were built to also assess the level of contamination from these neighbouring signals and Ser signal isolation. Phantoms (Phantoms 4, 8, 9, 10, 11 and 12, respectively) including serially decreasing Ser levels (30 mM, 20 mM, 10 mM, 5 mM, 2.5 mM, and 1.25 mM) were used to calculate the calibration factor for the measured concentrations. Preliminary *in vitro* measurements were obtained in order to develop prior knowledge of the spectral signature of Ser. Two phantoms (Phantoms 1 and 2) containing *in vivo* (~0.732 mM) and double *in vivo* (~1.464 mM) Ser concentrations were used to assess the test-retest reliability of the MRS protocol in measuring Ser.

Table 3-1. A summary of all the brain-mimicking phantoms that were built for this study is presented.

Phantom No.	Chemical component	C concentrations (mM)	Sphere Dia	Product No.
1	DL-Serine (Ser)	0.732 mM	3.937"	S5386-25G
	Creatine (Cr)	7.5 mM		C0780-50G
	N-Acetyl-L-Aspartic Acid (NAA)	8 mM		44,154-6
2	DL-Serine (Ser)	1.464 mM	3.937"	S5386 -25G
	Creatine (Cr)	7.5 mM		C0780-50G
	N-Acetyl-L-Aspartic Acid (NAA)	8 mM		44,154-6
3	DL-Serine (Ser)	30 mM	3.937"	S5386-25G
	Creatine (Cr)	7.5 mM		C0780-50G
4	DL-Serine (Ser)	30 mM	3.937"	S5386-25G
	N-Acetyl-L-Aspartic Acid (NAA)	8 mM		44,154-6
	3-(Trimethylsilyl)-1-propane-sulfonic acid (TPS)	1 mM		17,883-7
5	Creatine (Cr)	25 mM	3.937"	C0780-50G
	N-Acetyl-L-Aspartic Acid (NAA)	8 mM		44,154-6
6	L-Glutamic acid (Glu)	30 mM	1.969"	49449-100G
	N-Acetyl-L-Aspartic Acid (NAA)	8 mM		44,154-6
7	L-Glutamine (Gln)	30 mM	1.969"	49419-25G
	N-Acetyl-L-Aspartic Acid (NAA)	8 mM		44,154-6
8	DL- Serine (Ser)	20 mM	2.9530"	S5386-25G
	3-(Trimethylsilyl)-1-propane-sulfonic acid, sodium salt (TPS)	1 mM		17,883-7
9	DL- Serine (Ser)	10 mM	2.9530"	S5386-25G
	3-(Trimethylsilyl)-1-propane-sulfonic acid, sodium salt (TPS)	1 mM		17,883-7
10	DL- Serine (Ser)	5 mM	2.9530"	S5386-25G
	3-(Trimethylsilyl)-1-propane-sulfonic acid, sodium salt (TPS)	1 mM		17,883-7
11	DL- Serine (Ser)	2.5 mM	2.9530"	S5386-25G
	3-(Trimethylsilyl)-1-propane-sulfonic acid , sodium salt (TPS)	1 mM		17,883-7
12	DL- Serine (Ser)	1.25 mM	2.9530"	S5386-25G
	3-(Trimethylsilyl)-1-propane-sulfonic acid, sodium salt (TPS)	1 mM		17,883-7

3.2.2 Human participants:

As part of proof-of-concept application to measurements of endogenous levels of Ser in the human brain, four healthy volunteers (3 males, aged 24, 27 and 33 years, 1 female, aged 22 years) were recruited and Ser D-PRESS measurements were obtained twice, one week apart (except for the female participant; subject 1). Typically the periods for the onset of schizophrenia begin in the early adulthood or emerge in late adolescence; therefore, the ages of the participants make them appropriate subjects to compare to individuals with schizophrenia in a future study. All subjects gave written informed consent prior to the scan. The study was approved by the Health Sciences Research Ethics Board (HSREB), HSREB file number: 6319, of the University of Western Ontario.

3.2.3 Measurements:

MR examinations were performed on a clinical 3.0 T whole-body scanner (Siemens Biograph mMR scanner, a dual-modality PET/MRI imaging system^{55,56}, St. Joseph's hospital, London, Canada) using a standard Siemens 32-channel head coil whose plug configuration was adapted to this scanner. We implemented a D-PRESS pulse sequence on the 3.0 T scanner in an similar fashion to what our group previously implemented on a 4.0 T scanner.²⁹ The PRESS sequence is composed of an excitation 90° RF pulse (hamming filtered sinc; experimentally determined time-bandwidth product (R) for excitation: 8.750, duration of 2600 μ s) and two refocusing 180° RF pulses (Mao refocusing pulses^{53,54}; experimentally determined R = 6.000, duration of 7200 μ s) supplied in an external file. The D-PRESS pulse sequence inserts a high frequency-selective single-DANTE pulse within the standard symmetrical PRESS sequence at the midpoint between the two 180° refocusing pulses of the PRESS sequence. The basic pulse sequence structure is 90-TE/4-180-TE/4-DANTE-TE/4-180-TE/4 and the full pulse sequence diagram is presented in Figure 3-2. The 180° DANTE pulse (duration of 118.54 ms) comprises a series of short square RF pulses 0.086 ms in duration separated by a fixed delay of 4.48 ms which produces a frequency profile with a predictable repeating pattern of narrow passbands. The exact shape of the DANTE pulse is generated at run-time (online) by the pulse sequence in response to the parameters entered in the scanner

user interface (center frequency, passband full-width-at-half-maximum (FWHM) of 15 Hz, repeating at every 223 Hz intervals (the Frequency Domain Period (FDP)) and is amplitude-modulated with a Gaussian envelope (truncated at 5%), frequency domain FWHM = 14000 Hz). For this work, an FDP of 233 Hz was selected to ensure that the frequency difference between repeating passbands would be equal to the frequency difference between the Ser 3.83 ppm resonance and the NAA 2.01 ppm singlet. NAA was used as a reference peak to aid in phasing of the spectrum during post-processing as well as with the constraining of the spectral quantification template. Figure 3-3 represents the DANTE pulse used as well as its corresponding frequency profile estimated by its Fourier Transform.

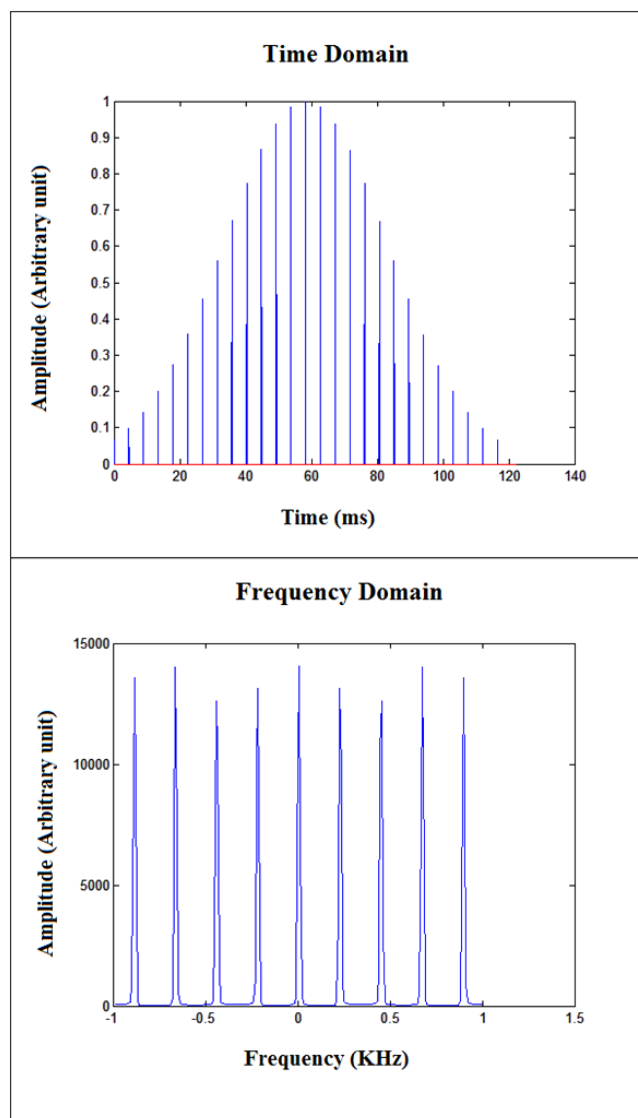


Figure 3-3. DANTE RF Pulse amplitude waveform in the time domain (top) and the corresponding frequency profile obtained by Fourier Transformation (bottom). DANTE pulse parameters were: passband width = 15 Hz; FDP = 223 Hz; number of points = 2560; Frequency Domain FWHM = 14000 Hz; amplitude modulation = Gaussian; amplitude modulation cut-off threshold = 5%.

A long echo time (286 ms) was used in these experiments since the DANTE-RF pulse's bandwidth of 15 Hz (duration of 118.54 ms), which was approximately equivalent to 0.11 ppm, was sufficient to isolate the resonance of serine at 3.83 ppm at 3.0 T. A clinically acceptable timeframe of approximately eight minutes was used to achieve a reasonable SNR due to the implementation of a long DANTE-RF pulse. Since the Ser signal intensity was susceptible to field drifts under the narrow band highly frequency-selective RF pulse during data acquisition, mainly produced by hardware imperfections, an assessment of scanner drift effects was performed for a scanning period of ~20 min. In order to minimize this effect, a parameter was implemented that compensates for frequency-drifts by enabling the movement of the passband of the DANTE RF pulse in the direction of the drift depending on its rate of movement during each experiment. The center frequency of the DANTE pulse was determined at run-time as 1.81 ppm downfield from the frequency measured for the NAA CH₃ peak in a spectrum acquired with a traditional PRESS acquisition (D-PRESS with the DANTE pulse OFF, TR = 2.0 s, TE = 286 ms, NA = 64). Spoiling gradient pairs along each of the three axes were applied immediately before and after the DANTE RF pulse to ensure the elimination of any unwanted signals outside the DANTE passbands. Water suppression was achieved through a WET water saturation module consisting of three variable flip angle RF pulses with 17.9 ms duration and Gaussian shape flanked by spoiler gradients.³⁷ An effective water suppression can be achieved with the DANTE-ON application since it eliminates any remaining water residuals and only refocuses signals that are affected by all of the RF pulses. The gradient scheme (including water suppression gradients) was kept constant in all acquisitions to maintain comparable lineshapes between acquisitions. Prior to acquiring data, the gradient crushers of this sequence were optimized in order to eliminate any unwanted coherences (see Appendix C). The main Ser data was acquired with the DANTE pulse ON (TR/TE = 2.000/286 ms; NA = 256; FDFWHM = 14000 Hz, 4 dummy scans; sampling points = 2048; phase cycling = 8-step). In order to provide a concentration reference (other than internal NAA), two separate water-unsuppressed acquisitions were obtained with the same echo and repetition time as the DANTE ON acquisition (TR/TE = 2000/286 ms), with (the DANTE frequency centered on water; FWHM = 15 Hz; NA = 8) and without the DANTE pulse application (NA = 8).

The separate DANTE-ON water-unsuppressed spectrum was obtained by setting the DANTE-RF pulse frequency centered on water and used for the correction of eddy currents in phantom experiments. A Lorentzian eddy current correction technique was used to eliminate lineshape distortions. Spectra and metabolite concentrations were quantified using Fitman (locally developed spectral fitting software)³³, a time-domain fitting algorithm. In order to evaluate reproducibility for the *in vitro* measurements, coefficients of variation (CV) were computed and the results were also analyzed statistically using one-way ANOVA using SPSS v.24 (IBM Corp, Armonk, New York, USA), respectively.

3.2.4 Experimental:

Phantom experiments:

In order to develop prior knowledge of the spectral signature of Ser, preliminary *in vitro* measurements were obtained. *In vitro* data was obtained from phantom 3 (buffered saline, inner diameter [i.d.] ~10 cm, pH 7.31) including a “high” concentration of Ser (30 mM) and Cr (7.5 mM). The data also demonstrates the ability to separate the Ser signal from the Cr singlet at 3.92 ppm. Considering that Ser consists of an ABX spin system and the DANTE pulse that was applied only to the X spins (compare Figure 3-4’s top and bottom traces).

In order to determine the linearity of Ser measurements with DANTE-PRESS, spectra were obtained from a series of Ser-only phantoms (Phantoms 4, 8, 9, 10, 11 and 12, respectively) with the following concentrations: 30 mM, 20 mM, 10 mM, 5 mM, 2.5 mM, and 1.25 mM. This data was also used to determine the effective number of protons participating to the DANTE-PRESS Ser signal. With a standard PRESS spectrum, one would assume the total Ser signal to originate from three protons, but the Gaussian passband over the 3.83 ppm Ser resonance, although consistent, does not provide a flat inversion profile over the range of resonances associated with the X spin of Ser. The effective number of protons must therefore be determined empirically from the slope of the linearity curve linking measured and known concentrations (Figure 3-5).

In order to determine the accuracy and precision of Ser measurements in phantoms, ten consecutive DANTE-PRESS spectra were obtained from within-session at baseline (no phantom repositioning, with different scanning adjustments) and between-session from the same phantom scanned a week later. For accurate adjustments of measurement parameters, additional tuning and manual adjustments of frequency, first- and second-order shim coils and water suppression were performed prior to each *in vitro* spectroscopy measurement. Two phantoms (Phantoms 1 and 2) containing either “*in vivo*” [~ 0.732 mM] or “double *in vivo*” [~ 1.464 mM] Ser concentrations were scanned during each session. Each phantom contained *in vivo* level Cr [~ 7.5 mM]. The results were interpreted and reported using descriptive statistics (means, standard deviations (SDs), and CVs) and any difference in the means of the unpaired measurements were assessed using a classical statistical method, one-way analysis of variance (ANOVA).

Prior knowledge of metabolite spectral signatures for Ser (30 mM), Cr (25 mM), Glu (30 mM), Gln (30 mM) and NAA (8 mM) were obtained from aqueous phantoms (Phantoms 4, 5, 6 and 7, respectively) prepared as above. NAA's CH_3 singlet was used as a chemical shift reference for all phantoms. Spectral quantification templates for *in vivo* data were formed from the combination of spectral signatures for the five metabolites (Ser, Cr, Glu, Gln, and Naa). The resulting spectra were used to construct a Ser quantification template consisting of 32 resonances and 5 metabolites constrained according to chemical shift, linewidth and phase (0^{th} and 1^{st} order). Each metabolite had a single amplitude parameter associated with its spectral signature.

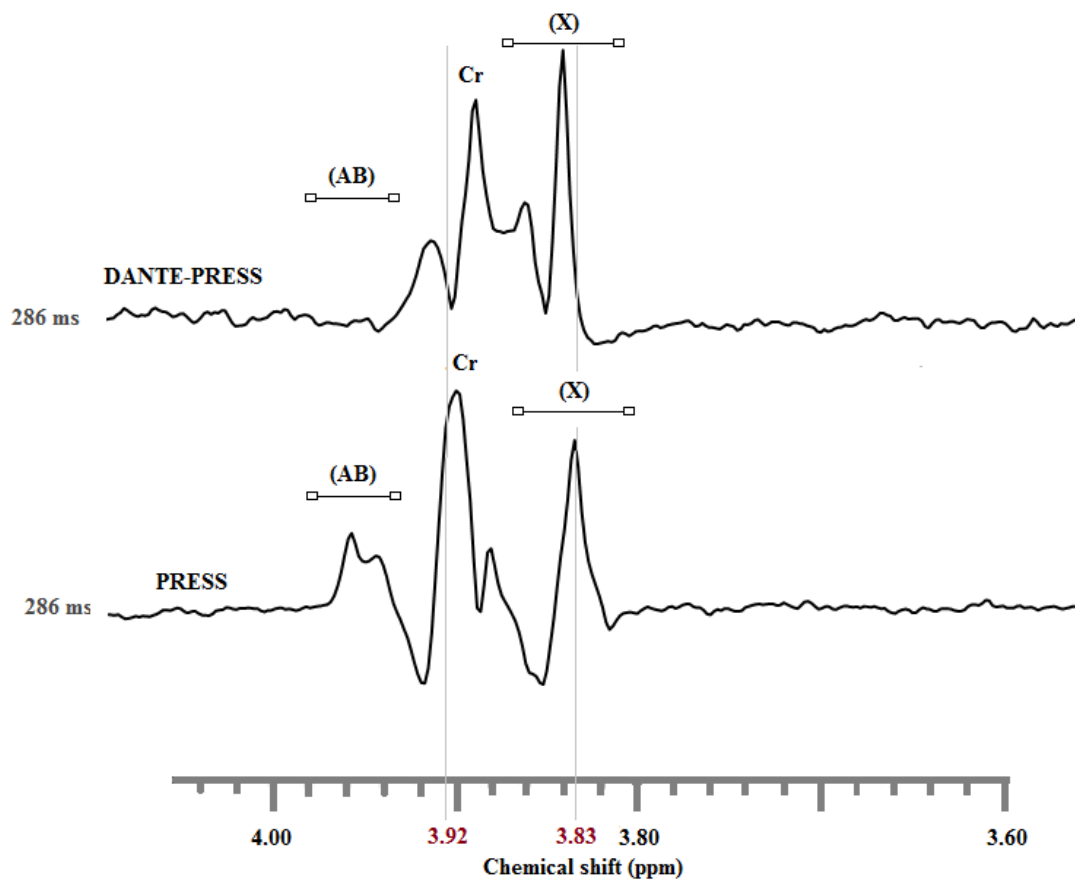


Figure 3-4. Spectra obtained from a phantom containing 30 mM of Ser and 7.5 mM of Cr, using an echo time of 286 ms with D-PRESS (top) and symmetrical PRESS with an echo time of 286 ms (bottom).

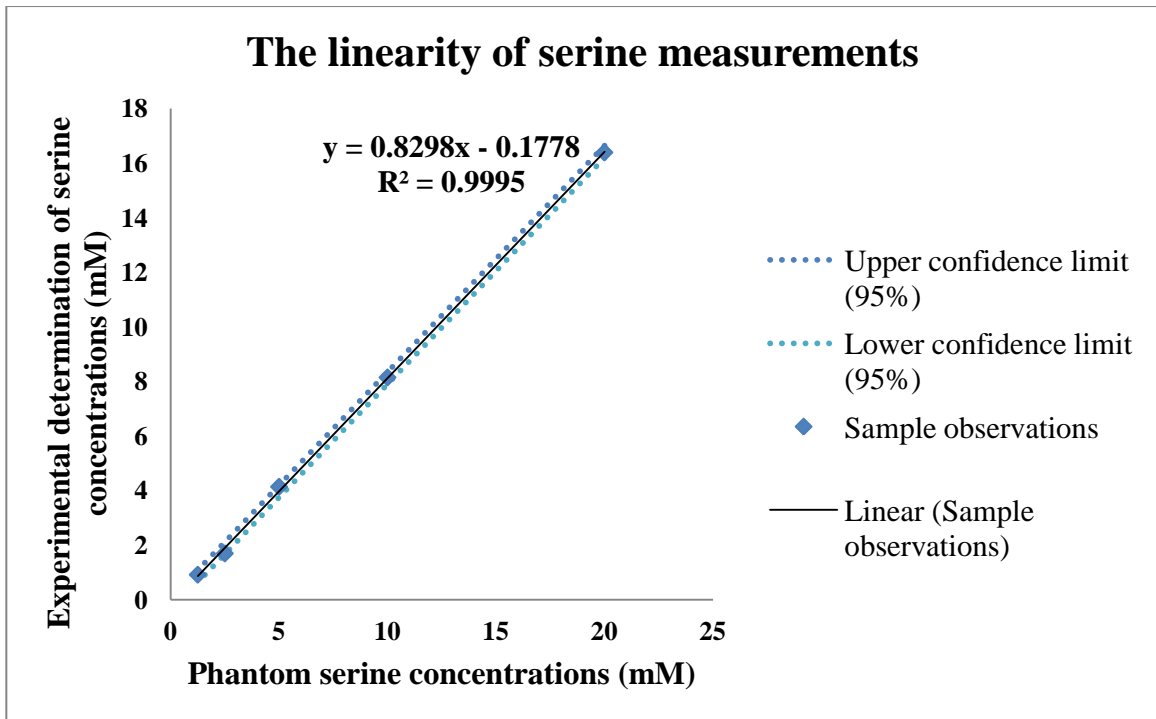


Figure 3-5. A series of phantoms with the following concentrations of serine were scanned: 20 mM, 10 mM, 5 mM, 2.5 mM, and 1.25 mM. A linear relationship between measured and known concentrations was confirmed ($r^2 = 0.9995$, (p-value < 0.001))

In vivo experiments:

To demonstrate the applicability of the D-PRESS technique for *in vivo* Ser measurements in the healthy human brain, measurements were obtained from a single voxel ($20 \times 20 \times 20 \text{ mm}^3$) (Figure 3-6) positioned in the left anterior cingulate's most rostral portion using 1 mm isotropic 3D MP-RAGE images for guidance (TR/TE/TI = 2000/2.98/900 ms; flip angle = 9° ; field of view = $256 \times 256 \times 176 \text{ mm}^3$; 176 slices; slice thickness = 1.00 mm).

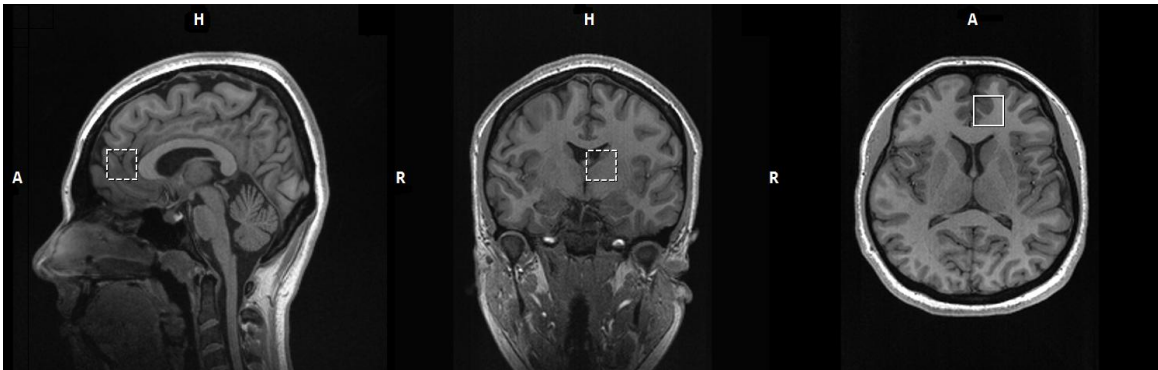


Figure 3-6. This figure illustrates the voxel ($20 \times 20 \times 20 \text{ mm}^3$) positioning in the left anterior cingulate in a healthy participant.

It was essential to use a careful voxel localization on repeat scans to reduce the amount of variability in concentration measurements. Accurate voxel re-localization was achieved by identifying local anatomical landmarks^{43,44} and using high resolution images⁴² to ensure reproducible voxel positioning between sessions. Voxel localization was achieved by mainly using the midsagittal image and by placing the voxel in the pregenual anterior cingulate cortex (anterior to the genu of the corpus callosum)⁵¹ with its inferior border located along the plane of the anterior-posterior commissure line.⁵² The voxel of interest was placed on the brain region which was dominated by gray matter (GM). Therefore, the tissue compositions of GM, white matter (WM), and cerebrospinal fluids (CSF) often used for correcting the water signal for tissue water content were not taken into consideration during metabolite quantification. Nevertheless, a tissue water content of 81% was assumed for all *in vivo* scans (i.e. 100% grey matter content was assumed).

The D-PRESS pulse sequence used the same parameters as those used in phantom experiments (DANTE passbands = 15 Hz (0.11ppm), amplitude modulation = Gaussian, FDP = 223 Hz, FDFWHM = 14000 Hz, TR/TE = 2000/286 ms; 4 dummy scans; sampling points = 2048; NA = 256; phase cycling = 8-step). These participants underwent two examinations seven days apart and two consecutive spectra were obtained at each session (within-session), except for the one female participant (subject 1). The First- and second-order shims were adjusted manually. The final *in vivo* template included the individual resonances of a total number of five metabolites (Ser, Cr, Glu, Gln and NAA), which were modeled and constrained. The time-domain iterative fitting algorithm used a tolerance value of 0.0001 that specified the percentage change in chi squared value which must have been achieved before the fit was considered completed. The minimum and maximum numbers of iterations were set to 50 and 5000 for both *in vitro* and *in vivo* templates respectively, the convergence criteria were usually met by the time 500 iterations were completed. The iterative fitting procedure was seeded with initial conditions and constraints to guide its convergence until the residuals of fit were minimized. The model contained peak parameters amplitude for each metabolite, with one parameter for chemical shift, Lorentzian width, zero-order phase, and delay time part of the quantification template.³³ There were a total number of five metabolite spectral signatures included in the template and the peaks from each spectral signature would change in amplitude together (grouped by amplitude constraints), but separate from the amplitude of other metabolites. Thus, a total number of nine fit parameters were implemented in the constraint file that were interpreted by the fitman fitting routine.

3.3 Results:

In a phantom solution (Phantom 3) containing a high level of Ser (30 mM) and *in vivo* concentration of Cr (7.5 mM), we demonstrated that the AB spin resonances of Ser displayed a J-coupling pattern acquired with D-PRESS (DANTE pulse ON) resonances were similar to those resonances acquired with a symmetrical PRESS sequence (DANTE pulse OFF) at the same echo time of 286 ms (see Figure 3-4). It can be gleaned from Figure 3-4 that Ser MRS spectra can be obtained without significant interference from the 3.92 ppm Cr resonances, which can be successfully suppressed.

Representative *in vitro* test-retest spectra are displayed in Figure 3-7. The *in vitro* spectra of Ser presents two vertical solid lines (A, B) that indicate the range of Ser resonances that were quantified and a single vertical dashed line (C) specifying the small residual signal produced from the Cr peak located at 3.92 ppm. In the *in vitro* experiments, this narrow-band frequency-selective technique enabled the suppression of the main confounding peak arising from a Cr singlet at 3.92 ppm (suppression factor ranging between 97% to 99% for the “*in vivo*” phantom and 99% on average for the “double *in vivo*” range experiments). As illustrated in Figure 3-7, there is an apparent systematic effect for these ten repeated acquisitions: the residuals of Cr signal increases as the scan number increases and this may be caused by the scanner drifts. The amount of drift was below detectable, so the acquisitions were used without correction. Some residual drift is nevertheless observable in the final spectra. Figure 3-8 indicates *in vitro* demonstration of ten repeated measurements that were obtained from “*in vivo*” (~0.732 mM) concentration phantom and from the “double *in vivo*” (~1.464 mM) concentration in two scanning sessions occurring one week apart. One-week repeat average concentration of the phantoms containing “*in vivo*” and “double *in vivo*” Ser concentrations at baseline were 1.13 ± 0.09 and 2.18 ± 0.13 , and one-week apart were 1.06 ± 0.10 and 2.23 ± 0.14 , respectively. The differences of the mean values were compared between sessions by conducting one-way ANOVA analysis and no statistically significant differences in the values were found for the *in vivo* ($F = 2.790$, $df = 18$, $p = 0.112$) and double *in vivo* ($F = 0.595$, $df = 18$, $p = 0.452$) measurements. The resulting coefficients of variation were low for both the *in vivo* (CV in the range of ~8-9%) and double *in vivo* (CV in the range of ~5-6%) measurements, demonstrating sufficient repeatability to warrant *in vitro* MRS measurements.

To assess whether field drifts can degrade the frequency calibrations, as confirmed by the measurements obtained from the water resonance with the DANTE application from phantom experiments, scanner drifts were monitored for a scanning period of ~20 min. The results indicated that, for that timeframe, the signal loss of the water peak is negligible due to this hardware imperfection (Signal loss < 1%, as verified in phantom experiments).

The average linewidth, full width at half maximum (FWHM), of the *in vivo* unsuppressed water signal was $\sim 13 \pm 2$ Hz at the echo time of 286 ms, after performing the first-order and second-order shimming adjustments. The *in vivo* spectra of Ser obtained with the DANTE application compares favorably with the spectrum obtained in *in vitro*, as illustrated in Figure 3-9. A stack of *in vivo* D-PRESS serine spectra obtained from the left anterior cingulate of three healthy participants, together with the standard PRESS spectrum acquired from subject 1, are presented in Figure 3-10. The signal near 3.83 ppm ascribes predominantly to the X spin system of Ser and some residual signal from the Cr peak at 3.92 ppm. As demonstrated in Figure 3-10, for the *in vivo* experiments a suppression factor of 4 ($\sim 75\%$) to 8 ($\sim 90\%$) was achieved to almost completely eliminate the Cr signal introduced from resonances at 3.92 ppm. This figure also illustrates the signals from additional potential contaminants from the neighbouring metabolites, including Gln and Glu, which were suppressed (as demonstrated in *in vitro* measurements) by average factors of approximately 3 ($\sim 67\%$) and 4 ($\sim 75\%$), respectively. Figure 3-11 displays an example of spectral fitting results, illustrating the data, the fitting line, the fit components, and the fit residuals. The addition of these metabolites' spectral signatures in the quantification template results in lower fit residuals and thus reduces variability of Ser measurements by taking these sources of contaminations into consideration.

The reproducibility of MRS measurements greatly depends on the quality and reproducibility of RF excitation parameter adjustments and availability of more advanced MRS adjustment capabilities, as illustrated in the MRS literature.³⁴ Therefore, the DANTE-PRESS sequence was further modified to implement inline adjustment capabilities. This enabled the optimization of several parameters of the pulse sequence, including fine-tuning of the frequency offset of the DANTE pulse and fine adjustments of the transmitter voltage of the RF pulses (Figures 3-12 and 3-13).

The calibration of these parameters and the use of advanced adjustments in each individual are essential to minimizing the degradation of spectral quality and signal loss. The optimization of the selected parameters was accomplished by using real-time monitoring of the measurements prior to the start of the data acquisition. In order to

generate proper pulse sequence profiles, the optimum flip angle values (for the excitation and the two refocusing RF pulses, concurrently) were determined at the beginning of each scanning session. To arrive at the final desired D-PRESS sequence functionality, the fine tuning of the adjustment of the frequency offset of the DANTE RF pulse was performed prior to obtaining each Ser-selected spectra. This is a critical step since any misadjustments in computing the DANTE-RF frequency offset cause significant signal loss and the proper fitting of the developed *in vivo* template for quantification is jeopardized.

The following MRS ratio of metabolite peaks of Ser to NAA and Ser to Cr were computed. MRS ratio concentrations were obtained from all of the healthy participants whose spectra are presented in Figure 3-10. Assuming identical relaxation times, the concentrations of the D-PRESS Ser and PRESS NAA signals obtained from the three healthy participants were compared, and the Ser-to-NAA concentration ratio was estimated to be 0.09 ± 0.01 (mean \pm SD, $n = 5$). This ratio is greater than the expected values (by ~32%, considering Ser 0.732 mM and NAA 10.3 mM) when compared to the findings in the literature.^{25, 45-49} The ratios of Ser-to-Cr were also obtained and the values were 0.20 ± 0.03 (mean \pm SD, $n = 5$), higher (by ~38%, considering Ser 0.732 mM and Cr 5.1 mM) than the estimations provided in the published studies.^{25, 45-50} Prior to implementing the inline adjustment technique, two repeated measurements from the first- and second-*in vivo* experiments (two male subjects; participant 2 and participant 4) were quantified. The MRS ratios of these measurements are presented in table 3-2. Although it is too early to draw firm conclusions regarding the *in vivo* data, inline adjustment capabilities appear to enhance the reproducibility of Ser *in vivo* measurements.

Table 3-2. MRS ratio summary * of all of the *in vivo* measurements are displayed. For all of the subjects, except subject 1, a second measurement was obtained within the same day. Pre adjustments include the measurements obtained prior to implementing the inline adjustment properties to the sequence.

Table 1
MRS ratio summary *

Ratio	Subjects (Pre adjustments)		Subjects (Post adjustments)		
	2	4	1	2	3
Session A:					
Ser/NAA	0.114	0.140	0.093	0.102	0.083
Ser/CR	0.230	0.265	0.177	0.229	0.165
Session B:					
Ser/NAA	0.177	0.254	—	0.096	0.099
Ser/Cr	0.344	0.495	—	0.204	0.210

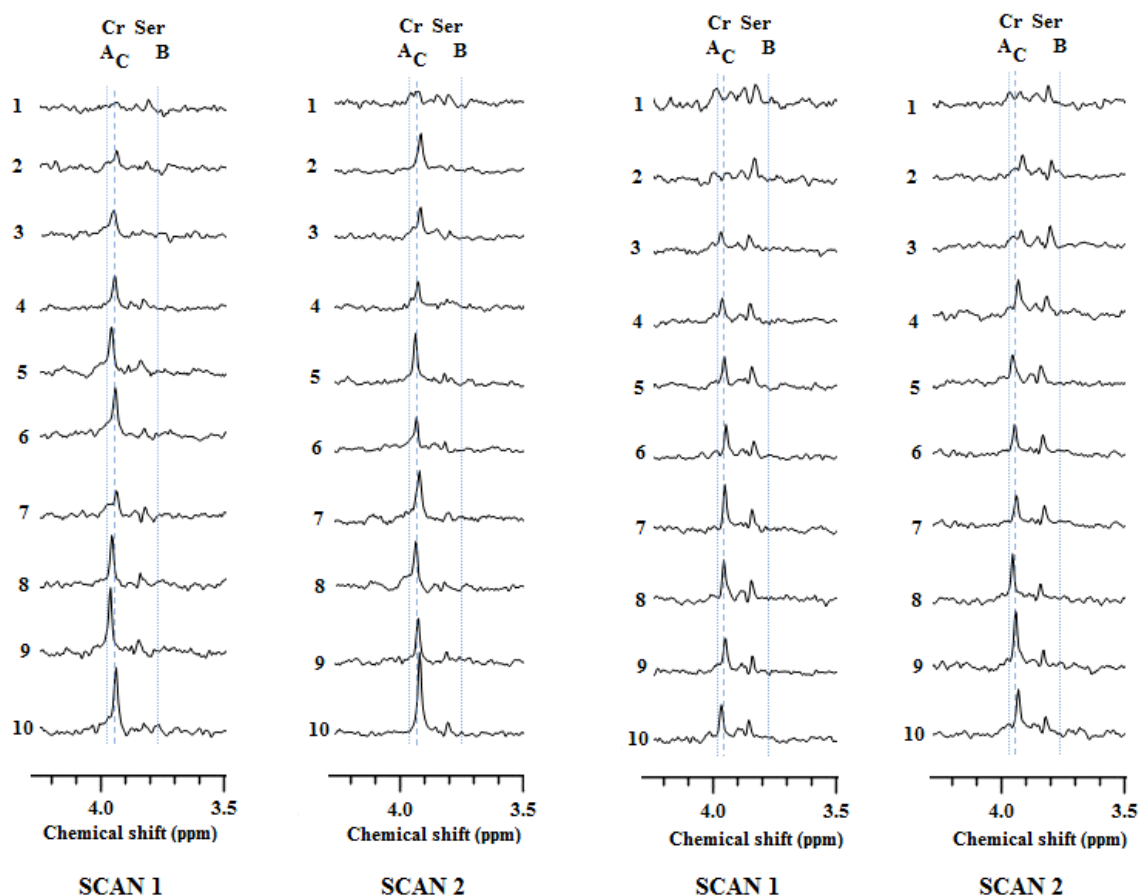


Figure 3-7. These spectra illustrate the 10 consecutive *in vitro* D-PRESS measurements obtained from two phantoms that contain *in vivo* serine concentrations and double *in vivo* serine concentrations, illustrated at the left and the right of the figure, respectively, at baseline & one week apart (indicated as SCAN 1 and SCAN 2, respectively). The two vertical solid lines (A, B) demonstrate the spectral width for Ser resonances and the Cr residuals generated from the peak at 3.92 ppm are indicated by the single vertical dashed line (C).

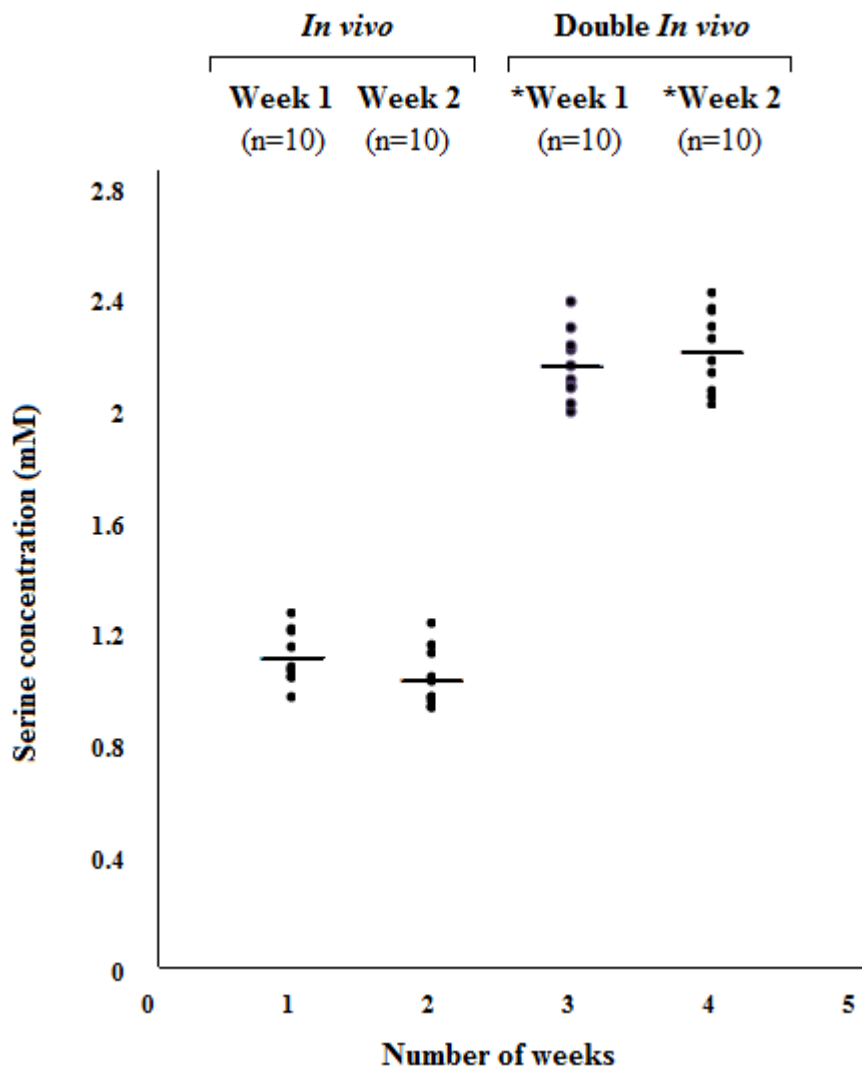


Figure 3-8. The average value of baseline *in vivo* & one week (Week 1 and Week 2) plus baseline double *in vivo* & one week (*Week 1 and *Week 2) were 1.13 ± 0.09 (CV = 8.3%), 1.06 ± 0.10 (CV = 9.9%), 2.18 ± 0.13 (CV = 5.7%) and 2.23 ± 0.14 (CV = 6.5%), respectively.

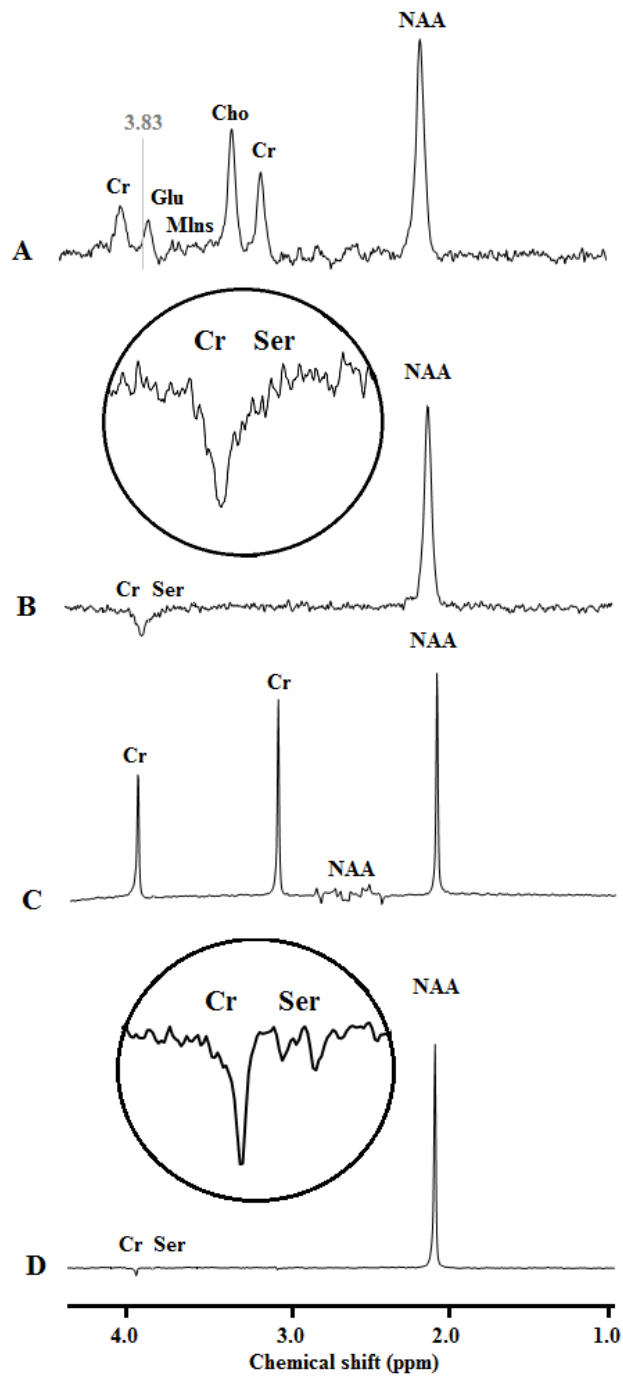


Figure 3-9. PRESS (A, C) and DANTE-PRESS (B, D) spectra (TE = 286 ms, TR = 2.0 s) were obtained from the anterior cingulate (A, B) and *in vitro* data acquired from a phantom composed of a solution of Ser and Cr (C, D). A LW correction factor of 2 Hz was applied to all of the four spectra.

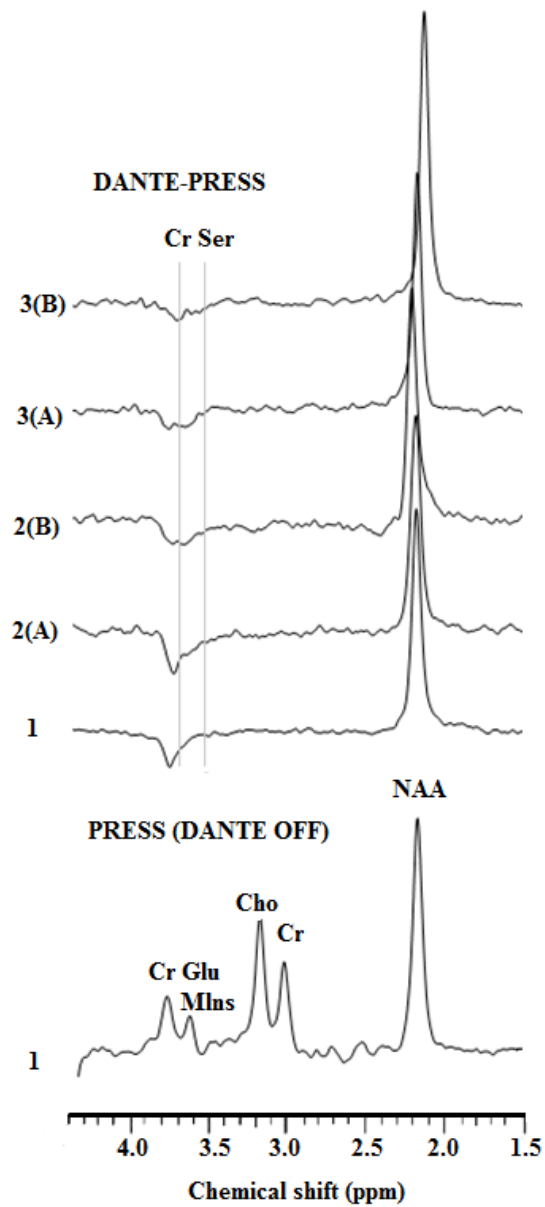


Figure 3-10 . A stack of *in vivo* DANTE-PRESS spectra obtained at TE=286 ms from the left anterior cingulate of three healthy participants. Two consecutive data-set were obtained within the same session from participants 2 and 3. The bottom trace is a standard PRESS spectrum obtained at TE=286 ms from participant 1.

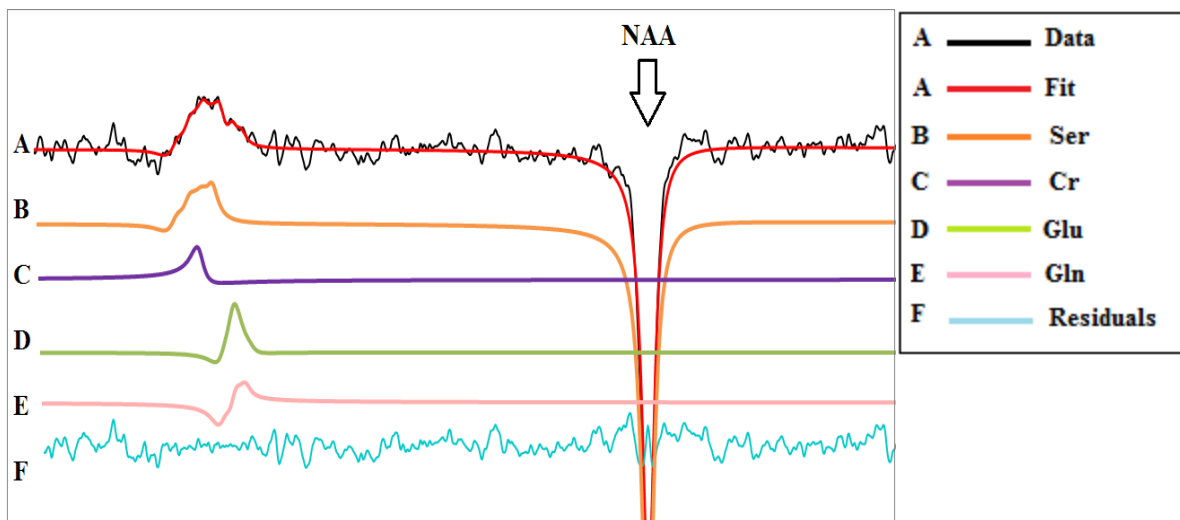


Figure 3-11. Representative of an *in vivo* spectrum. Line (A) represents the data in black and the fitting line in red, lines (B and C) illustrate the fitting components of serine in orange and creatine in purple, lines (D and E) represent the fitting components of glutamate in green and glutamine in pink, respectively. Line (F) shows the residuals in blue (data minus fit). LW correction factor of 2 Hz was applied.

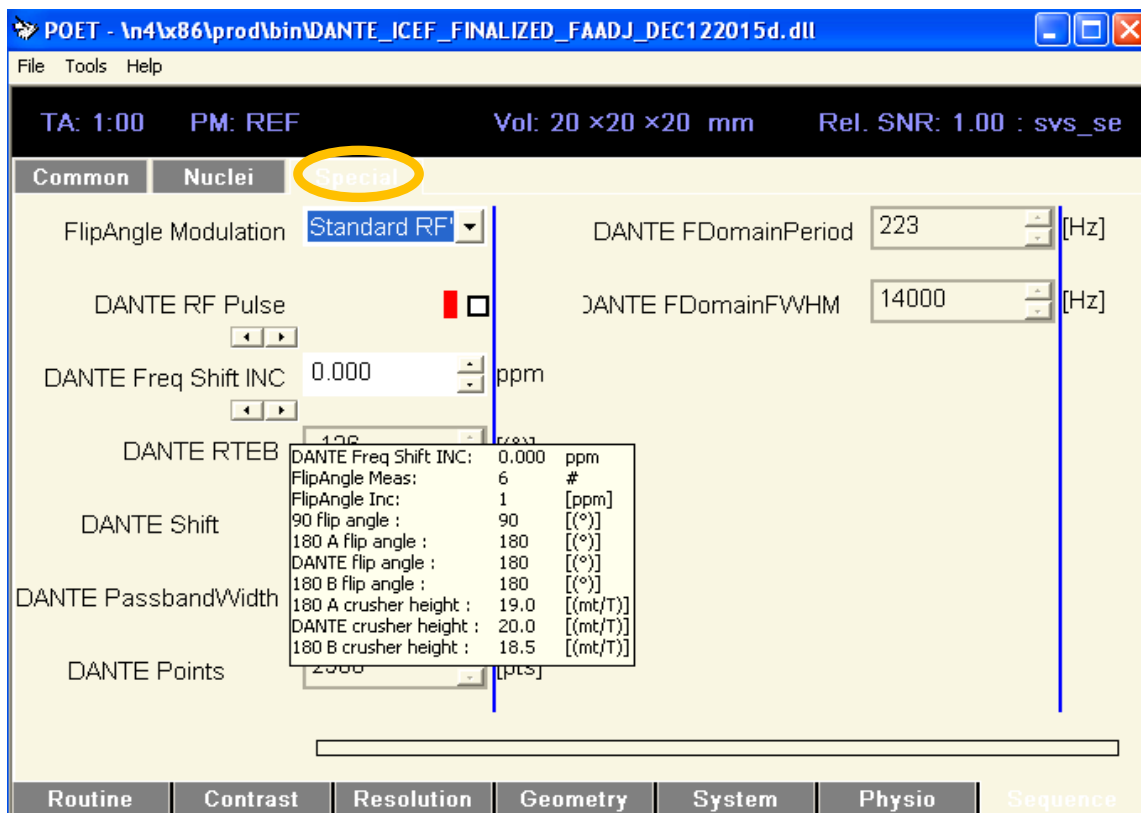


Figure 3-12. The “Special Card” illustrates the parameters which interact with the DANTE RF Pulse. The optimization of the DANTE frequency adjustments and the RF flip angle values are enabled through the use of this card.

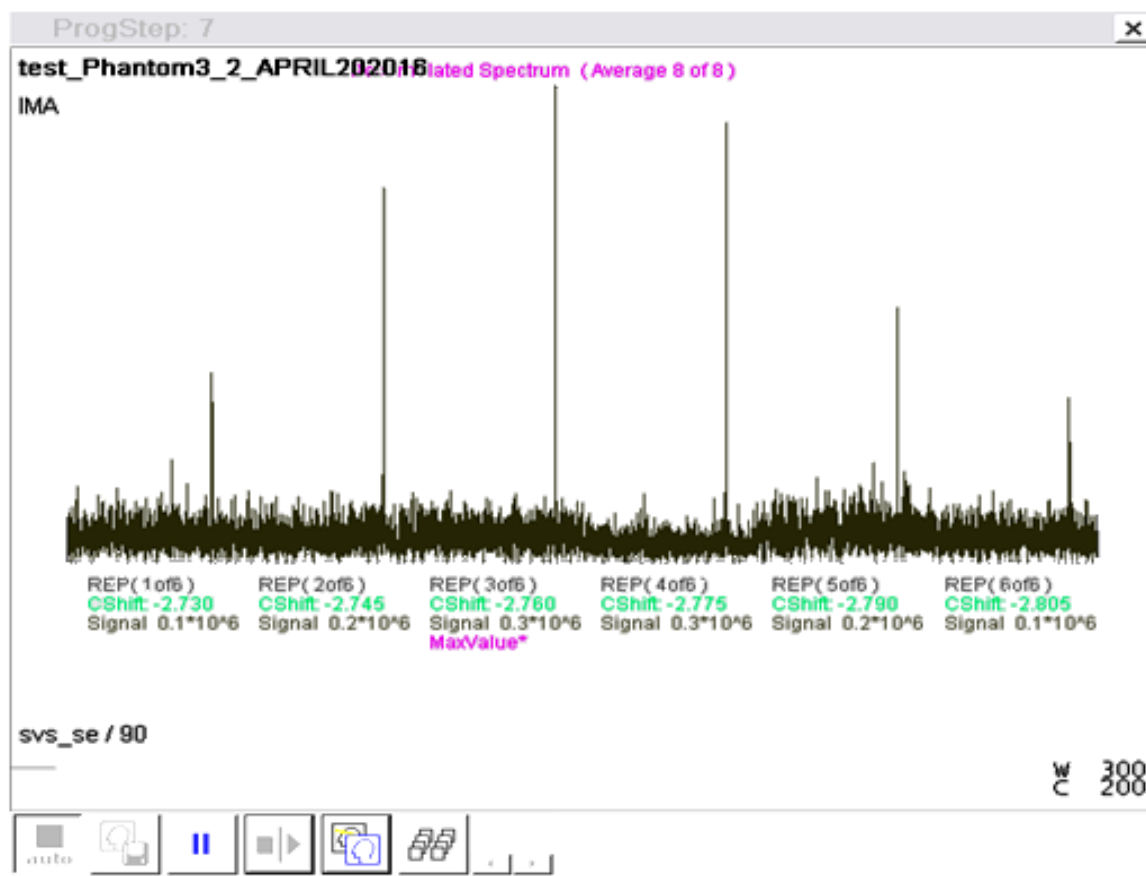


Figure 3-13. The inline display illustrates the DANTE RF pulse's chemical shift (CShift) value, the repetition number (REP), the signal value (Signal), and highlights the maximum value (MaxValue*) with a purple label.

3.4 Discussion:

This study demonstrated the first investigation of the reliability of the DANTE-PRESS method to detect *in vitro* Ser using a metabolite-selective single-voxel ^1H -MRS technique on a 3.0 Tesla clinical scanner. We evaluated the accuracy and precision of the measurements obtained in phantoms containing human brain mimicking concentration levels of Ser. This advanced ^1H -MRS technique, D-PRESS, is capable of isolating the resonances of Ser by significantly suppressing the resonances of Cr originating at 3.92 ppm and eliminating other interfering metabolites of Glu at ~ 3.74 ppm and Gln at ~ 3.75 ppm.

This study reports only the MRS ratio concentrations of Ser to other metabolites because of factors that make it difficult to compare the absolute numbers. The absolute values of NAA and Ser separately may vary significantly from scan to scan due to the voltage adjustments that were performed at the start of each scanning session in turn prior to each data acquisition. To investigate the absolute concentration, future studies may be able to take full advantage of voltage adjustments in obtaining higher SNR values by correcting the flip angle values based on the voltages.

A limitation of this report was that it did not incorporate the contributions from PEth and Eth metabolites, whose resonances may be refocused by the frequency-selective DANTE-RF pulse into the final quantification *in vivo* template. The Fitman program used for quantification applies the Levenberg-Marquardt minimization algorithm, an automated fitting procedure, which may result in quantification errors if certain metabolites are not included in the prior knowledge. The fitting procedure tends to compensate for the missing peaks by increasing or decreasing existing components of the fit, which may result in an over- or under-estimation of Ser signals. Therefore, in future studies, for a more precise quantification, it is critical to include all the neighbouring metabolites in the prior knowledge in order to assess the level of contamination and its effect on the concentrations of Ser.

A long, 118.54 ms DANTE pulse with a Gaussian waveform (5.0 % amplitude cut-off) was used to obtain a narrow refocusing bandwidth of 15 Hz. At field strength of 3.0

Tesla, the 15 Hertz bandwidth ensured significant suppression of the interfering singlet of Cr at 3.92 ppm and allowed for the detection of Ser. The use of a long echo time (TE = 286 ms) in these experiments was necessary to accommodate the long DANTE pulse. This can be a disadvantage of this method due to the associated substantial signal decay via transverse relaxation effects. On the other hand, it has been noted that macromolecular (MM) resonances are abundantly present at 4.00 ppm, near the Ser resonances at 3.83 ppm^{35,36} and their contribution to Ser signals is completely eliminated at such long echo times.

Despite the scanner drift that arises from hardware imperfections, including changes in the temperature over time and long scanning duration, the signal intensity and line shape of Ser obtained using the narrow-band 180° DANTE RF pulse still generates an acceptable signal-to-noise ratio for this low concentration metabolite. Nonetheless, the implementation of the extremely narrow radiofrequency RF pulse of DANTE (at a long echo time of 286 ms) is still susceptible to hardware-related frequency drift and restriction of participant head movement is critical to avoid motion-related frequency drifts.³⁹

In conclusion, this novel metabolite-selective ¹H-MRS method, dubbed D-PRESS, was the first attempt to measure endogenous human brain Ser levels at field strength of 3.0 Tesla. Results suggest *in vivo*-like concentrations of Ser can be measured reliably with little contamination from other metabolites. The implementation of inline adjustment capabilities to this custom D-PRESS ¹H-MRS sequence seemed critical to achieve reproducible Ser measurements *in vitro* and *in vivo*. Together the low CV values and the results obtained from the one-way ANOVA analysis for the *in vitro* findings suggest that the DANTE-PRESS sequence was capable of successfully detecting the signal of *in vitro* Ser with sufficient reproducibility and precision to justify assessment of test-retest reliability of endogenous *in vivo* levels. The proof-of-concept *in vivo* data showed that the technique is applicable to *in vivo* measurements. Further studies need to be performed in order to determine the reproducibility of these measurements in healthy controls and schizophrenic patients.

3.5 References:

1. Tsai GE, Lin PY. Strategies to enhance N-methyl-D-aspartate receptor-mediated neurotransmission in schizophrenia, a critical review and meta-analysis. *Current pharmaceutical design*. 2010 Feb 1; 16(5):522-37.
2. Kantrowitz JT, Woods SW, Petkova E, Cornblatt B, Corcoran CM, Chen H, Silipo G, Javitt DC. D-serine for the treatment of negative symptoms in individuals at clinical high risk of schizophrenia: a pilot, double-blind, placebo-controlled, randomised parallel group mechanistic proof-of-concept trial. *The Lancet Psychiatry*. 2015 May 31; 2(5):403-12.
3. Remington G, Foussias G, Fervaha G, Agid O, Takeuchi H, Lee J, Hahn M. Treating Negative Symptoms in Schizophrenia: an Update. *Current Treatment Options in Psychiatry*: 1-8.
4. Singh SP, Singh V. Meta-analysis of the efficacy of adjunctive NMDA receptor modulators in chronic schizophrenia. *CNS drugs*. 2011 Oct 1; 25(10):859-85.
5. Tsai G, Yang P, Chung LC, Lange N, Coyle JT. D-serine added to antipsychotics for the treatment of schizophrenia. *Biological psychiatry*. 1998 Dec 1;44(11):1081-9.
6. Mothet JP, Parent AT, Wolosker H, Brady RO, Linden DJ, Ferris CD, Rogawski MA, Snyder SH. D-serine is an endogenous ligand for the glycine site of the N-methyl-D-aspartate receptor. *Proceedings of the National Academy of Sciences*. 2000 Apr 25; 97(9):4926-31.
7. Wolosker H. D-serine regulation of NMDA receptor activity. *Sci STKE*. 2006 Oct 10; 356:-41.
8. Panatier A, Theodosis DT, Mothet JP, Touquet B, Pollegioni L, Poulain DA, Oliet SH. Glia-derived D-serine controls NMDA receptor activity and synaptic memory. *Cell*. 2006 May 19; 125(4):775-84.
9. Coyle JT, Tsai G, Goff D. Converging evidence of NMDA receptor hypofunction in the pathophysiology of schizophrenia. *Ann NY Acad Sci* 2003; 1003:318 –327.

10. Javitt DC, Zukin SR. Recent advances in the phencyclidine model of schizophrenia. *Am J Psychiatry*. 1991 Oct 1; 148(10):1301-8.
11. Tamminga CA. Schizophrenia and glutamatergic transmission. *Critical Reviews™ in Neurobiology*. 1998; 12(1-2).
12. Durrant AR, Heresco-Levy U. D-Serine in neuropsychiatric disorders: New advances. *Advances in Psychiatry*. 2014 Jun 19; 2014.
13. Olney JW, Farber NB. Glutamate receptor dysfunction and schizophrenia. *Archives of general psychiatry*. 1995 Dec 1; 52(12):998-1007.
14. de Bartolomeis A, Sarappa C, Magara S, Iasevoli F. Targeting glutamate system for novel antipsychotic approaches: relevance for residual psychotic symptoms and treatment resistant schizophrenia. *European journal of pharmacology*. 2012 May 5; 682(1):1-1.
15. Coyle JT. Glutamate and schizophrenia: beyond the dopamine hypothesis. *Cellular and molecular neurobiology*. 2006 Jul 1; 26(4-6):363-82.
16. Heresco-Levy U, Javitt DC, Ermilov M, Mordel C, Silipo G, Lichtenstein M: Efficacy of high-dose glycine in the treatment of enduring negative symptoms of schizophrenia. *Arch Gen Psychiatry* 1999; 56:29-36.
17. Simeon J, Fink M, Itil TM, Ponce D. (1970): d-Cycloserine therapy of psychosis by symptom provocation. *Comp Psychiatry* 11: 80–88.
18. Shleper M, Kartvelishvily E, Wolosker H. D-serine is the dominant endogenous coagonist for NMDA receptor neurotoxicity in organotypic hippocampal slices. *J Neurosci* 2005; 25: 9413–9417.
19. Matsui TA, Sekiguchi M, Hashimoto A, Tomita U, Nishikawa T, Wada K. Functional comparison of D-serine and glycine in rodents: The effect on cloned NMDA receptors and the extracellular concentration. *Journal of neurochemistry*. 1995 Jul 1; 65(1):454-8.
20. Stevens ER, Gustafson EC, Miller RF. Glycine transport accounts for the differential role of glycine vs. d-serine at NMDA receptor coagonist sites in the salamander retina. *European Journal of Neuroscience*. 2010 Mar 1;31(5):808-16.
21. Fossat P, Turpin FR, Sacchi S, Dulong J, Shi T, Rivet JM, Sweedler JV, Pollegioni L, Millan MJ, Olier SH, Mothet JP. Glial D-serine gates NMDA

- receptors at excitatory synapses in prefrontal cortex. *Cerebral cortex*. 2012 Mar 1; 22(3):595-606.
22. Panatier A, Theodosis DT, Mothet JP, Touquet B, Pollegioni L, Poulain DA, Olié SH. Glia-derived D-serine controls NMDA receptor activity and synaptic memory. *Cell*. 2006 May 19; 125(4):775-84.
 23. Schell MJ, Brady Jr RO, Molliver ME, Snyder SH. D-serine as a neuromodulator: regional and developmental localizations in rat brain glia resemble NMDA receptors. *The Journal of neuroscience*. 1997 Mar 1; 17(5):1604-15.
 24. Bauer D, Hamacher K, Bröer S, Pauleit D, Palm C, Zilles K, Coenen HH, Langen KJ. Preferred stereoselective brain uptake of d-serine—a modulator of glutamatergic neurotransmission. *Nuclear medicine and biology*. 2005 Nov 30; 32(8):793-7.
 25. Govindaraju V, Young K, Maudsley AA. Proton NMR chemical shifts and coupling constants for brain metabolites. *NMR Biomed* 2000; 13:–153.
 26. Choi C, Coupland NJ, Bhardwaj PP, Malykhin N, Gheorghiu D, Allen PS. Measurement of brain glutamate and glutamine by spectrally-selective refocusing at 3 tesla. *Magnetic resonance in medicine*. 2006 May 1; 55(5):997-1005.
 27. Choi C, Ogilvie CJ, Malykhin N, Ngo JT, Hartfeil MA, Coupland NJ. Detection of the myo-inositol 4.06-ppm resonance by selective J rewinding: Application to human prefrontal cortex in vivo. *Magnetic resonance in medicine*. 2005 Dec 1; 54(6):1536-40.
 28. Choi C, Dimitrov I, Douglas D, Zhao C, Hawesa H, Ghose S, Tamminga CA. In Vivo Detection of Serine in the Human Brain by Proton Magnetic Resonance Spectroscopy (¹H-MRS) at 7 Tesla. *Magn Reson Med*. 2009 Oct;64(4):1042-1046.
 29. Theberge J, Renshaw PF. In vivo measurements of brain serine with ¹H-MRS. In: *Proceedings of the 15th Annual Meeting of ISMRM, Berlin, Germany, 2007* (Abstract 1373).
 30. Green H, Wu X-L, Friedrich J, Freeman R. Selective Excitation at Two Arbitrary Frequencies. The Double-DANTE Sequence. *J Magn Reson* 1989, 81:646-652.

31. Phillips ML, Drevets WC, Rauch SL, Lane R. Neurobiology of emotion perception II: implications for major psychiatric disorders. *Biol Psychiatry* 2003; 54:515–528.
32. Hill K, Mann L, Laws KR, Stephenson CM, Nimmo-Smith I, McKenna PJ. Hypofrontality in schizophrenia: a meta-analysis of functional imaging studies. *Acta Psychiatr Scand* 2004; 110:243–256.
33. Bartha R, Drost DJ, Williamson PC. Factors affecting the quantification of short echo in-vivo ^1H MR spectra: prior knowledge, peak elimination, and filtering. *NMR in biomedicine*. 1999 Jun 1; 12(4):205-16.
34. Deelchand DK, Adanyeguh IM, Emir UE, Nguyen TM, Valabregue R, Henry PG, Mochel F, Öz G. Two-site reproducibility of cerebellar and brainstem neurochemical profiles with short-echo, single-voxel MRS at 3T. *Magnetic resonance in medicine*. 2015 May 1; 73(5):1718-25.
35. Behar KL, Rothman DL, Spencer DD, Petroff OA. Analysis of macromolecule resonances in ^1H NMR spectra of human brain. *Magn Reson Med* 1994;32:294–302.
36. Soher BJ, Pattany PM, Matson GB, Maudsley AA. Observation of coupled ^1H metabolite resonances at long TE. *Magn Reson Med* 2005; 53: 1283–1287.
37. Ogg RJ, Kingsley PB, Taylor JS. WET, a T1- and B1-insensitive water suppression method for in vivo localized ^1H NMR spectroscopy. *J Magn Reson B*. 1994; 104:1–10.
38. Labrie V, Roder JC. The involvement of the NMDA receptor D-serine/glycine site in the pathophysiology and treatment of schizophrenia. *Neuroscience & Biobehavioral Reviews*. 2010 Feb 28; 34(3):351-72.
39. Choi C, Coupland NJ, Bhardwaj PP, Kalra S, Casault CA, Reid K, Allen PS. T2 measurement and quantification of glutamate in human brain in vivo. *Magnetic resonance in medicine*. 2006 Nov 1; 56(5):971-7.
40. Coyle JT. NMDA receptor and schizophrenia: a brief history. *Schizophrenia bulletin*. 2012 Sep 1; 38(5):920-6. *Schizophr Bull*.2012.In press

41. Snyder ML, Lichstein HC. Sodium azide as an inhibiting substance for gram-negative bacteria. *Journal of Infectious Diseases*. 1940 Sep 1; 67(2):113-5.
42. Brooks WM, Friedman SD, Stidley CA. Reproducibility of 1H-MRS in vivo. *Magn Reson Med* 1999; 41:193–197.
43. Ozdemir ST, Ercan I, Sevinc O, Guney I, Ocakoglu G, Aslan E, Barut C. Statistical shape analysis of differences in the shape of the corpus callosum between genders. *the anatomical record*. 2007 Jul 1; 290(7):825-30.
44. P. Reimer, P. M. Parizel, J. F. Meaney and F. A. Stichnoth, *Clinical MR Imaging: A Practical Approach*, Springer-Verlag, Berlin, Heidelberg, 2010
45. Siegel GJ, Agranoff BW, Albers RW, Molinoff P. *Basic Neurochemistry: Molecular, Cellular, and Medical Aspects*, Raven Press, New York (1989).
46. Kumashiro S, Hashimoto A, Nishikawa T. Free D-serine in post-mortem brains and spinal cords of individuals with and without neuropsychiatric diseases. *Brain Res*. 1995 May 29; 681(1-2):117-25.
47. Hashimoto A, Oka T. Free D-aspartate and D-serine in the mammalian brain and periphery. *Progress in Neurobiology* 1997 Jul; 52(4):325-53.
48. Kreis R. Quantitative localized 1 H MR spectroscopy for clinical use. *Progress in Nuclear Magnetic Resonance Spectroscopy*. 1997 Sep 30; 31(2):155-95.
49. Klunk WE, Xu C, Panchalingam K, McClure RJ, Pettegrew JW. Quantitative 1H and 31P MRS of PCA extracts of post mortem Alzheimer's disease brain. *Neurobiol. Aging* 1996; 17: 349–357.
50. van Zijl P, Barker PB. Magnetic Resonance Spectroscopy and Spectroscopic Imaging for the Study of Brain Metabolism. *Annals of the New York Academy of Sciences*. 1997 May 1; 820(1):75-96.
51. Morey R, Brown VM. Neural systems for cognitive and emotional processing in posttraumatic stress disorder. *Frontiers in psychology*. 2012 Oct 30; 3:449-52.
52. Hansen TM, Olesen AE, Simonsen CW, Drewes AM, Frøkjær JB. Cingulate metabolites during pain and morphine treatment as assessed by magnetic resonance spectroscopy. *Journal of pain research*. 2014; 7:269.

53. Mao J, Mareci TH, Scott KN, Andrew ER. Selective inversion radiofrequency pulses by optimal control. *Journal of Magnetic Resonance* (1969). 1986 Nov 30;70(2):310-8.
54. Mao J, Mareci TH, Andrew ER. Experimental study of optimal selective 180 radiofrequency pulses. *Journal of Magnetic Resonance* (1969). 1988 Aug 1;79(1):1-0.
55. Retrieved on December 22, 2016 from <https://www.healthcare.siemens.com/magnetic-resonance-imaging/mr-pet-scanner/biograph-mmr>.
56. Delso G, Fürst S, Jakoby B, Ladebeck R, Ganter C, Nekolla SG, Schwaiger M, Ziegler SI. Performance measurements of the Siemens mMR integrated whole-body PET/MR scanner. *Journal of nuclear medicine*. 2011 Dec 1; 52(12):1914-22.

Chapter 4

4 Thesis summary:

In recent years, there has been a growing academic interest in *in vivo* detection of serine (Ser) concentrations in the human brain as our group, and other researchers, have investigated its significance and relevance to neuropsychiatric disorders.¹ Ser concentrations have been implicated in the pathophysiology of schizophrenia by a number of research findings.² Evidence suggests that alterations in the NMDA receptor, which causes glutamatergic abnormalities, are the main explanation for the negative and cognitive symptoms of schizophrenia, which may respond to the oral administration of D-serine supplements.³ The detection of the naturally occurring brain levels of serine has been impossible using standard proton Magnetic Resonance Spectroscopy (¹H-MRS), due to its comparatively weak signals, and neighboring strong signals. Advanced ¹H-MRS methods conducted at non-clinical, high-field strengths of 4.0 Tesla (T)⁴ and 7.0 T,⁵ have been capable of measuring the endogenous levels of human brain serine. Nonetheless, no earlier research has employed these techniques at the more widely available clinical field strength of 3.0 T.

In summary, this thesis has introduced an innovative ¹H-MRS DANTE-PRESS (D-PRESS) pulse sequence, implemented by inserting a spectrally-selective single-DANTE pulse into a standard symmetrical PRESS sequence. D-PRESS is capable of assessing endogenous levels of Ser by refocusing its signals and greatly suppressing the signals of other metabolites. D-PRESS uses a narrow radiofrequency pulse centred on a chosen spectral line of interest (i.e. the X spin of the Ser's ABX spin system) such that neighboring resonances remain unaffected. Chapter 3 summarizes findings from the evaluation of the test-retest reproducibility of Ser measurements in brain-mimicking phantoms, with two concentrations in the *in vivo* range. It also presents preliminary *in vivo* proof-of-concept data demonstrating the feasibility of Ser measurements at 3.0 T. Results demonstrated the reliability and reproducibility of Ser measurements obtained *in vitro* and suggests readiness for comparable work *in vivo*.

4.1 General remarks, limitations and implications:

The remainder of this chapter will highlight some of the advantages of the experimental protocol presented in this thesis. Despite the effort devoted to developing and implementing an advanced ^1H -MRS sequence in conjunction with MRS adjustment capabilities (see Appendix A), the following will identify any limitations and deficiencies in the existing practice that need to be addressed, and discuss ways of improving future studies.

4.2 The DANTE-PRESS protocol's advantages and limitations:

4.2.1 Advantages:

The D-PRESS pulse sequence consists of the addition of a frequency-selective, single-DANTE pulse with very narrow passband, into a symmetrical PRESS sequence (adapted from the MRI vendor's product PRESS sequence version VB20PSP4). The D-PRESS sequence introduced in Chapter 2 is capable of selectively exciting only the spins of interest in a very narrow range of radiofrequencies. Thus, a major advantage of the D-PRESS technique is that it offers an enhancement in sensitivity to distinguish proton signals from metabolites otherwise difficult to detect.^{6, 7} The selective pulse refocuses a particular resonance (or a group of resonances) within complex spectra while leaving adjacent resonances, which may hinder its measurement, unaffected.⁸ The most important advantage of the D-PRESS pulse sequence is that its metabolite-selective DANTE pulse is generated online in response to the user's input. The pulse sequence allows for online optimization of a variety of experimental parameters, including the pulse duration of the DANTE pulse that determines its selectivity,⁸ fine adjustments of the spoiler gradients (i.e. the height and the duration; see Appendix B), the modulation and the truncation value of the RF pulse (i.e. Gaussian), and the produced inversion-frequency profile of the pulse in order to achieve an acceptable excitation of a region of an NMR spectrum.⁹ Indeed, it is essential to select a suitable amplitude modulation function to improve the shape of the resulting frequency passband of the DANTE RF pulse.¹⁰ In this thesis a Gaussian-modulated DANTE RF pulse was implemented.⁸ In comparison to a rectangular

pulse, in most circumstances depending greatly on the selected waveform cut-off for a Gaussian shaped RF pulse, a Gaussian pulse with the same length generates a narrower profile.¹⁰ Although, a rectangular pulse is simpler in terms of implementation, it generates unwanted side lobes that may lead to refocusing of unwanted resonances.⁸ A sinc-modulated DANTE RF pulse would produce a more square refocusing profile but requires a longer pulse duration, pushing TE beyond the practical feasibility range.¹¹ A properly truncated, highly selective Gaussian modulation targets a narrow range of the NMR spectrum and eliminates the refocusing of the neighbouring resonances since its amplitude declines rapidly in the tails.⁸ For a detailed description of the user interface developed as part of this work for the online manipulation of D-PRESS pulse sequence parameters, see Appendix A.

4.2.2 Limitations and implications:

The implemented single-DANTE pulse allows the production of a frequency-domain inversion, with a profile repeating at a certain frequency interval (in Hz), which may cause the excitation of the unwanted metabolites elsewhere in crowded spectra other than the reference and the metabolite of interest.¹¹ For example, if a sideband of the DANTE pulse falls near the water peak, the pulse will interfere with water-suppression and the resulting baseline distortions hinder the detection of metabolites, including serine (the X spin, 3.83 ppm), near water (~ 4.7 ppm). Another obstacle arises when the difference between these repeating frequency passbands (a.k.a. Frequency Domain Period, FDP) is roughly less than 100 Hz, which may cause a reduction in the obtained SNR, as verified in our experiment. In our experiments, in order to overcome these challenges, we chose a reference metabolite (i.e. NAA) whose peak position is far away, 1.81 ppm (~ 223 Hz), relative to the resonance of the metabolite of interest (i.e. serine) within the spectrum of interest. This practice ensures the full separation of repeating passbands' profiles. However, it limits our choices in selecting a suitable reference peak.⁶ For future work, our recommendation is to implement a double-DANTE pulse that is capable of simultaneous excitation of spins, operating in two independent rotating referencing frames.⁷ The double-DANTE sequence was first introduced by Green et al. and allows for the production of two arbitrary frequencies in high-field NMR.^{7, 11} Not only will the

background contaminant signals be completely suppressed and only the desired metabolites will appear on the NMR spectrum, but the SNR value may not be affected when the frequency difference between passbands of interest is set to less than 100 Hz.

4.3 Biograph mMR PET/MRI 3.0 Tesla scanner:

The 3.0 T Biograph mMR MR-PET system scanner used in this study is an integrated multi-modal imaging device and may not be representative of all other typical 3.0 T MRI-only scanners (i.e. Siemens' Verio, Trio, Skyra and Prisma scanners). Aside from the reduction in the space within the bore of the MRI scanner⁶⁰ since the PET photodetectors are highly sensitive to temperature changes, a redesign of the gradient coils cooling system was required to monitor changes in heat.^{61, 62} The installation of the temperature sensors and the implementation of the liquid cooling approach⁶³ ensures the system to gain thermal stability and to operate at lower temperature in comparison to other conventional MRI systems.^{61, 63} The effective monitoring of the temperature of the detectors and the achieved thermal stability presumably aids in the reduction of the frequency drift. Although no data has been presented, it is possible that the rate of frequency drift may be more pronounced in other standard clinical 3.0 T scanners which may interfere with the spectral quality or reduce SNR. The loss in the SNR related to drift may be mitigated by dynamically adjusting frequency based on a measurement-based prediction of the drift rate as discussed in Chapter 3.

4.4 Ultra-high magnetic field of 7.0 Tesla versus 3.0 Tesla:

This work presents the first investigation of test-retest of endogenous measurements of serine at 3.0 T. The implementation of the single-voxel DANTE-PRESS technique on a clinical platform at 7.0 T relative 3.0 T will allow for a substantial increase in the signal to noise ratio (SNR) at higher B_0 , and an enhancement in spectral resolution due to an improvement in the separation of spectral lines of individual metabolites.^{13, 14} Since there will be an increase in the chemical shift dispersion, a higher FWHM value of the DANTE pulse (~35 Hz) will be required to target the resonance of serine at 3.83 ppm compared to the FWHM value of 15 Hz used at 3.0 T. Ultimately, due to the reduction in the duration

of the DANTE pulse (increased bandwidth/FHWM value), the implementation of a shorter TE value is possible, which in turn may reduce the attenuation of signal caused by J-coupling effects.¹² An increase in B_0 up to 7.0 T results in an improvement in the SNR (approximately 2-fold in comparison to 3.0 T).¹⁵ Because of the resulting improvement, a smaller number of averages can be used to produce an acceptable MRS spectra which will result in reduced scan time¹² (potentially lessening patient motion effects). Despite increases in spectral linewidths at 7.0 T¹⁶ compared to 3.0 T, they are outweighed by increases in spectral dispersion. Increases in spectral dispersion, interestingly, also contribute to the reduction in the amount of J-dephasing of the NMR spectrum; as the formerly strongly coupled metabolites become more weakly coupled (chemical shift difference over J ratio is decreased). This fact will lessen the amount of second-order J-coupling effects for the AB spins of Ser and will allow for a more precise and reliable quantification of metabolites with complex spectral signatures.¹⁷ Therefore, it is expected that the use of DANTE-PRESS at ultra-high field will lead to significant improvements in the detection of metabolites with low concentrations and a strongly coupled spins,¹⁵ such as serine.

A reasonable path for future work would be to compare the test-retest reliability of *in-vitro* and *in-vivo* Ser measurements obtained at the ultrahigh magnetic field of 7.0 T to that obtained at 3.0 T. The information would be useful to investigators planning studies of human brain serine when deciding which field strength to use and evaluating the cohort size required.

4.5 Caveats and future recommendations:

Some limitations associated with the D-PRESS protocol were presented in Chapter 3. This MRS technique measures both D-serine and L-serine within a region of interest, and cannot distinguish these metabolites individually. It also cannot provide information regarding the d-/l-serine ratio which has been suggested to be a therapeutic marker in these patients.¹⁸ Another important drawback that was not mentioned within Chapter 3 includes the accurate measurements of *in vivo* metabolite concentration relative to water concentrations of brain tissues. The calculations of the fractional components of the grey

matter (GM), white matter (WM), and cerebral spinal fluid (CSF) were not performed. Water content of GM equals 81% and WM equals 71%, as illustrated in the literature.¹⁹ Thus, in future *in vivo* work, accurate quantification of metabolite concentrations will need to correct for the fractional tissue content of the MRS volume.

4.6 Future work:

4.6.1 ¹H-MRS schizophrenia:

As stated before, it has been postulated that glutamatergic deficiency contributes to the pathophysiology of schizophrenia. Evidence suggests precise and reliable detection of glutamate (Glu) and glycine (Gly) in the human brain is crucial for research in neuropsychiatric diseases including schizophrenia.^{20, 21, 22} Glycine, an inhibitory neurotransmitter,²³ is an essential co-agonist²⁴ that may facilitate endogenous glutamatergic transmission by modulating the functional activity of N-methyl-D-aspartate (NMDA) receptor complex. Although detection of glycine using MRS methods with long echo times has been reported,²⁵ the assessment of this metabolite has been difficult due to its low abundance in the human brain and interference from macromolecules and myo-inositol.²² As mentioned in Chapter 1, measurements of glycine in schizophrenic patients using ¹H-MRS techniques have not yet been reported. Abnormalities in glutamate have been found in patients who suffer from schizophrenia.⁵¹ Glutamate quantification has been challenging due to its complex spectral signature and interferences from the neighbouring metabolites.²⁶ Metabolic abnormalities of glutamate in schizophrenia have been investigated by applying a non-invasive standard ¹H-MRS and the following will summarize most of these ¹H-MRS findings.

Clinical ¹H-MRS studies demonstrated higher than normal levels of glutamine²⁷ and glutamate²⁸ in the anterior cingulate of healthy participants under the influence of an antagonist known as ketamine. Similarly, elevated levels of glutamate in the precommissural dorsal-caudate (a dopamine-rich region)²⁹ and in the associative striatum and the cerebellum;³⁰ increased levels of Gln/Glu in the AC;³¹ elevated levels of glutamate in the prefrontal cortex and hippocampus;³² higher levels of GABA and

glutamate-glutamine (Glx) in the prefrontal cortex³³ of unmedicated, first-episode patients were observed by applying ¹H-MRS. Another group found elevated concentrations of glutamate in the prefrontal and hippocampal regions in schizophrenic patients.³⁴

Our group has also been capable of assessing abnormalities in the concentration of glutamatergic metabolites in these affected individuals by using single voxel ¹H-MRS methods. The following findings were reported by our group: higher glutamine levels in the AC and thalamus³⁵ and higher levels of glutamine in the left AC and thalamus³⁶ were observed in anti-psychotic naïve patients; lower levels of glutamate and glutamine and higher than normal levels of glutamine were found in the left region of AC and the thalamus³⁷ respectively in chronic patients. Another group also examined the concentration levels in glutamine in the medial prefrontal cortex in untreated patients and have found an increase in the concentration compared to the healthy groups.³⁸ Spectra obtained from the medial prefrontal cortex from adolescents who are at high genetic risk for developing schizophrenia have demonstrated a higher glutamate/glutamine concentration compared to healthy controls.³⁹ Conversely, in a study conducted in twins, the abnormalities in glutamate concentrations in schizophrenic patients were examined and their unaffected twins and the levels were found to be significantly lower in both groups compared to healthy subjects.⁴⁰ A different report had indicated an increase in glutamate and glutamine in the white matter portion of the brains of those in an elderly schizophrenic group.⁴¹ More importantly, longitudinal ¹H-MRS studies conducted in first episode patients after treatment have demonstrated the normalization and the reduction of glutamate levels in the associative striatum and the frontal lobe, respectively.^{42, 43} Similarly, other reports suggest which medicated first episode patients showed normalization of levels of GLX and GABA in the prefrontal cortex⁴⁴ and clinically stabilized patients had reduced levels of GLX in the anterior cingulate,^{45, 46} supporting the results obtained by our group previously.³⁷ Findings from a recent meta-analysis ¹H-MRS study indicate a rise in the medial frontal in Glu/Gln levels in the early stages of the illness and lower ratios in older patients.⁴⁷

The ^1H -MRS reports mentioned above provide *in vivo* information about the glutamate levels in patients diagnosed with schizophrenia. It is crucial to precisely and reliably assess the magnitude and extent of alterations in glutamatergic metabolites. These results indicate the growing appreciation of developing an effective technique, capable of detecting metabolites with difficult resonance structures at a high degree of precision. As indicated, the ^1H -MRS findings regarding glutamate concentrations have been inconsistent. A few factors have been proposed that may contribute to these mixed ^1H -MRS findings, including a variation in glutamate levels due to impaired functional integrity of the neurons,⁴⁸ the severity of the illnesses, the effects of anti-psychotic medications and methodological reasons.⁴⁹ The majority of the ^1H -MRS studies in terms of investigating the alterations in glutamate in schizophrenia patients have used magnetic field strengths lower than 4.0 T.⁵⁰ Reliable measurements of glutamate concentrations have been challenging at low magnetic fields, which may have led to the conflicting research results found in the literature.⁴⁹ Previous reports examined the reproducibility and sensitivity of ^1H -MRS measurements of glutamate and Glx in healthy subjects and in schizophrenic patients. The reproducibility of glutamate measures in healthy participants at 1.5 T and at 3.0 T was assessed. The results indicated a coefficient of variation (CV) ranging from 11.0 and 13.1% in the ACC and insula at 1.5 T⁵² and 13% at 3.0 T.⁵⁷ Another report indicated coefficients of variation in measurements of glutamate ranging from 5% to 10% in the cingulate gyrus of healthy participants at 3.0 T.⁵⁹ Measurements of glutamate were obtained at 1.5 T from patients with schizophrenia and the CV ranged from 20-50%⁵⁵ in the frontal lobe and 36-44% in the medial temporal lobe.⁵⁶ ^1H -MRS assessment of Glx at 3.0 T in patients with schizophrenia were obtained, and the results showed a CV range of 15–24% in the frontal and caudate regions.⁵³ Measures of glutamate provided a CV of approximately 2-3% in the ACC, conducted at 7.0 T.⁵⁴ Given the significant findings related to alterations in glutamate concentrations in schizophrenic patients and poor CVs (at field strengths < 7.0 T), it is crucial to apply more advanced and robust MRS sequences. DANTE-PRESS, a promising metabolite-selective approach, is better suited for the reliable and precise quantification of metabolites using low magnetic field strengths, and might enable achieving a lower CV range (with an estimated value of < 15% at 3.0 T), in measuring glutamate in patients with schizophrenia.

Since the D-PRESS technique is capable of improving the quantification of the selected metabolites by isolating their signals, the next logical step would be to utilize this technique in order to quantify difficult metabolites implicated in the etiology of schizophrenia such as glutamate, glutamine and glycine. The work would help develop a more comprehensive understanding of the neurochemical alterations in schizophrenia in order to provide design or monitor new treatments. Taken together, these findings suggest a rationale for investigating the abnormalities in glutamate, glutamine, glycine and serine with higher precision methods. Longitudinal studies of these metabolites may extend our knowledge of the pathophysiology of schizophrenia; allow the improvement of treatment response prediction and categorization of patient cohorts.⁵⁸ *In vivo* measurements of human brain serine, glycine and glutamate in schizophrenia could also allow the exploration of the possible link between abnormal glutamate levels in schizophrenia and endogenous activation of the NMDA glycine site.

4.7 References:

1. Durrant AR, Heresco-Levy U. D-Serine in neuropsychiatric disorders: New advances. *Advances in Psychiatry*. 2014 Jun 19; 2014.
2. Nunes EA, MacKenzie EM, Rossolatos D, Perez-Parada J, Baker GB, Dursun SM. D-serine and schizophrenia: an update. *Expert review of neurotherapeutics*. 2012 Jul 1; 12(7):801-12.
3. Tsai G, Yang P, Chung LC, Lange N, Coyle JT. D-serine added to antipsychotics for the treatment of schizophrenia. *Biological psychiatry*. 1998 Dec 1; 44(11):1081-9.
4. Theberge J, Renshaw PF. *In vivo* measurements of brain serine with ¹H-MRS. In: *Proceedings of the 15th Annual Meeting of ISMRM, Berlin, Germany, 2007* (Abstract 1373).
5. Choi C, Dimitrov I, Douglas D, Zhao C, Hawesa H, Ghose S, Tamminga CA. *In Vivo* Detection of Serine in the Human Brain by Proton Magnetic Resonance

- Spectroscopy (^1H -MRS) at 7 Tesla. *Magn Reson Med*. 2009 Oct; 64(4):1042-1046.
6. Turner CJ. Multipulse NMR in liquids. *Progress in nuclear magnetic resonance spectroscopy*. 1984 Dec 31; 16:311-70.
 7. Green H, Wu X L, Xu P, Friedrich J, Freeman R. Selective excitation at two arbitrary frequencies. The double-DANTE sequence, *Magn Reson*. 1989; 81,646–652.
 8. Bauer C, Freeman R, Frenkiel T, Keeler J, Shaka A J. Gaussian pulses. *Magn Reson Med*. 1984; 58, 442-457.
 9. Blondet P, Albrand JP, Von Kienlin M, Decorpst M, Lavanchy N. Use of rotating-phase DANTE pulses for in vivo proton NMR spectral editing with a single irradiation facility. *Journal of Magnetic Resonance (1969)*. 1987 Feb 1; 71(2):342-6.
 10. Friedrich J, Davies S, Freeman R. Shaped selective pulses for coherence-transfer experiments. *Journal of Magnetic Resonance (1969)*. 1987 Nov 30; 75(2):390-5.
 11. Morris GA, Freeman R. Selective excitation in Fourier transform nuclear magnetic resonance. *Journal of Magnetic Resonance (1969)*. 1978 Mar 31; 29(3):433-62.
 12. Tkáč I, Öz G, Adriany G, Uğurbil K, Gruetter R. In vivo ^1H NMR spectroscopy of the human brain at high magnetic fields: metabolite quantification at 4T vs. 7T. *Magnetic Resonance in Medicine*. 2009 Oct 1; 62(4):868-79.
 13. Ugurbil K, Adriany G, Andersen P, Chen W, Garwood M, Gruetter R, Henry PG, Kim SG, Lieu H, Tkac I, Vaughan T, Van De Moortele PF, Yacoub E, Zhu XH. Ultrahigh field magnetic resonance imaging and spectroscopy. *Magn Reson Imaging* 2003; 21:1263–1281.
 14. Vaughan JT, Garwood M, Collins CM, Liu W, DelaBarre L, Adriany G, Andersen P, Merkle H, Goebel R, Smith MB, Ugurbil K. 7T vs. 4T: RF power, homogeneity, and signal-to-noise comparison in head images. *Magn Reson Med* 2001; 46:24 –30.

15. Tkáč I, Andersen P, Adriany G, Merkle H, Uğurbil K, Gruetter R. In vivo ^1H NMR spectroscopy of the human brain at 7 T. *Magnetic resonance in medicine*. 2001 Sep 1; 46(3):451-6.
16. Otazo R, Mueller B, Ugurbil K, Wald L, Posse S. Signal-to-noise ratio and spectral linewidth improvements between 1.5 and 7 Tesla in proton echo-planar spectroscopic imaging. *Magn Reson Med* 2006; 56:1200–1210.
17. Mekte R, Mlynárik V, Gambarota G, Hergt M, Krueger G, Gruetter R. MR spectroscopy of the human brain with enhanced signal intensity at ultrashort echo times on a clinical platform at 3T and 7T. *Magnetic Resonance in Medicine*. 2009 Jun 1; 61(6):1279-85.
18. Yamamori H, Hashimoto R, Fujita Y, Numata S, et al. Changes in plasma D-serine, L-serine, and glycine levels in treatment-resistant schizophrenia before and after clozapine treatment. *Neurosci Lett*. 2014; 582:93-8.
19. Whittall KP, MacKay AL, Graeb DA, Nugent RA, Li DKB, Paty DW. In vivo measurement of T2 distributions and water contents in normal human brain. *Magn Reson Med* 1997; 37:34-43.
20. Javitt DC. Glutamate and schizophrenia: phencyclidine, N-methyl-D-aspartate receptors, and dopamine-glutamate interactions. *Int Rev Neurobiol* 2007; 78:69–108.
21. Eulenburg V, Arnsen W, Betz H, Gomeza J. Glycine transporters: essential regulators of neurotransmission. *Trends in biochemical sciences*. 2005 Jun 30; 30(6):325-33.
22. Choi C, Bhardwaj PP, Seres P, Kalra S, Tibbo PG, Coupland NJ. Measurement of glycine in human brain by triple refocusing ^1H -MRS in vivo at 3.0 T. *Magnetic Resonance in Medicine*. 2008 Jan 1; 59(1):59-64.
23. Legendre P. The glycinergic inhibitory synapse. *Cell Mol Life Sci* 2001; 58:760–793.
24. Eulenburg V, Arnsen W, Betz H, Gomeza J. Glycine transporters: essential regulators of neurotransmission. *Trends Biochem Sci* 2005; 30: 325–333.
25. Huisman TAGM, Thiel T, Steinmann B, Zeilinger G, Martin E. Proton magnetic resonance spectroscopy of the brain of a neonate with nonketotic

- hyperglycinemia: in vivo-in vitro (ex vivo) correlation. *EurRadiol* 2002; 12:858–861.
26. Maddock RJ, Buonocore MH. MR spectroscopic studies of the brain in psychiatric disorders. In *Brain Imaging in Behavioral Neuroscience 2011* (pp. 199–251). Springer Berlin Heidelberg.
 27. Rowland LM, Bustillo JR, Mullins PG, Jung RE, Lenroot R, Landgraf E, Barrow R, Yeo R, Lauriello J, Brooks WM. Effects of ketamine on anterior cingulate glutamate metabolism in healthy humans: a 4-T proton MRS study. *Am J Psychiatry*. 2005;162:394–396
 28. Stone JM, Dietrich C, Edden R, Mehta MA, De Simoni S, Reed LJ, Krystal JH, Nutt D, Barker GJ. Ketamine effects on brain GABA and glutamate levels with 1H-MRS: relationship to ketamine-induced psychopathology. *Mol Psychiatry*. 2012; 17:664–665.
 29. de la Fuente-Sandoval C, Leon-Ortiz P, Favila R, Stephano S, Mamo D, Ramirez-Bermudez J, Graff-Guerrero A. Higher levels of glutamate in the associative-striatum of subjects with prodromal symptoms of schizophrenia and patients with first-episode psychosis. *Neuropsychopharmacology*.2011; 36:1781–1791.
 30. de la Fuente-Sandoval C, Leon-Ortiz P, Azcarraga M, Stephano S, Favila R, Diaz-Galvis L, Alvarado-Alanis P, Ramirez-Bermudez J, Graff-Guerrero A. Glutamate levels in the associative striatum before and after 4 weeks of antipsychotic treatment in first-episode psychosis: a longitudinal proton magnetic resonance spectroscopy study. *JAMA Psychiatry*. 2013; 70:1057–1066.
 31. Bustillo JR, Rowland LM, Mullins P, et al. 1H-MRS at 4 tesla in minimally treated early schizophrenia. *Mol Psychiatry*. 2010; 15:629–636.
 32. Olbrich HM, Valerius G, Rüsç N, Buchert M, Thiel T, Hennig J et al. Frontolimbic glutamate alterations in first episode schizophrenia: evidence from a magnetic resonance spectroscopy study. *World J Biol Psychiatry*2008; 9: 59–63.
 33. Kegeles LS, Mao X, Stanford AD, Girgis R, Ojeil N, Xu X, Gil R, Slifstein M, Abi-Dargham A, Lisanby SH, Shungu DC. Elevated prefrontal cortex gamma-aminobutyric acid and glutamate-glutamine levels in schizophrenia measured in

- vivo with proton magnetic resonance spectroscopy. *Arch Gen Psychiatry*. 2012; 69:449–459.
34. van Elst LT, Valerius G, Büchert M, Thiel T, Rüscher N, Bubl E, Hennig J, Ebert D, Olbrich HM. Increased prefrontal and hippocampal glutamate concentration in schizophrenia: evidence from a magnetic resonance spectroscopy study. *Biological psychiatry*. 2005 Nov 1; 58(9):724-30.
 35. Théberge J, Williamson KE, Aoyama N, Drost DJ, Manchanda R, Malla AK, Northcott S, Menon RS, Neufeld RW, Rajakumar N, Pavlosky W. Longitudinal grey-matter and glutamatergic losses in first-episode schizophrenia. *The British journal of psychiatry*. 2007 Oct 1;191(4):325-34.
 36. Théberge J, Williamson KE, Aoyama N, Drost DJ, Manchanda R, Malla AK, Northcott S, Menon RS, Neufeld RW, Rajakumar N, Pavlosky W. Longitudinal grey-matter and glutamatergic losses in first-episode schizophrenia. *The British journal of psychiatry*. 2007 Oct 1;191(4):325-34
 37. Théberge J, Al-Semaan Y, Williamson PC, Menon RS, Neufeld RW, Rajakumar N, Schaefer B, Densmore M, Drost DJ. Glutamate and glutamine in the anterior cingulate and thalamus of medicated patients with chronic schizophrenia and healthy comparison subjects measured with 4.0-T proton MRS. *American Journal of Psychiatry*. 2003 Dec 1.
 38. Bartha R, Williamson PC, Drost DJ, Malla A, Carr TJ, Cortese L, Canaran G, Rylett RJ, Neufeld RW. Measurement of glutamate and glutamine in the medial pre-frontal cortex of never-treated schizophrenic patients and healthy controls by proton magnetic resonance spectroscopy. *Arch Gen Psychiatry*. 1997; 54:959–965.
 39. Tibbo P, Hanstock C, Valiakalayil A, Allen P. 3-T proton MRS investigation of glutamate and glutamine in adolescents at high genetic risk for schizophrenia. *Am J Psychiatry*. 2004;161:1116–1118
 40. Lutkenhoff ES, van Erp TG, Thomas MA, et al. Proton MRS in twin pairs discordant for schizophrenia. *Mol Psychiatry*. 2010;15:308–318

41. Chang L, Friedman J, Ernst T, Zhong K, Tsopelas ND, Davis K. Brain metabolite abnormalities in the white matter of elderly schizophrenic subjects: implication for glial dysfunction. *Biol Psychiatry* 2007; 62: 1396–1404.
42. de la Fuente-Sandoval C, Leon-Ortiz P, Azcarraga M, Stephano S, Favila R, Diaz-Galvis L, Alvarado-Alanis P, Ramirez-Bermudez J, Graff-Guerrero A. Glutamate levels in the associative striatum before and after 4 weeks of antipsychotic treatment in first-episode psychosis: a longitudinal proton magnetic resonance spectroscopy study. *JAMA Psychiatry*. 2013; 70:1057–1066.
43. Goto N, Yoshimura R, Kakeda S, Nishimura J, Moriya J, Hayashi K, Katsuki A, Hori H, Umene-Nakano W, Ikenouchi-Sugita A, Korogi Y, Nakamura J. Six-month treatment with atypical antipsychotic drugs decreased frontal-lobe levels of glutamate plus glutamine in early-stage first-episode schizophrenia. *Neuropsychiatr Dis Treat*. 2012; 8:119–122.
44. Kegeles LS, Mao X, Stanford AD, Girgis R, Ojeil N, Xu X, Gil R, Slifstein M, Abi-Dargham A, Lisanby SH, Shungu DC. Elevated prefrontal cortex gamma-aminobutyric acid and glutamate-glutamine levels in schizophrenia measured in vivo with proton magnetic resonance spectroscopy. *Arch Gen Psychiatry*. 2012; 69:449–459.
45. Tayoshi S, Sumitani S, Taniguchi K, et al. Metabolite changes and gender differences in schizophrenia using 3-Tesla proton magnetic resonance spectroscopy (1H-MRS). *Schizophr Res*. 2009; 108:69–77.
46. Rowland LM, Kontson K, West J, Edden RA, Zhu H, Wijtenburg SA, Holcomb HH, Barker PB. In vivo measurements of glutamate, GABA, and NAAG in schizophrenia. *Schizophr Bull*. 2013; 39:1096–1104.
47. Marsman A, van den Heuvel MP, Klomp DW, Kahn RS, Luijten PR, Hulshoff Pol HE. Glutamate in schizophrenia: a focused review and meta-analysis of ¹H-MRS studies *Schizophr Bull*.
48. Maddock RJ, Buonocore MH. MR spectroscopic studies of the brain in psychiatric disorders. In *Brain Imaging in Behavioral Neuroscience 2011* (pp. 199-251). Springer Berlin Heidelberg.

49. Merritt K, McGuire P, Egerton A. Relationship between glutamate dysfunction and symptoms and cognitive function in psychosis. *Neuropsychopharmacology of Psychosis: Relation of Brain Signals, Cognition and Chemistry*. 2015 Apr 22:86.
50. Rothman DL, De Feyter HM, de Graaf RA, Mason GF, Behar KL. C-13 MRS studies of neuroenergetics and neurotransmitter cycling in humans. *NMR Biomed* (2011) 24(8):943–5710.
51. Marsman A, van den Heuvel MP, Klomp DW, Kahn RS, Luijten PR, Pol HE. Glutamate in schizophrenia: a focused review and meta-analysis of 1H-MRS studies. *Schizophrenia bulletin*. 2013 Jan 1; 39(1):120-9.
52. Jang DP, Lee JM, Lee E, Park S, Kim JJ, Namkoong K, Yoon KJ, Kim IY, Kim SI. Interindividual reproducibility of glutamate quantification using 1.5-T proton magnetic resonance spectroscopy. *Magnetic resonance in medicine*. 2005 Mar 1; 53(3):708-12.
53. Mullins PG, Rowland L, Bustillo J, Bedrick EJ, Lauriello J, Brooks WM. Reproducibility of 1H-MRS measurements in schizophrenic patients. *Magnetic resonance in medicine*. 2003 Oct 1; 50(4):704-7.
54. An1 Z, Ganji1 S, Choi C. Reproducibility of glutamate, GABA and glycine in human brain, as measured by optimized 1H MRS at 7T. In: *Proceedings of the 23rd Annual Meeting of ISMRM, Toronto, Canada, 2015 (Abstract 4659)*
55. Stanley JA, Drost DJ, Williamson PC, Carr TJ. In vivo proton MRS study of glutamate and schizophrenia. *NMR Spectroscopy in Psychiatric Brain Disorders*. 1995 Apr 1; 47:21-44.
56. Kegeles LS, Shungu DC, Anjilvel S, Chan S, Ellis SP, Xanthopoulos E, Malaspina D, Gorman JM, Mann JJ, Laruelle M, Kaufmann CA. Hippocampal pathology in schizophrenia: magnetic resonance imaging and spectroscopy studies. *Psychiatry Research: Neuroimaging*. 2000 May 15; 98(3):163-75.
57. Schubert F, Gallinat J, Seifert F, Rinneberg H. Glutamate concentrations in human brain using single voxel proton magnetic resonance spectroscopy at 3 Tesla. *Neuroimage*. 2004 Apr 30; 21(4):1762-71.

58. Stone JM. Glutamatergic antipsychotic drugs: a new dawn in the treatment of schizophrenia? *Therapeutic advances in psychopharmacology*. 2011 Feb 1; 1(1):5-18.
59. Mullins PG, Chen H, Xu J, Caprihan A, Gasparovic C. Comparative reliability of proton spectroscopy techniques designed to improve detection of J-coupled metabolites. *Magnetic resonance in medicine*. 2008 Oct 1; 60(4):964-9.
60. Daftary A. PET-MRI: challenges and new directions. *Indian Journal of Nuclear Medicine*. 2010 Jan 1; 25(1):3.
61. Vandenberghe S, Marsden PK. PET-MRI: a review of challenges and solutions in the development of integrated multimodality imaging. *Physics in medicine and biology*. 2015 Feb 4; 60(4):R115.
62. Peng BJ, Wu Y, Cherry SR, Walton JH. New shielding configurations for a simultaneous PET/MRI scanner at 7T. *Journal of Magnetic Resonance*. 2014 Feb 28; 239:50-6.
63. Carrio I, Ros PR, editors. *PET/MRI: Methodology and Clinical Applications*. Springer Science & Business Media; 2013 Dec 9.

Appendix A: DANTE-PRESS (the sequence and the special Card)

The D-PRESS sequence and the user interface for its parameters were developed using the source code of the MRI scanner manufacturer's product source as a starting point. This was provided by, and in collaboration with, Dr. Gerald Moran, from Siemens Canada under the terms of the Master Research Agreement between Lawson Health Research Institute and Siemens Canada. As described in Chapter 4, a custom DANTE-PRESS pulse sequence was programmed, as well as an associated user interface, allowing more advanced pulse sequence parameter modification capabilities. The Integrated Development Environment for Applications (IDEA) provided by the manufacturer is the pulse programming environment and set proprietary C++ classes that were used to implement the D-PRESS method, interface and online post-processing capabilities. The new features of the D-PRESS are included in the "sequence/special" card of the scanner's user interface.

DANTE-PRESS parameters:

Once a user clicks on the "DANTE RF Pulse" check box, it adds the DANTE RF Pulse and its crusher gradients to the standard symmetrical PRESS pulse sequence as the second refocusing pulse (non-slice selective), transforming this double spin echo sequence into a triple spin echo sequence. Once the DANTE RF Pulse checkbox is enabled, all parameters related to the DANTE RF Pulse appear on the "Special Card".

A DANTE pulse is formed by the convolution of a rectangular function with a comb function and multiplied by an amplitude modulation function (i.e. Gaussian):

$$comb\left(\frac{t}{\Delta t}\right) \otimes rect\left(\frac{t}{\tau}\right) \bullet gauss\left(\frac{\beta}{2} \sqrt{\frac{\pi}{\ln 2}} t\right) \quad \text{Equation A-1}$$

Where t is time, Δt is the time between each rectangular pulse, τ is the duration of each rectangular pulse and β is the damping coefficient of the Gaussian envelope.

Since the DANTE pulse is composed of individual hard pulses, the frequency profile of DANTE pulses is accurately represented by its Fourier Transform:

$$|\Delta t| \text{comb}(\Delta t f) \bullet \tau \text{sinc}(\tau f) \otimes \frac{2}{\beta} \sqrt{\frac{\ln 2}{\pi}} \text{gauss}\left(\frac{2}{\beta} \sqrt{\frac{\ln 2}{\pi}} f\right) \quad \text{Equation A-2}$$

which can be seen to be a comb function multiplied by a sinc function and convolved with a Gaussian. Therefore, one can control the frequency profile of DANTE pulses by setting three parameters: Δt (period), τ (Duration), and β (damping coefficient) to express these parameters in a more practical form: FDP = $1/\Delta t$, Sinc FWHM = $1.2068/\tau$ and Gauss FWHM = β .

Of course, since the DANTE pulse is a digitized waveform, other parameters, such as the number of digitization points and the amplitude cut-off for the Gaussian modulation, must be used for the pulse sequence to construct a specific DANTE pulse.

The following will briefly introduce how the parameters related to this pulse have been implemented in the MRI scanner user interface.

The “DANTE Modulation” drop menu enables the user to select the shape of the DANTE RF pulse amplitude modulation: Sinc, Gaussian or none (square). In this thesis all the experiments were performed using the Gaussian modulation.

The “DANTE AM Cut-off” parameter represents the fraction of maximum amplitude of the waveform to cut-off the Gaussian waveform, which would otherwise be infinite. In all of the experiments presented in this thesis, this value was set to 0.05, i.e. 5%, and verified by phantom experiments.

The “DANTE Passband Width” represents the Full Width Half Maximum of all passbands, which is represented in parts per million (ppm). A tool tip has been programmed to display the resulting calculated duration of the DANTE RF pulse in milliseconds (ms).

The “DANTE Shift” sets the carrier frequency for the Dante RF pulse. Its value is relative to the reference frequency determined during the frequency adjustment of the pulse sequence, presented in parts per million (ppm).

The “DANTE F Domain Period” variable, circled in purple in Figure A-1, represents the distance in between two successive passbands in the frequency domain. In this thesis, we used the acronym FDP to represent this quantity. The value is represented in Hertz (s^{-1}). The use of this parameter is essential to allow the user to excite both the resonance of the metabolite of interest and a resonance of a reference metabolite simultaneously. The reference metabolite can be used as a phase reference, amplitude reference or chemical shift reference in the final spectrum.

The “DANTE Points” parameter represents the number of digitization points of the DANTE RF pulse waveform.

The “DANTE F-Domain FWHM” represents the Full Width Half Maximum (FWHM) in Hertz of the intrinsic sinc modulation of the frequency profile of the DANTE pulse. This is typically set to a very large value so that consecutive passbands have practically the same amplitude.

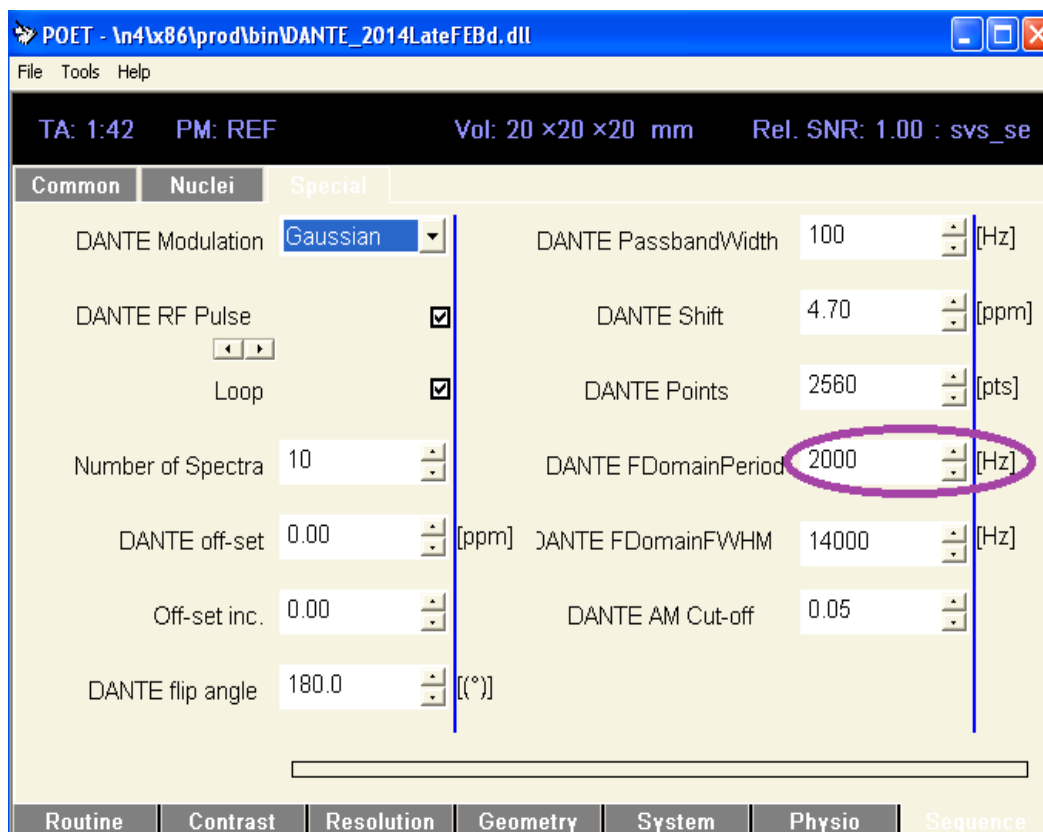


Figure A-1. The “Special Card” illustrating the parameters which interact with the DANTE RF Pulse.

The optimization parameters:

Several options were added to the special card (circled in orange), such as tools allowing the run time optimization of selected sequence parameters before the start of the data acquisition. The calibration of these parameters ensures that the final desired pulse sequence functionality is achieved and increases the spectral quality and reproducibility.

A. The “Flip Angle Modulation” drop menu:

The user interface provides a drop menu of “FlipAngle (FA) Modulation” that offers the option of calibrating either the excitation pulse flip angle, the DANTE pulse flip angle, or the flip angle of both non-DANTE refocusing pulses simultaneously. By placing the cursor near the user interface entry field, a tool tip displays the current RF pulse and

gradient crusher parameters, including the flip angle values and the gradient crushers' amplitude. The starting value of each flip angle is entered manually by the user along with the incremental step value and the desired number of measurements. Following the calibration measurement loop, the optimum flip angle value observed can/should be entered manually prior to the start of the acquisition of the final spectrum. When the optimization is completed, prior to the start of acquisition of the final data, the "Standard RF" option must be selected to disable the calibration loop and enable normal looping (average and measurement loops).

B. The "DANTE Frequency Shift Increment" parameter:

The user interface provides another parameter adjustment loop, "DANTE Freq Shift INC", which allows the user to fine tune the adjustment of the frequency offset of the DANTE RF pulse. This is important since the passbands are so narrow. Misadjustment of the DANTE frequency offset can result in significant signal loss.

Additionally, the field defines the number of measurements desired and the incremental step in chemical shift of this adjustment loop.

Following the calibration of the DANTE Frequency shift, the optimum chemical shift value can/should be entered manually by the user prior to the start of data acquisition.

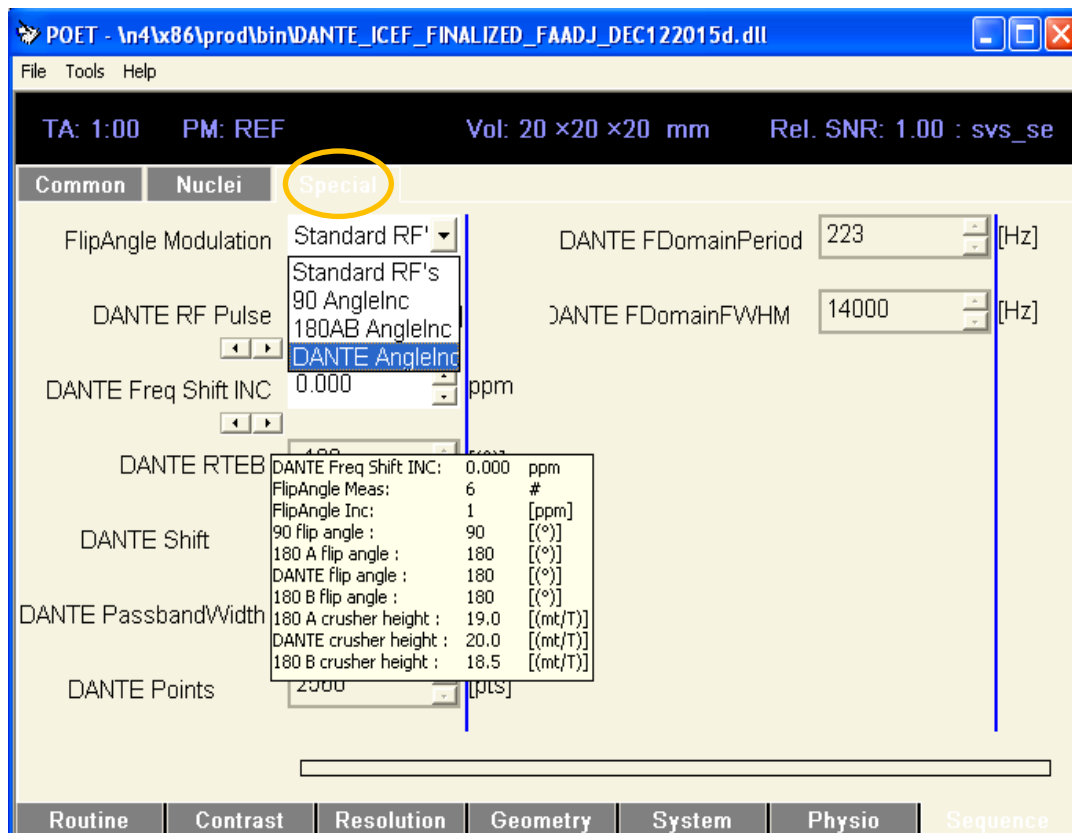


Figure A-2. This figure illustrates the modulation parameters including the drop-down menu for the “Flip Angle Modulation” and the “DANTE Frequency Shift INC” parameters.

Appendix B: DANTE Radio Frequency (RF) Pulse

The generation of the DANTE-PRESS sequence is enabled by the implementation of the DANTE-RF pulse along with its flanking crusher gradients in the pulse sequence as the second non-slice selective refocusing pulse into a symmetrical PRESS sequence (Version VB20PSP4, based on modification of Siemens product SVS_SE source code). The following code/snippet includes the customized process of the implementation of this “Arbitrary” Gaussian-modulated, frequency-selective, DANTE RF pulse within the sequence at run time. The DANTE-RF pulse can be prepared with the following statement and used in the *fSEQRun* portion of the sequence:

```
prepArbitrary (pMrProt, pSeqExpo, myRFPulseArray, EffectiveAmplitudeIntegral)
```

Example code snippet:

```
/* In Global Declarations */

sSample myRFPulseArray[IRF_MAX_ENVELOPE_ELEMENTS]
/*DANTE waveform vector*/

sRF_PULSE_ARB myRFPulse;
/*DANTE RF Pulse Object*/

fSEQInit (....)
{
....
/* Sequence Special Card Simple DANTE-RF Pulse Variable Declaration */
PARAM ("DANTE RF Pulse", &u_bBoolTestDante, false, "Enables or Disables
the implementation of the Dante RF Pulse and its crusher gradients in
the pulse sequence as the second non-slice selective refocussing
pulse.");

PARAM("DANTE PassbandWidth", "[Hz]", &u_lBandwidth, 0, 100, 1, 15, " The
'DANTE PassbandWidth' represents the bandwidth of the Dante RF pulse. ");

PARAM("DANTE Points", "[pts]", &dante_pts, 0,8192 , 1, 2560, " The
'DANTE Points' represents the number of points of the Dante RF pulse
waveform.");

PARAM("DANTE AM Cut-off","", &dante_cut, 0, 1, 0.01, 0.05, "The 'DANTE
AM Cut-off' represents the fraction of maximum amplitude of the waveform
to cut-off the Gaussian waveform.");
....
}
fSEQPrep(....)
{
....
```

```

/* The Gaussian modulated DANTE-RF Pulse is calculated: */
// Set the pulse duration based on the user-requested passband width and
amplitude modulation.

/* Compute DANTE RF pulse duration in seconds for Gaussian */

dante_beta = u_lBandwidth;
/* set passband FWHM for Gaussian modulation */

dante_dur = 4.0/ pi / dante_beta * sqrt(log(2) * 1.0 * log(dante_cut));

p3=dante_dur;
/* puts duration in seconds in shorter variable name for use in long
formulas below */

/* Calculate other DANTE-RF pulse properties */

dante_timeres = dante_dur/dante_pts;
/* calculate square pulse length in number of points */

dante_nsqpts = (int) (dante_tau/dante_timeres);
/* calculate time domain period in number of points */

dante_ndtpts = (int) (dante_deltat/dante_timeres);

/** Calculate the DANTE-RF shape ***/
// ("Gaussian Pulse ON\n");

t=0;
tinc = dante_dur/(dante_pts-1); /*time increment*/

for (i=0;i<dante_pts;i++) {

    /* set phase to a constant for now */
    myRFPulseArray[i].flPha = float (0.);

    /* compute within-block index */
    k=i % dante_ndtpts;

    if (k < dante_nsqpts) {
        myRFPulseArray[i].flAbs = float (1.0 * exp(pi * pi / 4.0 /
            log(2) * dante_beta * dante_beta * (t-p3/2.0) * (t-p3/2.0)));
        } else
    {
        myRFPulseArray[i].flAbs= float (0.);
    }

    dRealAmpl += (myRFPulseArray[i]).flAbs *
cos((myRFPulseArray[i]).flPha);
    dImagAmpl += (myRFPulseArray[i]).flAbs *
sin((myRFPulseArray[i]).flPha);

    t=t+tinc;
} //end of for-loop

```

```
dEffectiveAmplIntegral = sqrt(dRealAmpl*dRealAmpl +  
dImagAmpl*dImagAmpl);  
  
} //end of fSEQPrep  
fSEQRun(.....)  
{  
    myRFPulse.run();  
} //end of fSEQRun
```

Due to the RF hardware limits provided by the Biograph mMR 3.0 T scanner the maximum duration of an RF pulse cannot exceed 100 ms. Thus, the example code above allows for the implementation of an arbitrary DANTE-RF pulse with a duration of equal and less than 100 ms in total ($\sim \Rightarrow 20$ Hz). One possible way to implement long duration RF pulses is to split these pulses into shorter durations with small delays between them. In order to generate an arbitrary DANTE-RF pulse with duration higher than 100 ms (i.e. 118.54 ms, equivalent to a FWHM equal to 15 Hertz at 3.0 Tesla) and to compensate for this hardware limitation, two arbitrary Gaussian modulated DANTE-RF pulses must be implemented each with durations equal and less than 100 ms. This is the approach that was used in this thesis to achieve DANTE passbands of 15 Hertz.

Appendix C: Inline Display



The “Inline display” enables the real time monitoring of the measurement loops. The standard MRS signal post-processing options on the MRI scanner provide basic abilities to display individual spectral traces as they are being acquired as well as the accumulated spectrum averaged from all traces acquired at any given time. These traces display only one spectrum at a time (no option for displaying multiple measurements) and represent only the signal from the receiver channel with the largest signal (not the channel-combined data).

Programming within the manufacturer’s Image Calculation Environment (ICE) allows the user to implement custom behaviors for the inline display. The following will provide examples of the inline display functions implemented as used during calibration loops for acquisition performed in a phantom (*in vitro* data). Optimization scans are executed by using a smaller number of averages (total 1 to 8) to reduce the timeframe of these scans. The following parameters were optimized and their results were displayed in the inline display:

(A) The calibration of the flip angle values for the excitation pulse and the refocusing RF pulses (the calibration of the flip angle value for the DANTE RF pulse is not demonstrated in the following examples):

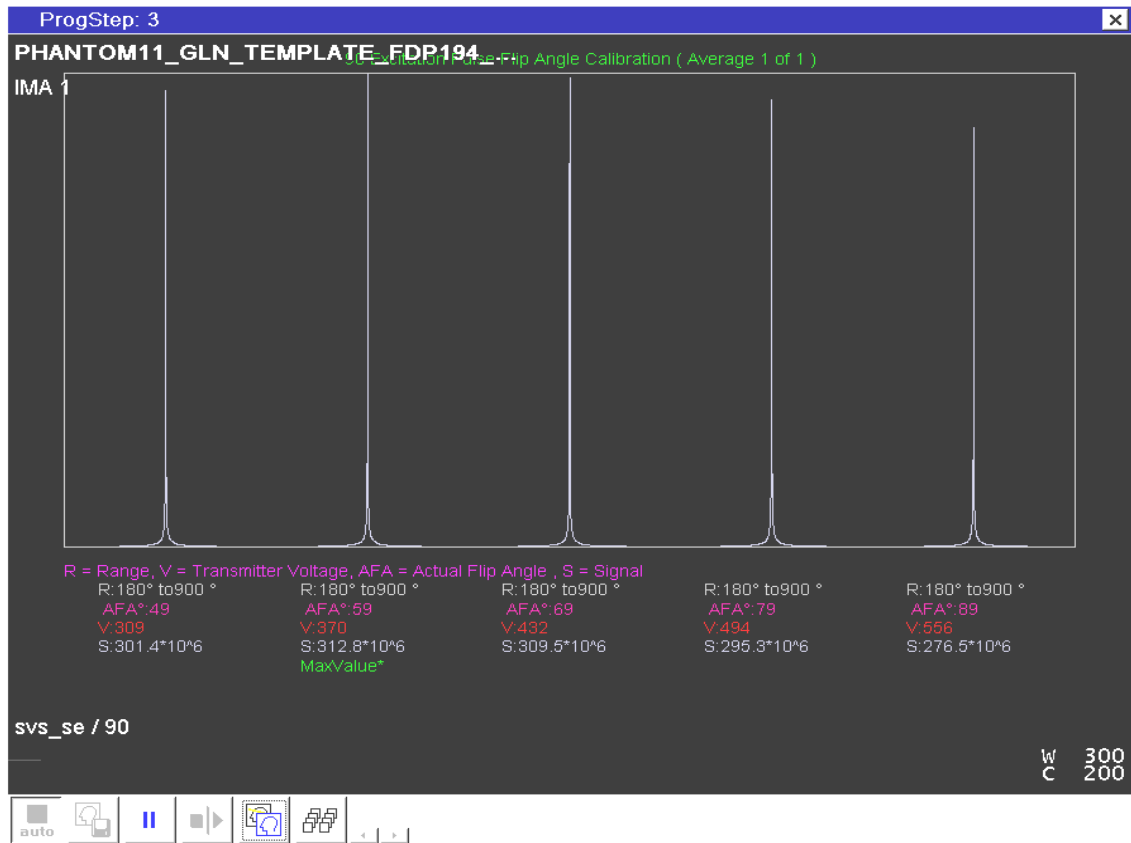


Figure C-3. The inline display illustrates the RF pulse’s flip angle (FA) value, indicating the production of the maximum signal along with the actual FA (AFA), transmitter voltage (V), the signal value (S), and highlights the maximum value with a green label (MaxValue*).

The inline display during fine calibration of the flip angle (FA) for the 90° Excitation pulse of the D-PRESS sequence using the water unsuppressed signal (1 average, 4 dummy scans) is displayed in Figure C-3. In this example, the excitation pulse voltage of ~370 V produced maximum signal.



Figure C-4. The inline display illustrates the RF pulse’s flip angle (FA) value, indicating the production of the maximum signal along with the actual FA (AFA), transmitter voltage (V), the signal value (S), and highlights the maximum value with a green label (MaxValue*).

Figure C-4 illustrates the inline display during the simulations fine calibration of the flip angle (FA) for the two 180° Refocusing RF pulses of the D-PRESS sequence using the water unsuppressed signal (1 average, 4 dummy scans). This example demonstrates that for both refocusing pulses the voltage of ~516 V produced maximum signal

The calibration of the flip angle values for the 90° Excitation pulse and the 180° refocusing pulses of the D-PRESS sequence enables the determination of the optimal flip angle value, which ensures the reduction in signal loss and the degradation in spectral quality.

(B) The calibration of the offset of the DANTE pulse's carrier frequency.

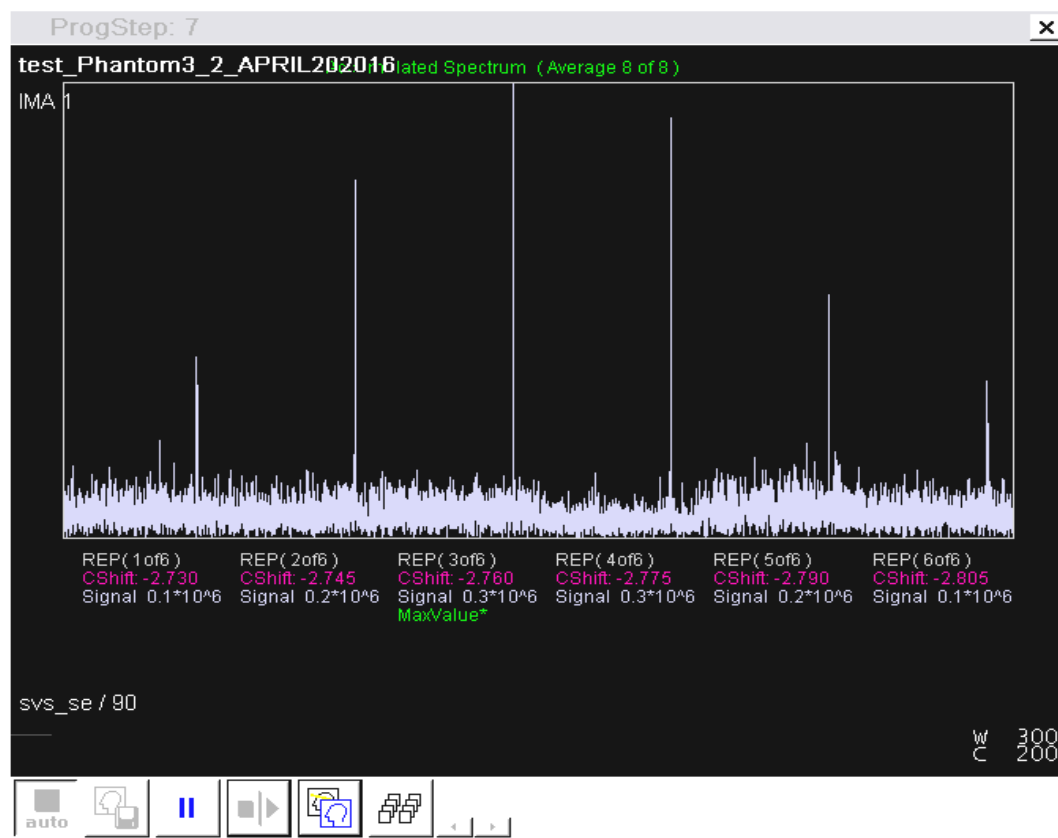


Figure C-5. The inline display illustrates the DANTE RF pulse's chemical shift (CShift) value, the repetition number (REP), the signal value (Signal), and highlights the maximum value with a green label (MaxValue*).

Fine adjustment of the center frequency of the DANTE pulse using N-AcetylAsparate Acid as the chemical shift (CS) reference metabolite was obtained from an *in vitro* experiment. The inline display during the calibration of the DANTE chemical shift (8 averages, 4 dummy scans) is displayed above (Figure C-5).

In this example, the CS value was incremented in steps of 0.015 ppm. The precise relative CS value of NAA is ensured and corresponds to 2.01ppm on an absolute ppm scale.

(C) DANTE chemical shift (CS) calibration for the water resonance:



Figure C-6. The inline display illustrates the calibration of the DANTE chemical shift for the water peak and highlights the maximum value with a green label (MaxValue*).

The Water unsuppressed concentration is used as a reference and is acquired with and without the DANTE pulse. CS fine tuning is used for the DANTE ON water reference. The inline display demonstrates the channel-combined magnitude spectrum (8 averages, 4 dummy scans (Figure C-6)).

In this example, the CS value of 0.030 ppm produces the maximum signal, as indicated by the MaxValue* label. The 0.030 ppm CS value was chosen and was entered manually by the user prior to the start of data acquisition to obtain the DANTE ON water reference spectrum. This spectrum can be compared with the DANTE OFF water signal to estimate the magnitude of signal losses, if any, due to the use of the DANTE pulse, yet another 180° pulse with possible flip angle imperfection.

Appendix D: Gradient Crusher Optimization

In the D-PRESS pulse sequence, every 180° RF pulse was flanked by crusher gradients in order to selectively produce signal from the triple spin echo. In order to prevent interference from unwanted coherences (FIDs and spin echo, and stimulated echos), the area of the crusher gradients of the 180° RF pulses was optimized and modified accordingly.

The screenshot shows the POET software interface with the 'Special' tab selected. The 'DANTE RTEB' parameter is highlighted with a red box and a white arrow. The 'DANTE Shift' parameter is set to 0.000 [ppm]. The 'DANTE PassbandWidth' is set to 15 [Hz]. The 'DANTE Points' is set to 2560 [pts]. The 'DANTE FDomainPeriod' is set to 223 [Hz]. The 'DANTE FDomainFWHM' is set to 14000 [Hz]. The 'DANTE Freq Shift INC' is set to 0.0000000 [ppm]. The 'ICE LineWidth EXPFilter' is set to 1.0000 [ppm].

The following table lists the crusher gradient values shown in the interface:

Crusher	Value [mT/m.us]
Fid1crushing	144.38
Fid2crushing	88.58
Fid3crushing	163.05
Fid4crushing	141.52
SE12crushing	32.77
SE14crushing	138.66
SE13crushing	181.71
SE24crushing	194.47
SE23crushing	237.51
SE34crushing	120.00
SE123crushing	293.32
SE234crushing	45.53
SE134crushing	101.34
ST123crushing	107.24
ST234crushing	215.99
ST134crushing	160.18

The bottom of the interface shows a log window with the following text:

```

2016/11/23 09:29:16:569 [\n4\pkg\MrServe eTrace.h:555]
PERFORMANCE WARNING: .MSR.seq_wip7.* dura ied = 300 ms
..... dRfEnergyInSRFs exc = 0
..... dRfEnergyInSRFs rf ref 1 =
..... dRfEnergyInSRFs rf ref 2 =
FINAL FINAL FINAL dRfEnergyInSRFs 104.489
FINAL FINAL FINAL dRfEnergyInSBBs 0
..... dRfEnergyInSRFs exc = 24.4242
..... dRfEnergyInSRFs rf ref 1 = 74.9839
..... dRfEnergyInSRFs rf ref 2 = 125.544
FINAL FINAL FINAL dRfEnergyInSRFs 128.913
FINAL FINAL FINAL dRfEnergyInSBBs 0

```

Figure D-7. This figure illustrates how the values for the gradient crusher areas can be visualized at run-time by the user in response to changes in the pulse sequence timing and the crusher gradient amplitude allowing for efficient adjustments of gradient crushing resulting in the elimination of the unwanted coherences adequately.

By placing a cursor near the user interface entry field, a tool tip displays the calculation of the total area of the crusher gradients by taking into account the contribution of the gradient crusher of one, two, three, or four RF pulses, along all three axes. During the calibration of the gradient crushers, the user can therefore estimate roughly what parameter values to use in order to effectively remove the unwanted coherences or quickly identify unwanted coherences with weak gradient crushing.

The following optimized gradient values of the following RF pulses were manually entered by the user after the optimization procedure was completed:

(RF²): Height of 19 mT/m, duration of 2000 ms

(RF³): Height of 20 mT/m, duration of 2000 ms

(RF⁴): Height of 18.5 mT/m, duration of 4000 ms.

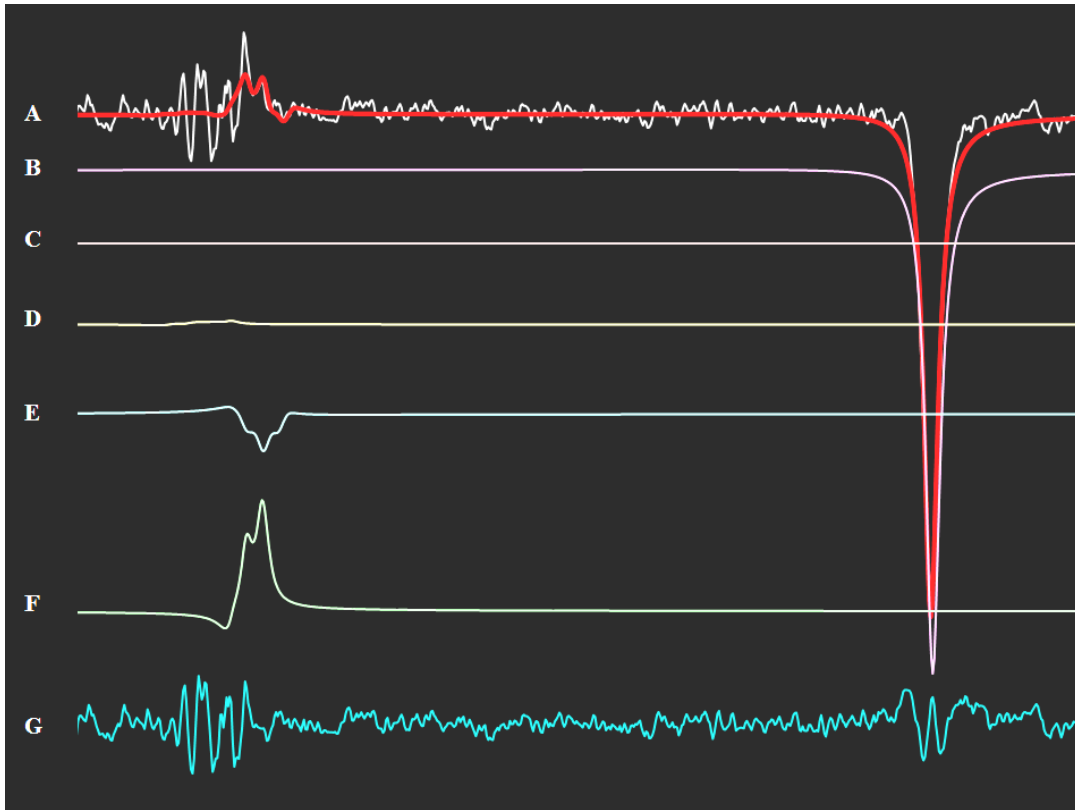


Figure D-8. Representative of an *in vivo* spectrum obtained prior to optimizing the height of the gradient crushers. Line (A) represents the data in white and the fitting line in red, lines (B, C and D) illustrate the fitting components of NAA, Cr and Ser in purple, orange and yellow, respectively, lines (E, F) represent the fitting components of Gln in blue and Glu in green, respectively. Line (G) represents the residuals in blue (data minus fit). LW correction factor of 2 Hz was applied. As illustrated the residuals are considerably large and the template does not fit the data properly.

The *in vivo* spectrum above was obtained from a healthy participant, with the D-PRESS sequence using an echo time of 286 ms (DANTE ON at 3.83 ppm, FDP 223 Hz) prior to gradient crusher optimization. The initial *in vivo* data obtained contained significant interference from unwanted coherences, the *in vitro* template did not fit the data properly, and the serine concentration obtained was inconsistent from scan to scan.

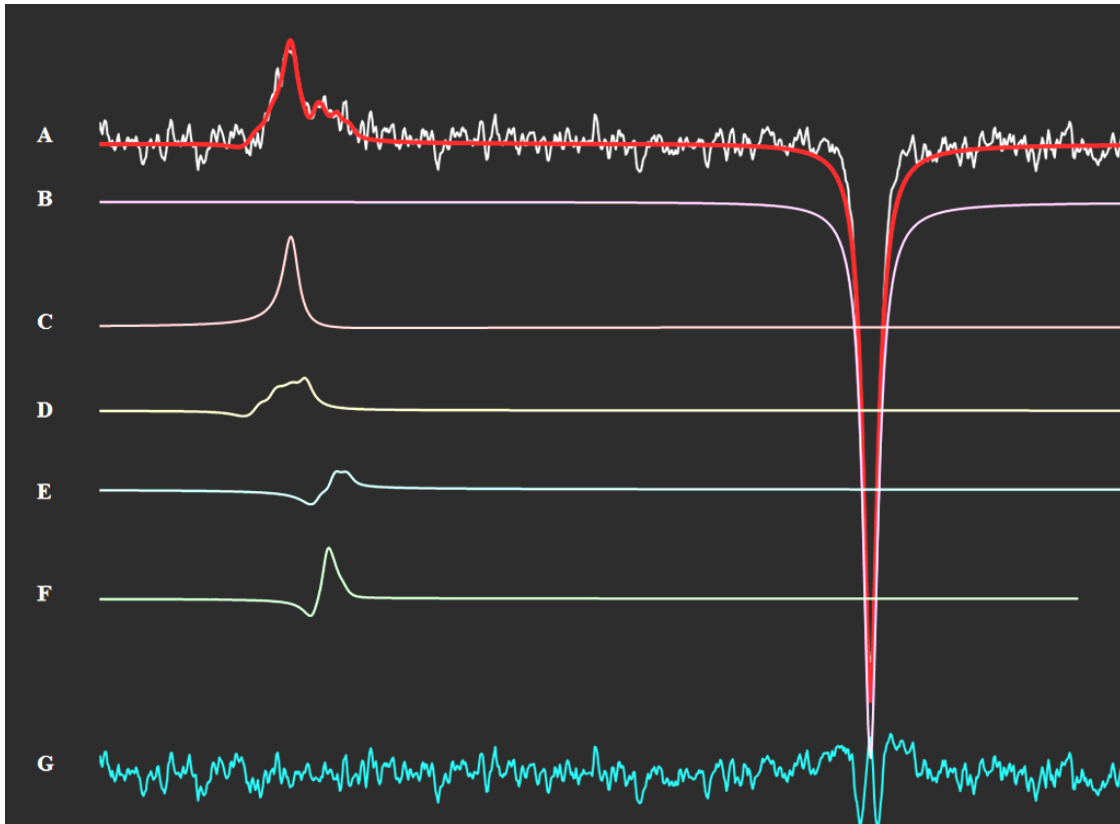


Figure D-9. Representative of an *in vivo* spectrum acquired after the optimizing of the gradient crushers was performed. Line (A) represents the data in white and the fitting line in red, lines (B, C and D) illustrate the fitting components of NAA, Cr and Ser in purple, orange and yellow, respectively, lines (E, F) represent the fitting components of Gln in blue and Glu in green, respectively. Line (G) represents the residuals in blue. LW correction factor of 2 Hz was applied. As illustrated the residuals are negligible and the template fits the data properly.

The spectrum above was acquired with an updated protocol from the same healthy participant, but using the gradient crusher amplitude values obtained after optimization. The *in vivo* data obtained with the new protocol and optimized parameters (gradients) eliminated unwanted coherences and produced data that could be better modeled by the metabolite spectral signatures of Cr, Ser, Glu and Gln (notice the flat residuals)

Appendix E: Ethics Approval



Research Ethics

Western University Health Science Research Ethics Board HSREB Annual Continuing Ethics Approval Notice

Date: June 29, 2016

Principal Investigator: Dr. Terry Thompson

Department & Institution: Schulich School of Medicine and Dentistry\Schulich School of Medicine & Dentistry, Lawson Health Research Institute

Review Type: Delegated

HSREB File Number: 6319

Study Title: Improving Magnetic Resonance Imaging Hardware and Software at 1.5 and 3 Tesla

HSREB Renewal Due Date & HSREB Expiry Date:

Renewal Due -2017/06/30

Expiry Date -2017/07/28

The Western University Health Science Research Ethics Board (HSREB) has reviewed the Continuing Ethics Review (CER) Form and is re-issuing approval for the above noted study.

The Western University HSREB operates in compliance with the Tri-Council Policy Statement Ethical Conduct for Research Involving Humans (TCPS2), the International Conference on Harmonization of Technical Requirements for Registration of Pharmaceuticals for Human Use Guideline for Good Clinical Practice (ICH E6 R1), the Ontario Freedom of Information and Protection of Privacy Act (FIPPA, 1990), the Ontario Personal Health Information Protection Act (PHIPA, 2004), Part 4 of the Natural Health Product Regulations, Health Canada Medical Device Regulations and Part C, Division 5, of the Food and Drug Regulations of Health Canada.

Members of the HSREB who are named as Investigators in research studies do not participate in discussions related to, nor vote on such studies when they are presented to the REB.

The HSREB is registered with the U.S. Department of Health & Human Services under the IRB registration number IRB 00000940.

Ethics Officer, on behalf of Dr. Joseph Gilbert, HSREB Chair

Ethics Officer: Erika Basile ___ Katelyn Harris ___ Nicole Kaniki ___ Grace Kelly Vikki Tran ___ Karen Gopaul ___

Curriculum Vitae

Name: **Homa Javadzadeh**

**Post-secondary
Education and
Degrees:**

Master of Science

Department of Medical Biophysics
Western University
London, Ontario, Canada
2013-2016

Thesis: *MEASURING BRAIN SERINE WITH ¹H-MRS AT 3.0 TESLA*

Supervisors: Dr. Jean Théberge, PhD, FCCPM and Dr. Peter Williamson, MD, FRCPC.

Honours Bachelor of Science

B.Sc. in Neuroscience and Integrative Biology (Life Sciences)
University of Toronto, Toronto, ON
2005-2010

**Honours and
Awards:**

Schulich Graduate Scholarship
2015-2016

**Related Work
Experience**

Research Assistant
Department of Medical Biophysics
University of Western Ontario, Lawson Health Research Institute
Supervisor: Dr. Jean Théberge, PhD, FCCPM

Presentations and Abstracts:

Oral presentations

Javadzadeh H. Théberge J. *In vivo* ¹H-MR spectroscopy of endogenous brain serine. Proceedings of 2015 Psychiatry Research Day, London, ON.
(Selected for an oral presentation)

Javadzadeh H. Théberge J. *In vivo* Measurements of Brain Serine with ¹H-MRS. Presented at the 2014 TOFS (Talks on Fridays), St. Joseph's hospital, London, ON.

Poster presentations

Javadzadeh H. Théberge J. Assessment of serine quantification reproducibility using advanced ^1H -MRS in the human brain at 3.0 Tesla. In: Proceedings of the 24th Annual Meeting of ISMRM, Singapore, 11/05/2016

Javadzadeh H. Théberge J. Assessment of serine quantification reproducibility using advanced ^1H -MRS in the human brain at 3.0 Tesla. In: Proceedings of the 24th Annual Meeting of ISMRM, Singapore, MR Spectroscopy Study Group 12/05/2016 (*Abstract 4310*).

(Selected for a poster presentation)

Javadzadeh H. Théberge J. ^1H -MR spectroscopy measurements of endogenous brain serine. Proceedings of 2016 London Health Research Day, ON.

Javadzadeh H. Théberge J. *In vivo* ^1H -MR spectroscopy of endogenous brain. Presented at the 2015 10th Annual London Imaging Discovery, London, ON.

(Poster First Place Winner)

Javadzadeh H. Théberge J. *In vivo* ^1H -MR spectroscopy of endogenous brain serine. Proceedings of 2015 London Health Research Day, ON.

(Selected as the top 80 presenters).

Javadzadeh H. Théberge J. *In vivo* ^1H -MR spectroscopy of brain serine at 3.0 Tesla. Poster presented at the 2014 London Health Research Day, London, ON.

Submitted Abstracts

Javadzadeh H. Théberge J. ^1H -MRS measurement of serine in phantoms and demonstration in the human brain at 3.0 Tesla. In: Proceedings of the 23rd Annual Meeting of ISMRM, Toronto, Canada, 2015 (*Abstract 5729*).

Javadzadeh H. Théberge J. 3.0 Tesla ^1H -MRS measurements of human brain serine. In: Proceedings of the 22nd Annual Meeting of ISMRM, Milan, Italy, 2014 (*Abstract 2139*).